ESCUELA TÉCNICA SUPERIOR DE NÁUTICA

UNIVERSIDAD DE CANTABRIA

Trabajo Fin de Grado

Definición geométrica y construcción 3D de una hélice.

Geometric definition and 3D construction of a propeller

Para acceder al Título de Grado en

INGENIERÍA MARINA

Autor: David Espinosa García

Director: Jesús María Villar González

Diciembre – 2017

ESCUELA TÉCNICA SUPERIOR DE NÁUTICA

UNIVERSIDAD DE CANTABRIA

Trabajo Fin de Grado

Definición geométrica y construcción 3D de una hélice.

Geometric definition and 3D construction of a propeller

Para acceder al Título de Grado en

INGENIERÍA MARINA

Diciembre – 2017

Contenido

RESUMEN

En este trabajo se pretende poner en práctica las aptitudes y conocimientos que se han adquirido en la universidad durante el Grado en Ingeniería marina, llevando a cabo un diseño en 3D de una hélice manejando un programa CAD (diseño asistido por ordenador), poniendo así en prácticas conocimientos de dibujo. Por otra parte se demuestran conocimientos de hélices marinas y propulsión naval. También cabe destacar que aunque la impresión en 3D por medio de una impresora no es una disciplina impartida en la universidad, podría ser considerada como una prolongación de las técnicas aprendidas en “sistemas de representación”. En nuestro caso se realiza una impresión de una hélice común, para poder ver así físicamente la realidad de lo aprendido de modo teórico durante los años de estudios.

Usando programas de diseño proporcionados por la universidad y otras versiones de programas gratuitos o de software libre, se llevará a la práctica el modelado de una hélice de una serie sistemática conocida.

Este trabajo muestra la utilidad de las nuevas tecnologías para generar o realizar procesos que tiempo atrás se realizaban manualmente, consumiendo gran cantidad de horas hombre. Las facilidades actuales son enormes, a la hora de realizar piezas.

Las nuevas tecnologías son importantes para el desarrollo de piezas con precisiones elevadas, donde el factor de error del hombre no es admisible y la capacidad de las maquinas es mucho mayor. Igualmente la repetitividad de los acabados finales también es una ventaja a favor de las máquinas. No obstante, como toda máquina carece de personalidad y criterio, sigue siendo imprescindible que en este proceso el hombre intervenga para hacer valoraciones y tomar decisiones que un proceso de mecanizado automático no puede.

1. JUSTIFICACIÓN Y OBJETIVOS

En este trabajo se pretende construir una hélice, seleccionando sus parámetros básicos y desarrollando su geometría por medio de un diseño asistido por ordenador.

Una vez logrado el diseño con el CAD se realizará una impresión en 3D (tres dimensiones), buscando así una hélice materializada, y pudiendo comprobar que nuestro desarrollo académico se asemeja a la realidad industrial que hemos visto en ocasiones.

Cabe destacar que el campo de la definición o descripción geométrica de la hélice, es un tema poco desarrollado tanto a nivel académico como profesional.

En el proceso de asociar una hélice a una carena y un motor hay 2 facetas bien definidas:

1- El trabajo del diseñador, que establece los parámetros fundamentales de la hélice (diámetro, paso, Area Ae/Ao, revoluciones, número de palas, espesor, material, etc) para que cumpla el cometido esperado, y
2- El trabajo del fundidor, que busca entre su colección de modelos para crear moldes aquel que mejor se ajusta a los parámetros que le indican, y con el desarrolla todo el proceso hasta obtener la pieza final.

Sin embargo, la labor del creador del modelo para el fundidor no es apenas conocida. Ello se debe a que los modelos no se deterioran con el uso y salvo para nuevas formas de hélices, no se necesitan nuevos modelos. El trabajo del modelista era tradicionalmente una mezcla de escultor, geómetra, matemático y ebanista.

En el presente TFG nos adentramos en esa actividad del modelista, y creamos

un molde “digital”, que finalmente convertimos en molde “físico” al imprimirlo
Este trabajo TFG es especialmente satisfactorio para cualquier ‘constructor’, ya que se va a llegar al resultado final de una hélice física impresa en 3D en PLA (un tipo de polímero usado en las máquinas de impresión actualmente).

2. Introducción a impresoras 3D.

Se puede decir que Las impresoras 3D son máquinas nacidas de las nuevas tecnologías. Por medio de un software de diseñador se crea un objeto o se copia la forma de un objeto real. A partir de ahí se puede reproducir un objeto físico materializando formas, volúmenes y dimensiones, permitiendo así hacer objetos exclusivos o que cumplan o satisfagan unas necesidades específicas para un usuario determinado. Producción a medida.

Estas impresoras trabajan por medio de una fuente de datos que generan distintos programas dando coordenadas en los tres ejes, los cuales van guiando el extrusor de la maquina por el cual sale el plástico fundido que se introduce por la parte superior, creando una líneas superficiales en los ejes X e Y, cuando las capas depositadas en estos dos ejes son finalizadas la impresora sube a una capa superior eje Z, en el cual vuelve a aportar material para crea un segundo nivel del material, se puede decir que la impresión se realiza por la deposición de capas sucesivas.

Las dimensiones de las maquinas dependen de muchos factores, pero se pueden modificar ya que este tipo de impresoras son de diseño abierto, (las licencias/patentes correspondientes son prácticamente no restrictivas) lo cual permite al usuario hacerla del tamaño que quiera. En el caso que nos ocupa, nuestra impresora dispone de una base de impresión de 20*20*20, lo cual permite también acometer productos mayores, aunque en ese caso será preciso unir varias partes-componentes, estas uniones se realizaran por medios de formas, las cuales encajaran unas con otras para obtener así una pieza final formada por 4 partes.

2.1. Historias de la impresión 3D

La impresión 3D comienza en el año 1984, donde Charles Hull inventa la estereolitografía (SLA), este método fue patentado y consistía en un haz de luz ultravioleta que focalizaba sobre la superficie de un líquido foto-polimérico. Ese líquido es una resina que cura o solidifica por medio del haz de luz ultravioleta. Estos rayos van dibujando la figura sobre la superficie de ese líquido, y va solidificando esta superficie.

Después de que se ha formado la primera capa superficial sólida, la plataforma que contienen la cubeta con el líquido donde se está imprimiendo la pieza en 3D cambia la posición de su base, haciendo que una capa de líquido se superponga a la última capa solidificada, y se reinicia el proceso de dibujado y solidificación. El objeto sólido se construye como superposición de rebanadas solidificadas. En la imagen1 se muestra un esquema del proceso

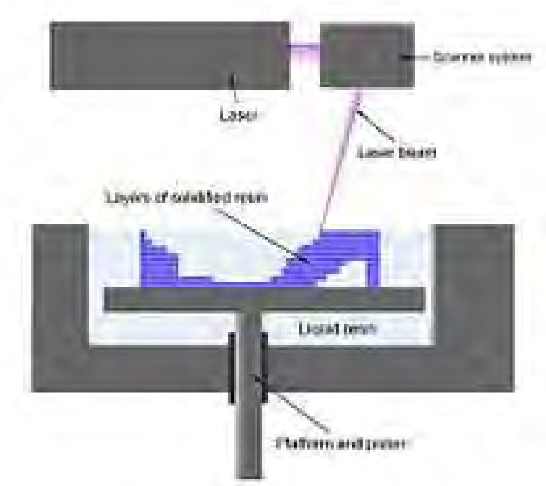

Imagen 1. Referencia [5]. Esquema de una sección vertical de una máquina de impresión por luz ultravioleta. Se aprecia la cubeta, la resina líquida, la plataforma móvil que va descendiendo, la resina solidificada que va conformando la pieza, y el cabezal proyector del rayo de luz focalizado en la superficie del líquido.

El segundo gran avance fue en el año 1993, es la impresión 3D por deposición de material o inyección de materia termoplástica. (Ver imagen 2). Fue desarrollado por El MIT, este método consisten en calentar un material hasta el punto de fusión. El material semilicuado es extruido a través de una boquilla, de manera continua, de modo que produce un filamento fino de material en estado semifluido, y lo va depositando sobre la superficie ya solidificada de las capas anteriores y por sucesivas capas de deposición se va generando la figura deseada.

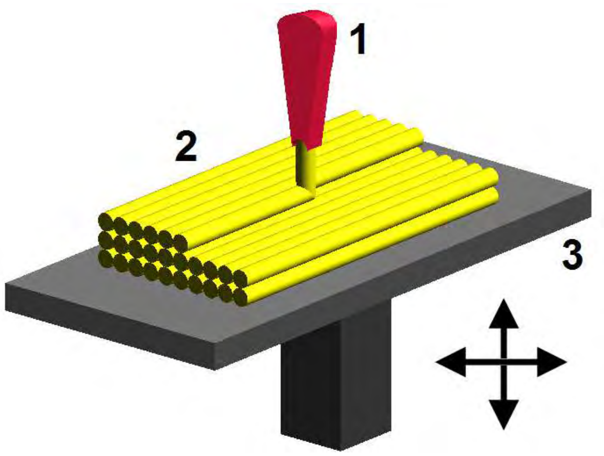

Imagen 2. Referencia [6], Funcionamiento de impresión por deposición de capa. El movimiento relativo entre la boquilla de extrusión 1 y la plataforma 3 hacen que el filamento 2 vaya quedando posicionado conformando la pieza.

El tercer gran avance fue en el año 1999 cuando la Universidad de Wake Forrest, usa la tecnología de impresión 3D para hacer implantes en humanos (imagen 3). Surgen así los primeros órganos modificados mediante implantes arteriales por objetos impresos en 3D y recubiertos por células del paciente.

Imagen 3. Referencia [7]. Resultado de impresión para implante.Sobre una reticula bio-compatible impresa en 3D, puede crecer tejido biológico

En el año 2000 se hace otro gran avance y se crea una impresora que funcionan por fusión selectiva por medio de un láser (SLM). (imagen4)

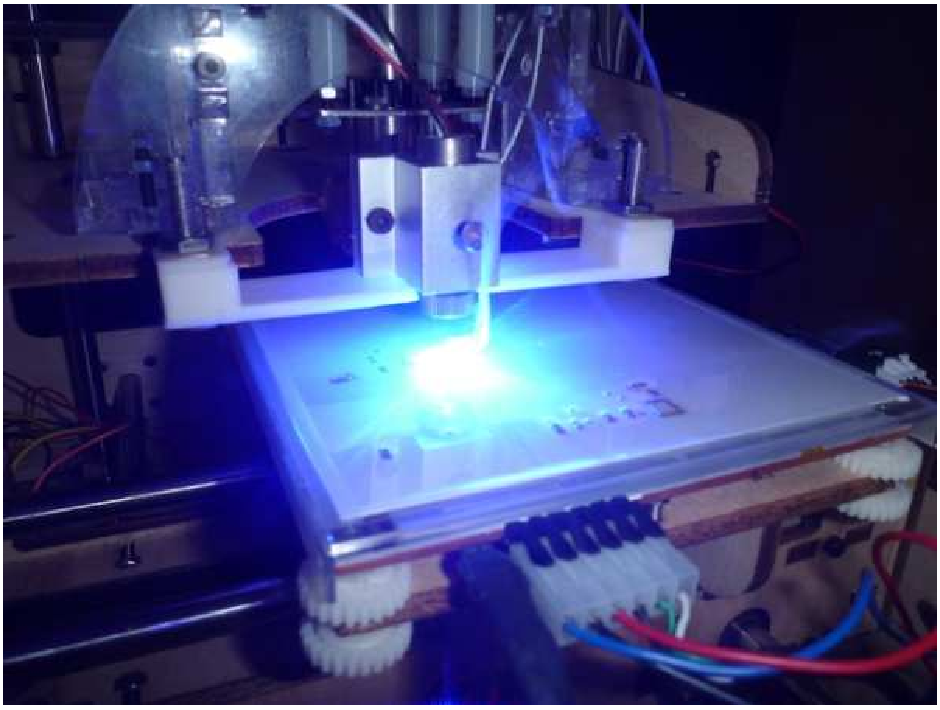

Imagen 4. Referencia [8]. Impresora por fusión selectiva. Similar a la resina curada por luz, pero en este caso el material es polvo en lugar de líquido

En el año 2006 se ofrece la primera impresora 3D de código abierto, (licencias y patentes liberadas) dejando así que cualquier persona pueda usar los códigos para poder hacer su propia impresora en casa.

En el año 2009 sale la primera impresora 3D comercial, en formato de KIT para montar en casa, basándose en el concepto de REPRAP.

3. Producción actual de hélices.

Las primeras hélices marinas se hacían completamente a mano gracias a personas capaces de plasmar en madera por medio del tallado, las formas y dimensiones que aportaba un ingeniero en planos (también conocidos como sabanas). El escultor o tallador de hélices invertía mucho tiempo en realizar un pre-molde en madera para generar la hélice.

En la actualidad las maquinas CNC han sustituido en muchos lugares a un tallista o escultor de hélices. Esas máquinas, son capaces de reproducir con precisión milimétricas los planos y formas creados por un ingeniero, ya que son capaces de desplazar su cabezal en todas las direcciones, siendo así muy versátiles para un tallado con precisión. (Imágenes 5, 6 y 7).

Imagen 5. Referencia [9]. Modelo o noyo de Pala de hélice realizada por CNC Está en fase de enmasillado y lijado. Después se le aplicará un acabado en pintura Se usará como plantilla para conformar el molde de arena de moldeo

Imagen 6 Referencia [9]. Máquina CNC realizando desbaste para crear un modelo, noyo o pre-molde de una pala de hélice. Se aprecia también el futuro núcleo de la hélice (paso fijo)

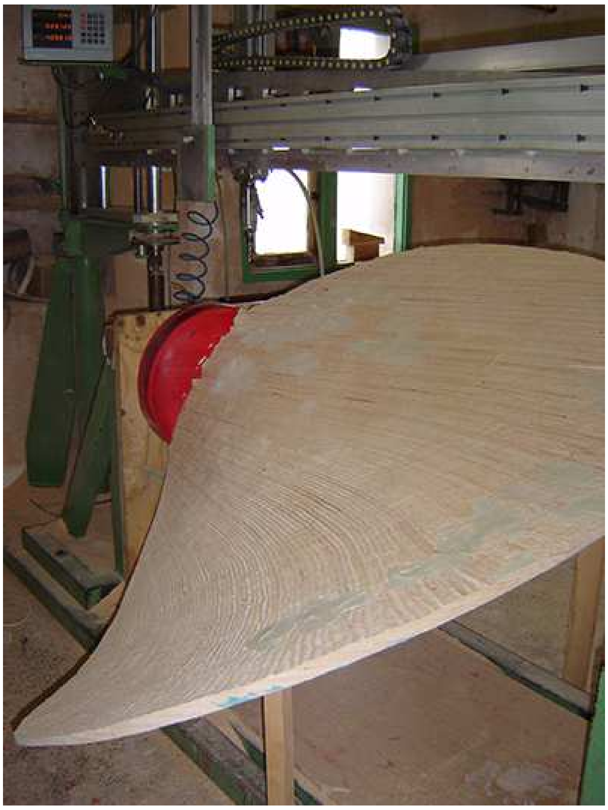

Imagen 7. Referencia [9]. CNC y pala de hélice en fase final de rectificado. Se aprecia por la forma de la raíz de la pala que es postiza o de paso variable.

Una vez se obtiene el pre-molde (o modelo) de una pala de la hélice, el fundidor puede hace un molde hembra con arena de moldeo. Reposicionando el modelo tantas veces como palas tenga la hélice, y recubriéndolo con arena que posteriormente se hace endurecer, se construye el molde para la colada. Su forma es como un ‘negativo de la hélice, Donde la hélice tendrá material, el molde tiene ‘hueco’. Ese molde hueco (hembra) conforma la pieza final cuando en su interior enfría y solidifica un caldo, aleación de materiales metálicos en distintas proporciones y homogéneos entre sí. Al realizar el vertido (imagen 8) generamos la hélice, la cual no tiene la calidad de acabado final ya que presentará un acabado superficial tosco, y también puede presentar pequeñas imperfecciones.

Imagen 8. Referencia [9]. Volcado de colada en molde de hélice. En este caso operación manual realizada por 2 operarios con indumentaria protectora. La hélice es de unos 130 cm de diámetro.

Una vez realizada la hélice y sacada del molde, se hacen diversas comprobaciones para asegurar que no existen grietas, poros o fisuras ni en el interior ni en el exterior. Para detectar los posibles poros superficiales se hace un ensayo de líquidos penetrantes. Para ello se usan dos espray, el primero se aplica en la hélice y se deja penetrar, se pasa un trapo y una vez eliminada la capa superficial, se da el siguiente, este reaccionara con el primero (que ha podido quedar en las zonas de poros), marcando las zonas de imperfecciones. Los lugares con imperfecciones se tendrán que reparar, para ello se retira parte del material con una dremel y se aportar material en la zona afectada.

Las hélices, una vez moldeadas con la aleación colada prevista, son sometidas a varios procesos como desmoldeo, eliminación de mazarotas y bebederos, , mecanizado del núcleo, desbastado, rectificado, afinado y pulido, para dejarlas en condiciones óptimas. (imágenes 9 y 10).

Imagen 9. Referencia [9]. Desbastado por fresado CNC de la hélice creada por colada. El soporte en el suelo es una plataforma móvil controlada por el CNC, como el brazo portaherramienta visible arriba a la derecha.

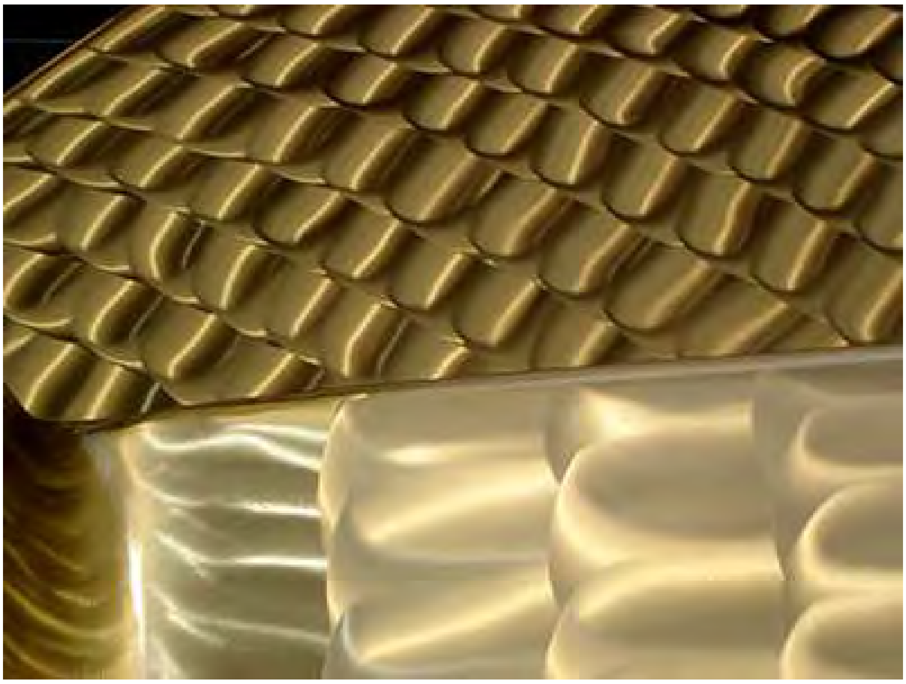

Imagen 10.Referencia [9]. Acabado final de hélice. Se aprecian las 'aguas' o 'escamas' visuales características de un pulido final con herramientas manuales. Esa apariencia es la evidencia de la aplicación de una herramienta de pequeña huella en posiciones sucesivas. La pequeña huella ha de ser compatible con la forma alabeada (no plana) de la superficie, y el operario debe tener la destreza debida para lograr la superfie prevista en el diseño.

En estas páginas web que se indican seguidamente podemos visualizar los procesos actuales que se llevan a cabo para generar una hélice.

http://www.propellerscorp.com/fabricacion-helices-barcos
http://www.casusopropellers.com/desarrollo-y-produccion

Las hélices una vez construidas, tendrán que pasar controles dimensionales validándolas para darles un certificado, este es realizado por empresas que certifican que sus medidas son correctas, también se ensaya una probeta del material del cual está hecha, es un ensayo de rotura.

4. Alternativas emergentes para la producción de hélices.

Las producciones de hélices actuales llevan una gran cantidad de procesos para llegar a una hélice funcional.

Aunque el material fundido que se vierte en el molde pueda ser bastante homogéneo, no ocurre lo mismo con el producto solidificado final. A medida que La colada de metales vertida en el molde, este tiende a calentarse, mientras que aquel metal tiende a enfriarse y hacerse más viscoso. Todo el proceso de llenado del molde sigue unas leyes complejas de dinámica de fluidos, con gran intercambio de calor, y material en la frontera de cambio de estado, liquido, sólido y gas-vapor. El material solidificado no presenta una estructura homogénea en todo su conjunto. El material superficial se enfría a distinta velocidad que el núcleo o zonas más profundas, produciendo así material de distintas cualidades.

Se puede decir que la zona superficial al enfriarse más rápida tendrá un comportamiento más frágil, pero una gran dureza superficial y la zonas internas un comportamiento más dúctil ya que se enfría más lentamente.

Una de las nuevas tecnologías para la realización de piezas puede ser la aportación de material por capas o laminación. Eso empezó a realizarse con plásticos, pero hoy en día las impresoras por capa o impresoras 3D son capaces de imprimir o hacer piezas en materiales muy variados: metálicos, cerámicos, plásticos, ceras, acrílicos, entre otros.

Hay empresas que en este momento se encuentran haciendo impresiones en metal por medio de maquinaria de este tipo, pese a que actualmente es muy costosa.

En la siguiente dirección url se encuentra una web donde se comentan estas experiencias actuales, http://imprimalia3d.com/noticias/2016/11/08/008196/preparan-una-impresora-3d-metal-bajo-coste-mediante-soldadura-mig .

5. Eleccion del metodo para la digitalizacion de la helice.

Queríamos materializar una hélice que fuese representativa. Tenemos libertad para elegir, y nos hemos decantado por un tipo común, muy reconocible. Está creada a partir de la serie sistemática B de Wageningen, también conocida como la serie de Troost, quien fue uno de sus desarrolladores
Esta serie de hélices se caracteriza por dos cualidades fundamentales:

A- Su comportamiento en cuanto a rendimiento y cavitación es muy bueno

B- Su definición geométrica ha sido publicada y divulgada, por lo que tal información es gratuita y de dominio público.

Este último motivo es especialmente poderoso para nuestra elección, ya que subraya el carácter académico y auto-pedagógico de este trabajo,

La información disponible sobre esta serie sistemática es muy completa., Además de las tablas y graficas que muestran las curvas KT, KQ y rendimiento de propulsión aislado también se ha publicado la definición matemática de la geometría de las palas y de cada sección.

En el artículo “a Further mathematical and computer analysis on the definition of Wageningen B series” de Peter Van Oossanen, que se incluye en el **Anexo 1 y Referencia [1]**, se da información suficiente sobre ello.

La información se da en forma de funciones que definen el paso, el espesor de la pala, el ancho de la pala o arco, la posición del borde de ataque, la posición del punto de mayor espesor de la sección, etc. En general la variable independiente en esas leyes es la distancia radial de la estación, definida por un parámetro adimensional, r/R, siendo R el radio de la hélice, y r el radio de la estación particular.

Sin embargo muchos de los datos que allí aparecen son tablas de interpolación, que no aportan la completitud que necesitamos para el trabajo.

La simple interpolación lineal, o incluso parabólica, sobre los puntos de las tablas originales publicadas por los divulgadores de la serie B no garantizaría el perfecto alisado de las superficies.

Por ello, se realizó el “alisado” los datos de las tablas con unas funciones matemáticas de ajuste suave (lo cual mejora la pura interpolación). Esas funciones matemáticas tendrán que ser de continuidad C2 (continuidad de la segunda derivada de la curva), para asegurar la suavidad de curvatura de la superficie.
Para materializar el cálculo hemos usado una hoja tipo Excel, de la cual existen versiones tipo Opensource, como es libre Office, compatible con Excel.
Respecto a las funciones spline de suavizado, hemos usado un addon para Excel, que añade unas funciones de interpolación tipo spline.

XonGrid Interpolation Add-in
http://xongrid.sourceforge.net/ y dentro de ella se admite un alisado o fitting.

Aparte de esas funciones matemáticas podremos obtener una malla de puntos tan densa como queramos, que nos dará la precisión elevada requerida para nuestro propósito aunque la forma final a construir siempre estará definida por secciones discretas.

Los datos que se han tomado para la hélice son los que se pueden encontrar en el **Anexo 1 y Referencia [1] ; y Anexo 3 y Referencia [3]**, donde se encuentran las tablas de la publicación.

También dentro de este **Anexo 1 y Referencia [1],** se puede encontrar las definiciones de los parámetros de la hélice, los cuales son importantes para poder entender la geometría de la misma.

En el **Anexo 2 y Referencia [2],** se habla de los parámetros característicos de la hélice y sobre el área extendida de la hélice, como se representa en los planos.

La hélice que hemos decidido construir tendrá los siguientes parámetros característicos:

Diámetro	D, 1200 mm	
Numero de palas,	Z	3
Relación Paso/Diámetro	p/D	0.9
Relación de área disco	Ae/Ao	0.55
Rake	15º	
Skew	ninguno	

Esos bastan para concretar una hélice de la serie B.

La elección ha sido arbitraria, con la única intención de obtener una geometría usual, sencilla, de diseño conservador, como las muchas que se pueden ver en barcos relativamente pequeños, pesqueros o de recreo, Las hélice de barcos con mayor ‘carga’ de empuje suelen tener menos paso y más Ae/Ao, así como más palas.

En la imagen 11 mostramos la geometría de la pala. Se aprecian la citadas leyes de cuerdas (c), posición del borde de ataque (le, leading edge), ídem de salida (te, trailing edge), ídem del punto de máximo espesor en cada sección (mt), y espesor máximo en cada sección (t)

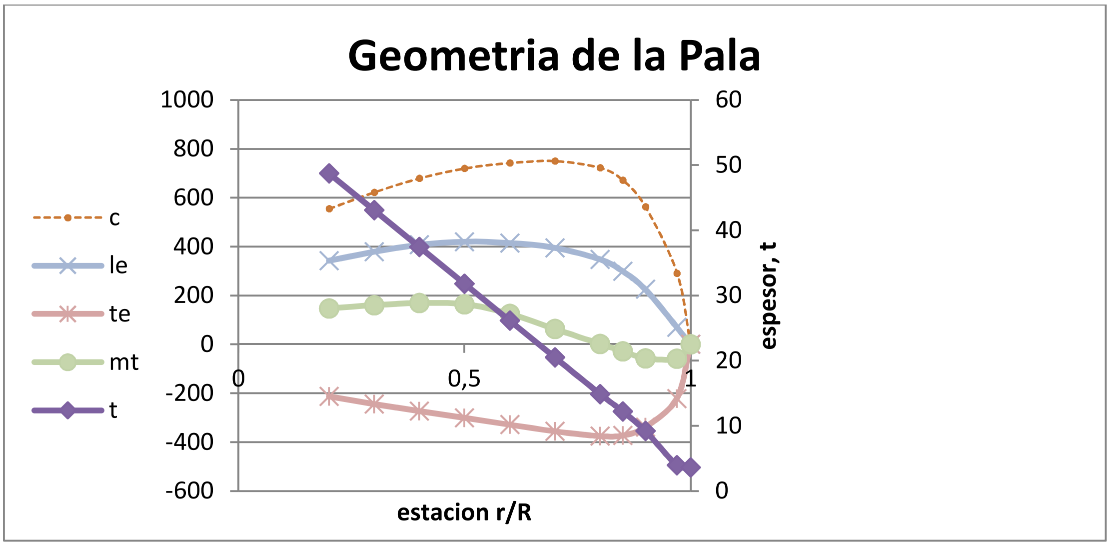

Imagen 11. Geometría de la pala de hélice. Leyes de variación de los parámetros más representativos de la secciones trasnversales de la pala, en función de su posición radial.

La Imagen 12 nos muestra uno de los perfiles.

Hay que advertir que no tiene la forma del perfil real. Es lo que se llama, vista extendida. No se tiene en cuenta el giro correspondiente a su paso, ni el rake y skew que corresponda a su estación r/R.

En la imagen 12 se ve un corte de la hélice a un radio determinado r/R = 0.2. Es el desarrollo sobre un plano del corte (intersección) de la pala con un cilindro de radio r.

Esa es la forma usual en la que se representan en los planos las secciones de las palas.

Son representaciones adecuadas para los estudiosos de la hidrodinámica, pero no sirven para los constructores. Antes de que puedan ser utilizadas para construir hay que hacerles algunas manipulaciones relacionadas con el paso, el enrollado (wrapped), y la inclinación de la generatriz de la pala (rake).

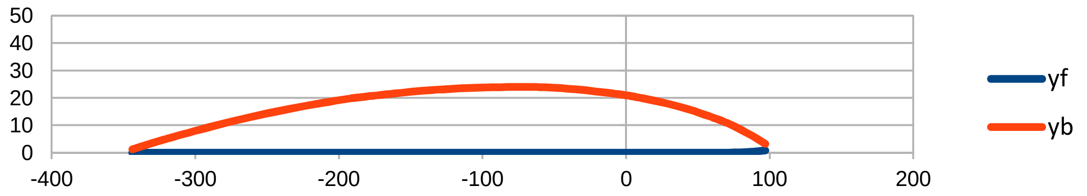

Imagen 12. Perfil de una sección de hélice. Es una representación extendida y 'desenrrollada', en plano y sin paso, de una sección cilíndrica de la pala. El borde de ataque sería el de la derecha, la cara 'de presión' la inferior, y la de 'succión' la superior. La coordenada x=0 corresponde a la línea de referencia de la pala, generatriz.

Seguidamente mostramos el aspecto más realista, desde el punto de vista de representación en sistema diédrico, que tendrían algunas secciones tal como se calculan a partir de la formulación de la serie sistemática. La representación es en planta y alzado (sistema diédrico).

En la planta (imagen 13) se representa solo secciones de una pala, cuya línea de referencia (perpendicular al eje de la hélice) esté en vertical. Además solo se han representado unas pocas secciones, próximas a la raíz, y a media pala, para no complicar en exceso una representación a la que no estamos acostumbrados.

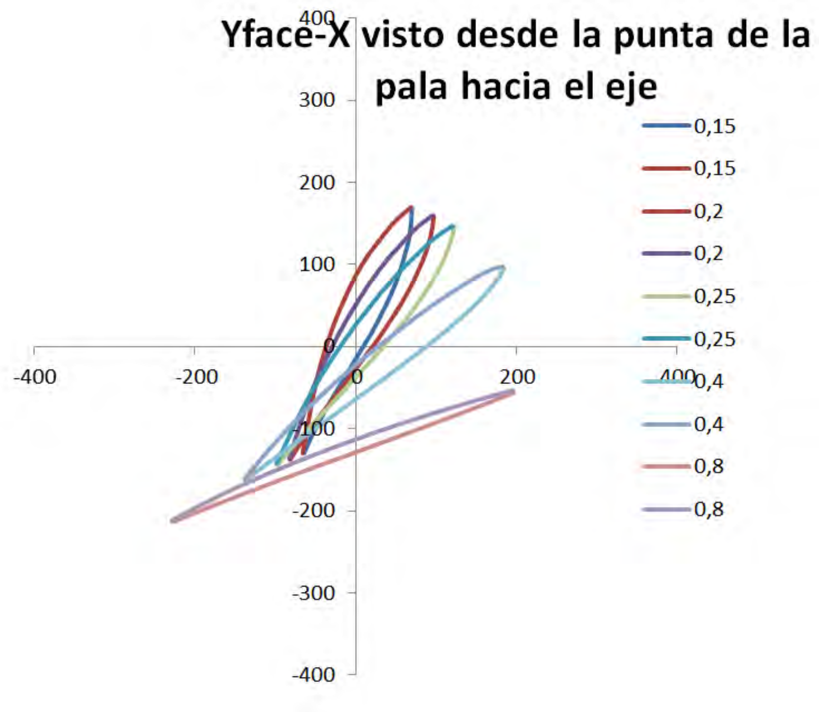

Imagen 13. Yface-X Visto desde la punta de la pala hacia el eje. Varias secciones de pala, correspondientes a las estaciones 0.15, 0.20,..0.80. En cada sección se diferencia la cara de succión y de presión de cada perfil. Las secciones más próximas a la punta de la pala tienen perfiles en forma de arco de circunferencia.

La imagen 14 es más fácil de interpretar, y corresponde a un alzado de una pala, donde los arcos de circunferencia con centro en el origen de coordenadas (eje de la hélice) son las secciones cilíndricas que se han representado.

También se aprecia la línea imaginaria que uniría los puntos de mayor espesor de cada estación.

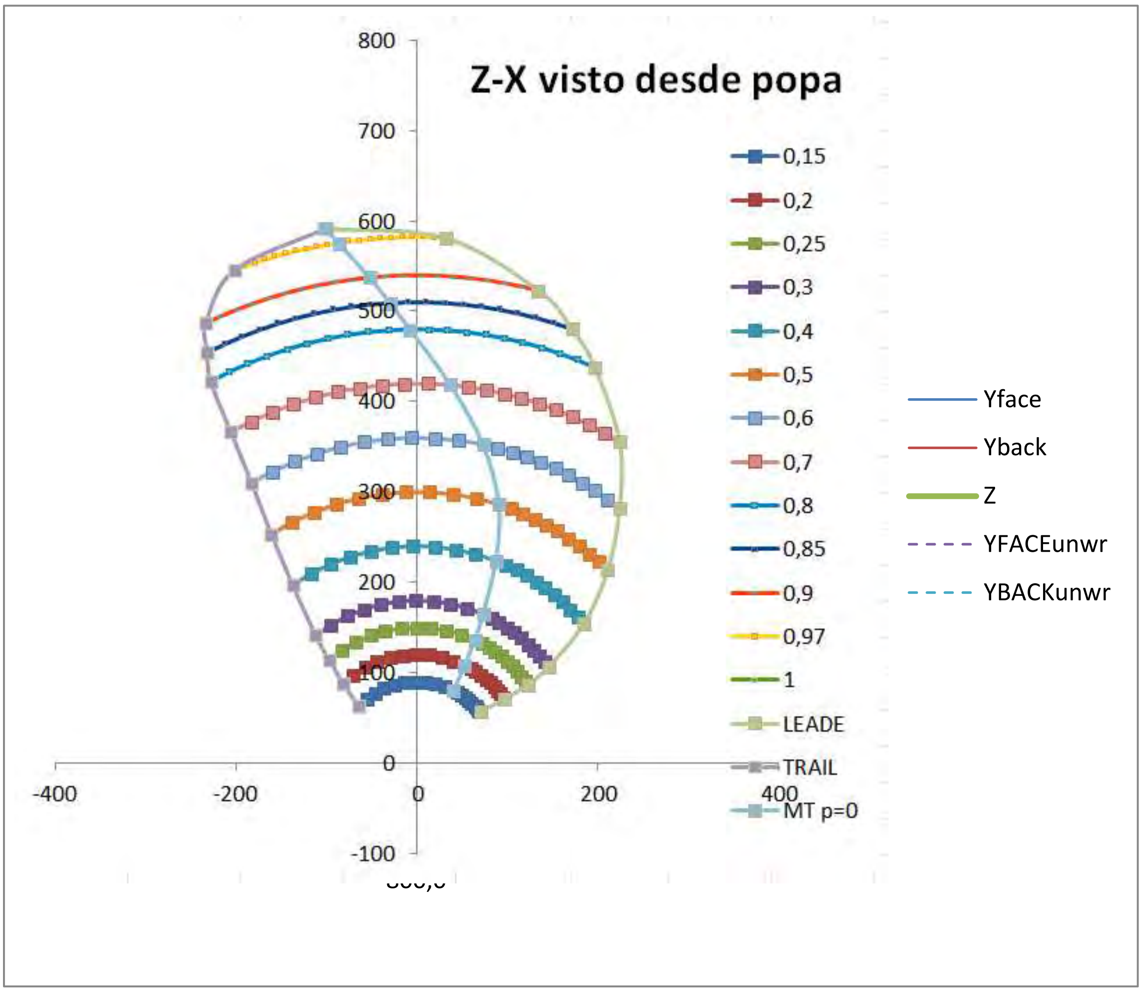

Imagen 14. Plano frontal de una hélice. En este caso la forma se corresponde con el perfil real aparente de la pala. El borde de ataque está a la derecha. Las representaciones usuales son vistas desde la popa. En este caso hélice dextrógira.

Ahora bien toca el paso más importante, el programa de diseño si puede dibujar estos perfiles curvos, permitiendo hacer superficies, llegando así a desarrollar las caras Face y Back de la hélice.

Por medio de la hoja de cálculo de Excel, podremos obtener las coordenadas cartesianas (x,y,z) de los puntos que definen las diversas secciones de la pala.

Finalmente tendremos 2 caras en cada pala, la de presión (face) y la de succión (back)

6. Definición de las superficies en el CAD. Otras opciones para introducir las superficies.

Las tablas de coordenadas xyz de los puntos calculados, serán exportadas como un archivo de texto e importadas en el programa de CAD. Una vez hecho, crearemos en el CAD dos superficies (back y face) que pasen por los puntos.

Queda así conformada una pieza delimitada por esas superficies. Hacemos algunos retoques para adaptar a la pala una base de unión al núcleo, y tendremos la pala finalmente concluida.

Como es una prueba de concepto, haremos que la pala sea postiza a un núcleo macizo.

En las imágenes 15 y 16, se muestra la pala conformada en el CAD.

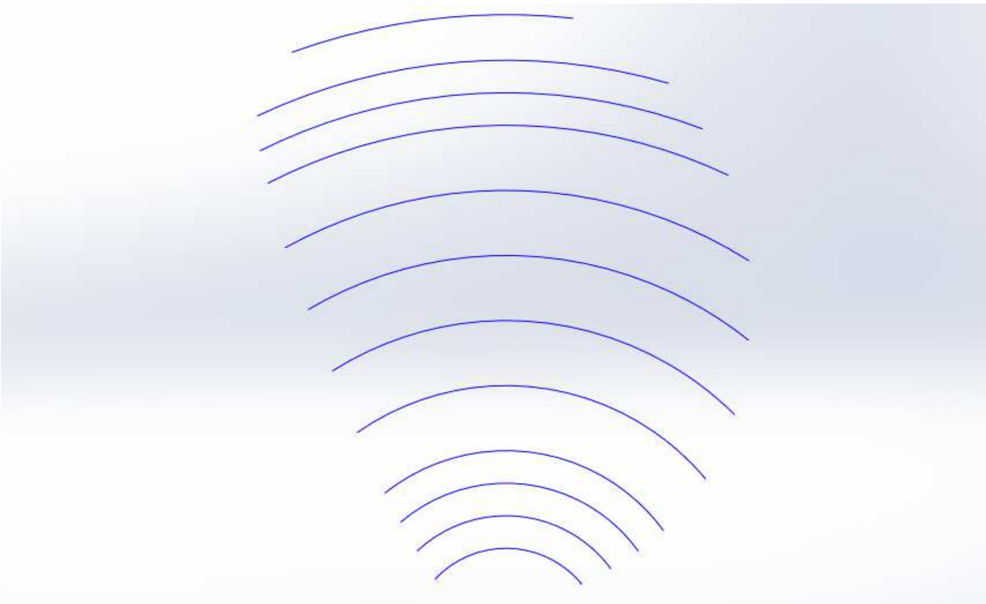

Imagen 15. Frontal de pala de hélice del archivo CAD. Solo se aprecian un conjunto de perfiles (vistos 'de canto') correspondientes a unas determinadas estaciones.

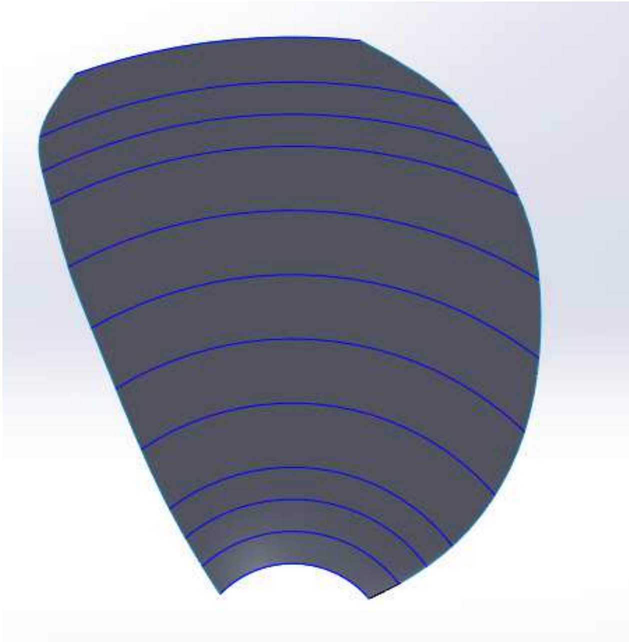

Imagen 16. Frontal de hélice con superficies visto desde CAD. El programa permite visualizar una superficie que pasa por los perfiles.

Exportación del CAD: La salida del CAD que necesitamos para la siguiente fase es un fichero en formato STL. Normalmente es una de las opciones de formato de exportación que brindan los CAD más usuales.

el fichero STL contiene toda la geometría necesaria para poder representar el modelo digital.

7. Programas de impresión.

En el **Anexo 4** se encuentra el manual del programa de impresión (CURA) utilizado para la realización de este trabajo. Allí se describe el funcionamiento del programa y la instalación del mismo.

en este caso vamos a usar un programa libre llamado Cura. Los programas de impresión aceptan el formato STL, , y el programa calcula un ‘rebanado’ a partir del cual produce un conjunto de instrucciones en un código que pueda ser entendido por una máquina CNC como es la impresora 3D. El programa de rebanado nos permite exportar ese código (en formato gcode) en forma de fichero. El software de gestión de la impresora sabrá interpretarlo para imprimir la forma real. Las imágenes 17 y 18 muestan algunos momentos de la operación.

Las características a tener en cuenta en la impresión son los siguientes.

<u>Rebanado</u>: es el espesor de cada una de las capas que van a conformar la pieza impresa. Cuanto más delgada, mayor será la calidad o suavidad de las superficie acabada.

No es un valor totalmente libre, ya que debe estar en cierta relación con el diámetro de la boquilla del extrusor de la impresora.

En el caso de esta impresión de usa boquilla de 0.35 mm, y el espaciado entre capas será de 0.2 mm. Esta calidad sería una calidad media, pero se pretende que la impresión no dure demasiado tiempo. A menor diámetro de boquilla y menor espesor de capa, mayor calidad, pero también mayor tiempo necesario para la impresión.

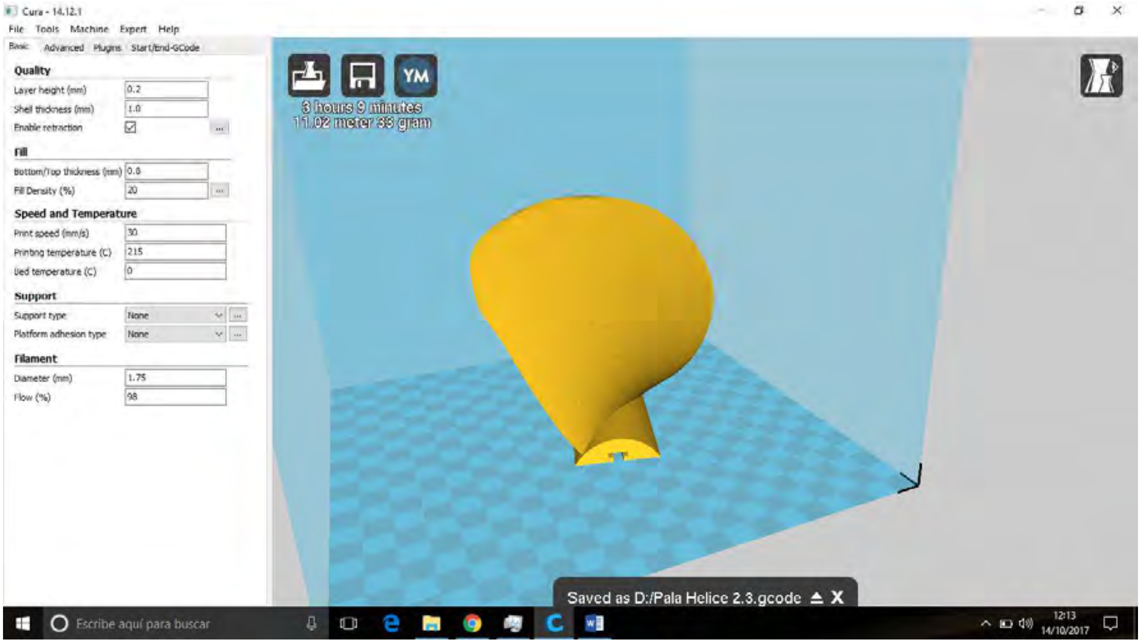

Imagen 17. Copia de pantalla del programa de impresión CURA. Aspecto que tendrá la pieza impresa, y algunos parámetros de la configuración de esa impresión.

<u>Relleno</u>: se mide como % o densidad de volumen. (Volumen de filamento/volumen de la pieza). Este parámetro es uno de los más importantes en relación con la resistencia de la pieza, y con el tiempo necesario para imprimirla.

En este caso imprimiremos a un 20% de densidad. La densidad se refiere al grado de relleno de la parte interna de la pieza. Lo que se pretende es formar una retícula espacial de líneas superpuesta que dan rigidez a la pieza pero la mantienen aligerada en su interior. Desde el exterior no se aprecia la influencia del grado de relleno, ya que no afecta a sus capas superficiales, ni a la zona de superficie exterior de cada capa.

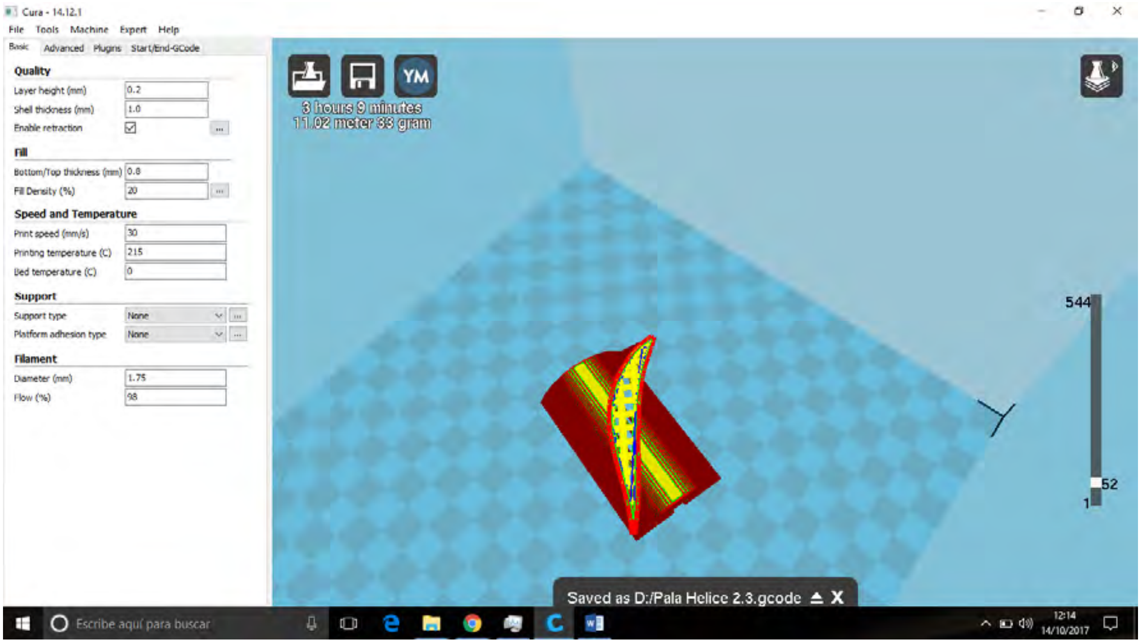

Imagen 18. En la pantalla del programa se aprecia un estado intermedio de la impresión. Ya se ha concluido la parte de la raíz de la pala, y va por la capa 52 de 544. Se puede ver que el interior de la pieza, en amarillo tiene un reticulado con 'huecos', distinto del cordón continuo que conforma el contorno de la pala. El corte es una sección plana, horizontal, 'rara'. No es la representación usual en planos de hélices.. La previsión de la máquina es realizar una pala completa en 3 h y 9 minutos

En nuestro caso vamos a trabajar un plástico conocido como PLA (poly lactic Acid), el cual no necesita una cama caliente para impresión, a diferencia del ABS (Acrilo Butil Styrene), el otro producto alternativo más común para material de impresión. Ambos son termoplásticos, cuyo punto de fusión para extruir está en unos 200ºC.. Sin embargo el PLA tiene un punto de plastificación de unos 60º. Pese a todo, a temperatura ambiente de 25º, es un material robusto.

Nuestra impresora es capaz de hacer una hélice en plástico pero, como se muestran en la imagen 19, y en la referencia [11] , ya existen máquinas capaces de imprimir en metal hélices reales.

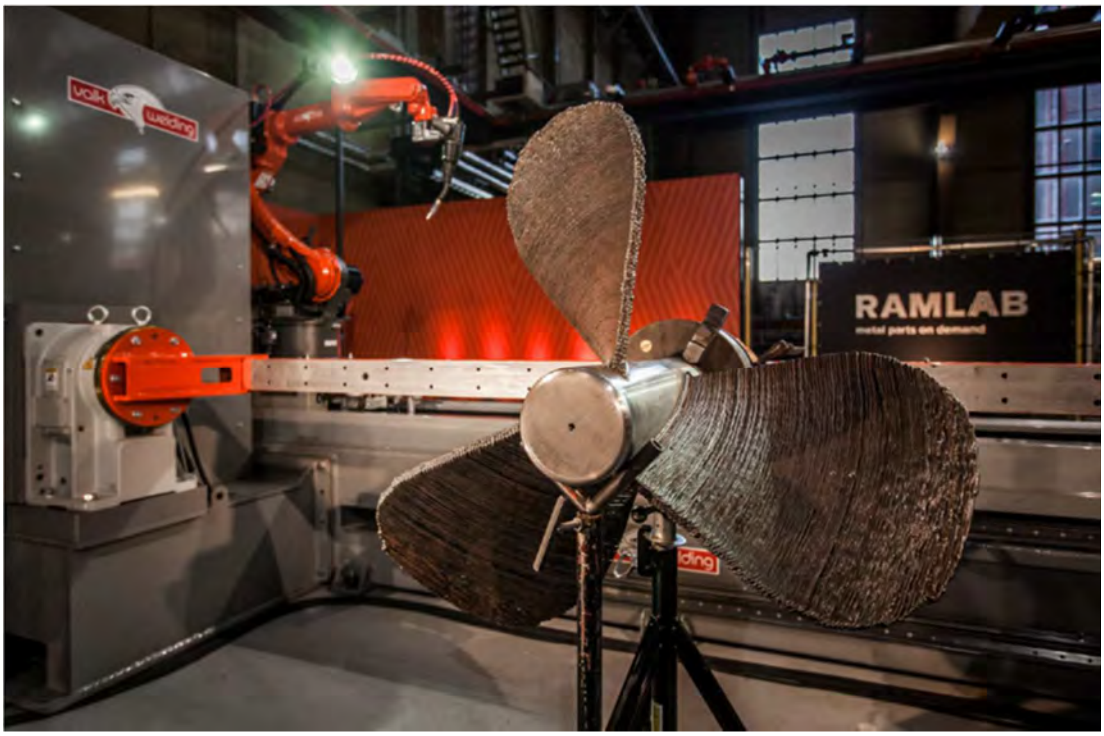

Imagen 19 Referencia [11]. Hélice construida con una impresora 3D en material metálico. Está destinada a un remolcador, y ha sido clasificada por el Bureau Veritas (año 2017)

8. Resultado de la impresión.

El objetivo final era materializar nuestra idea, fabricar hélices con tecnología de impresión 3D, y lo hemos logrado.

En las siguientes imágenes (20 a 31) se muestran diversos momentos de la impresión de varias hélices

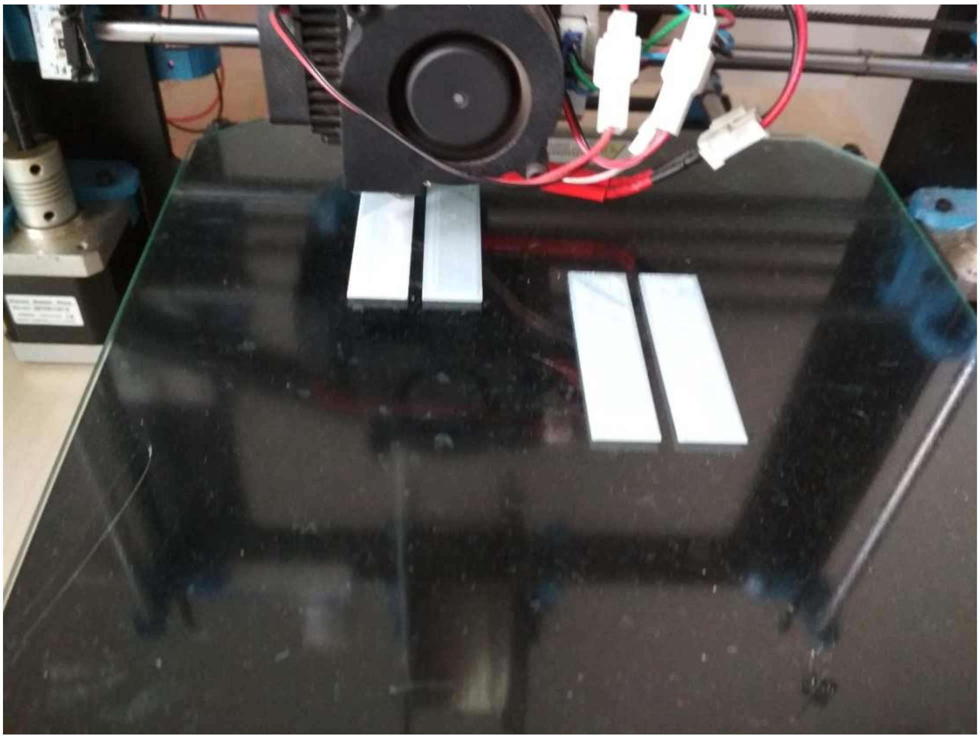

Imagen 20. El inicio. Se muestra las primeras capas de deposición de material de dos palas, realizadas simultáneamente. No se pasa a una capa superior hasta no haber terminado todo el trabajo (en todas las piezas) en la capa en curso.

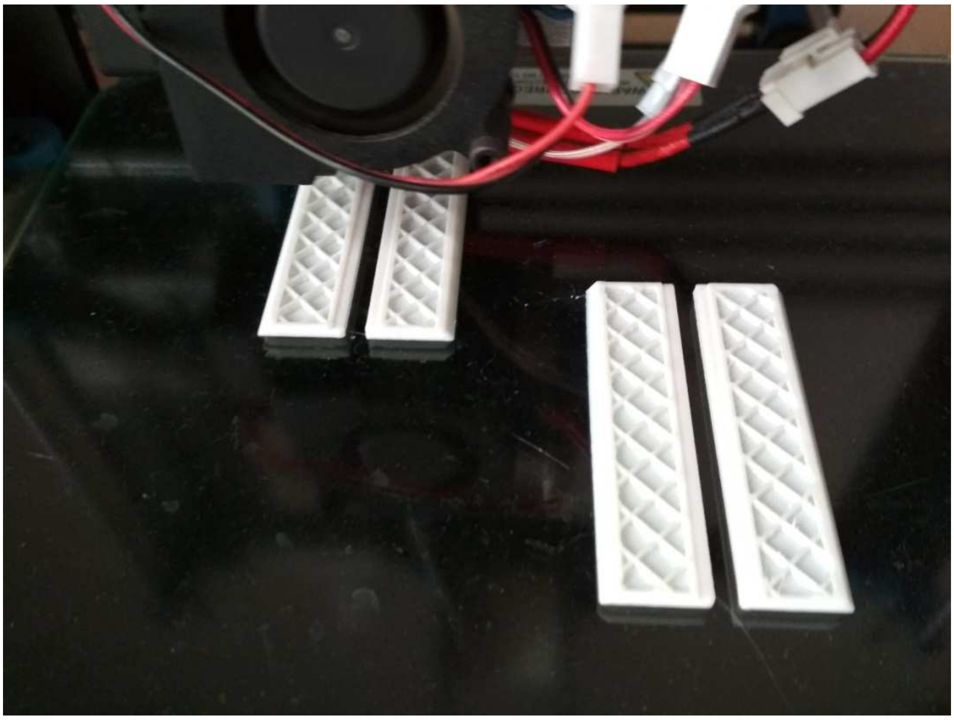

Imagen 21. La impresión progresa hacia arriba, hacia la punta de pala de la hélice. El interior de la pieza se conforma con un mallado especial, para ahorro de material y peso, tiempo y dinero.

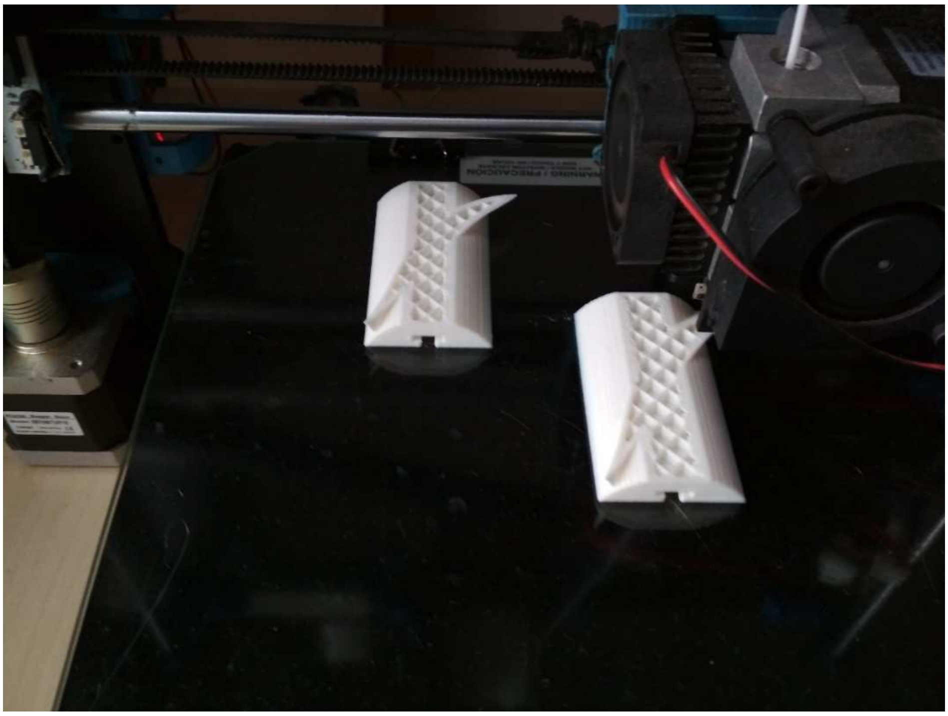

Imagen 22. Se empieza a ver la forma de las secciones de la raíz de la pala Las dos palas progresan al unísono, aunque el cabezal de extrusión trabaja alternativamente en una y otra manteniendo el mismo nivel de capa horizontal.

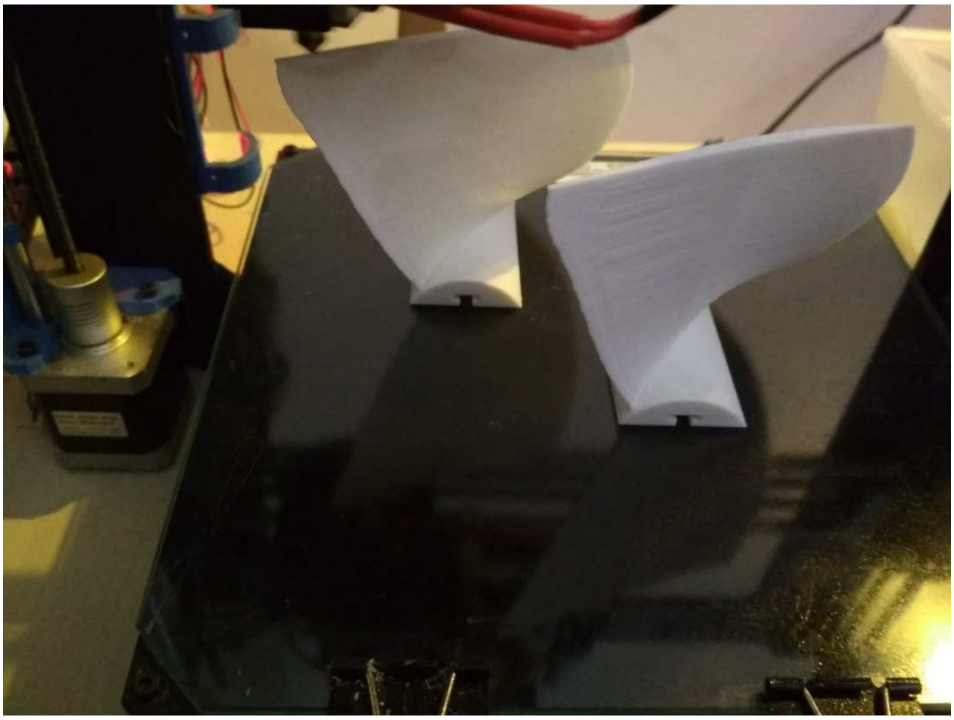

Imagen 23. Estamos casi al final de la impresión de dos palas

Imagen 24. Una pala finalizada.

Imagen 25. Vista desde otra posición. La geometría de la pala es una forma de notable complejidad para ser construida por medios mecánicos.

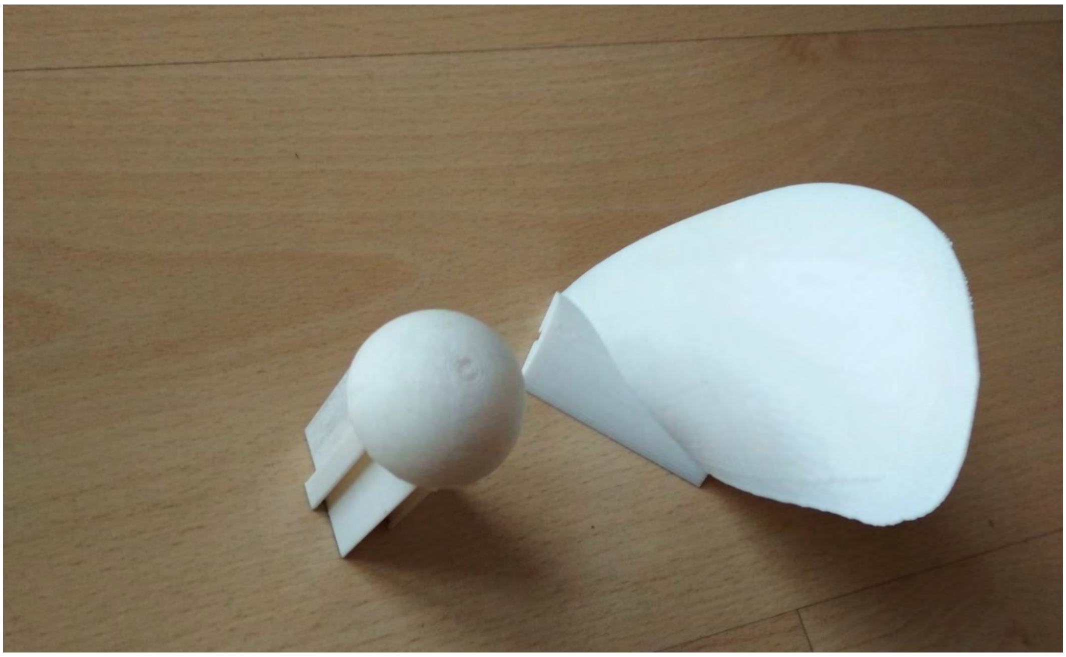

Imagen 26. Pala de hélice y un núcleo especialmente concebido para este ejemplo. Facilita la unión entre palas sin necesidad de otros elementos mecánicos (tornillos, etc..).

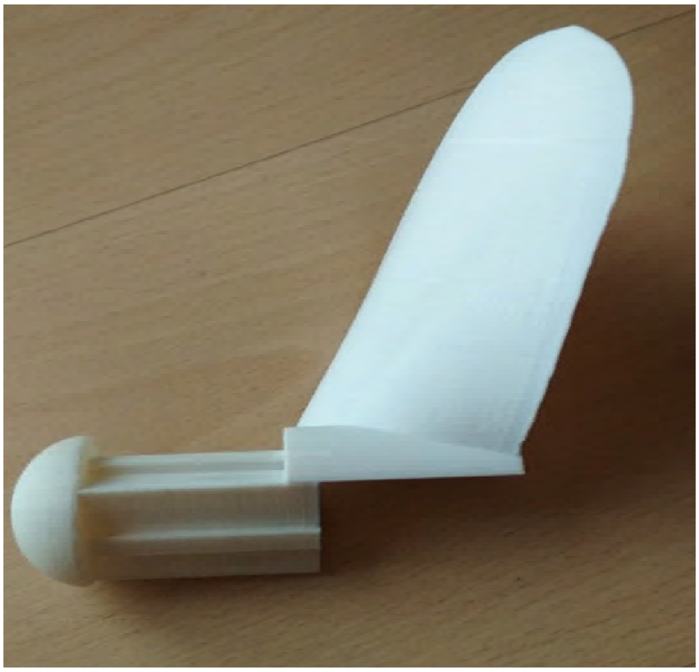

Imagen 27. La forma de unión es por una T por la cual se encaja las palas con el núcleo.

Imagen 28. Otra vista de unión entre una pala de hélice y el núcleo.

Imagen 29. Otra hélice completa, vista desde popa.

Imagen 30. Vista desde proa y bordes de ataque.

Imagen 31. Vista lateral de hélice con encaje en núcleo con tres palas.

9. Coste económico para la realización de una hélice.

No vamos a hacer un presupuesto formal al uso de un servicio industrial, sino que vamos a dar algunos datos para hacernos idea de los costes relacionados en este trabajo.

9.1. Coste de los materiales y maquinaria.

Para realizar la hélice hace falta una impresora, en este caso el coste de la impresora esta sobre unos 600€. Se trata de un producto de gama media-baja, para uso doméstico por modelistas y aficionados.

El material de extrusión, filamento de impresión, utilizado es plástico PLA, que se comercializa en rollos de 1 kg, y su coste es de unos 20€ / kilo. Esta pieza (una pala) ha necesitado 33 gr. Para 4 piezas (la hélice completa, 3 palas + 1 núcleo) serían unos 150 g de material (con una densidad de relleno del 20%), esto supone un coste de 3€.

El coste económico de la energía eléctrica consumida dependerá de las horas de impresión y el consumo. La impresora tiene una fuente de alimentación de unos 200 watios, una pieza tarda unas 3 h, el total de piezas a imprimir es 4, tardando unas 12 h de impresión. Puede asumirse un coste de energía de 1€.

Amortización de maquinaria, mantenimiento y varios, se puede agregar 1€ más por pieza, ya que en ese coste se agrega también la laca necesaria para fijar las piezas, aceite para el engrase de la máquina, entre otras cosas. Eso hace un valor de unos 4 € más de coste económico.

Se puede hablar que el coste económico material de producir estas 4 piezas, la hélice completa (3 palas + 1 núcleo) es de 8€.

9.2. Coste económico por diseño.

Se puede decir que un operador de programas de diseño asistido por ordenador (CAD) puede tardar en introducir los parámetros y realizar la pieza entre 2h y 16h. Este tiempo varia tanto porque depende mucho dela experiencia del operador, y de la calidad de la fuente de datos, ya que datos erróneos pueden causar mucho trabajo de corrección..

Si valoramos a unos 20€/h, el trabajo de esta persona al realizar el diseño supone un coste entre 40€ y 320€. Este es el coste económico más importante, y depende mucho de la cualificación del operador, y de la fuente de datos. Por concretar una cifra digamos, en nuestro caso, 100 €.

9.3. Desarrollo de las tablas por medio de una serie sistemática.

La preparación de una hoja de cálculo para generar una nube de puntos de la geometría de la hélice podríamos estimarla en unas 40 horas de una persona bien cualificada en esa materia. Igualmente el coste horario también es muy relativo, dependiendo de la disponibilidad, cualificación, etc. Supongamos 30 €/h. Resultaría unos 1200 €.

Ese coste estaría clasificado conceptualmente del mismo modo que la impresora 3D. Son herramientas, cuyo coste es necesario como inversión, pero que se manifiesta como amortización en cada una de las piezas que se producen con ella.

De tal manera, que una vez disponible la herramienta, el coste de obtener los datos para una hélice concreta podrían cifrarse en un tiempo de 1 h, y un coste de 40 € (20 €/h +20 €/hélice = 40 €)

9.4. Conclusión del coste económico.

Por todo lo dicho, podemos cifrar un coste por hélice ‘original’, a la unidad, de

8 + 40 + 100 = 150 € aprox.

No obstante, aumentando la cantidad de unidades producidas y mejorando la productividad de los operadores, el coste de una hélice como la descrita podría estar en unos 15 €,

El precio final de comercialización quedaría muy condicionado por cuestiones como oportunidad, exclusividad, implantación, publicidad, etc. Admitiendo márgenes de beneficio muy grandes, según diversos segmentos de mercado.

De cualquier modo que se cuantifique el coste de la producción de una hélice por un sistema de impresión 3D, es claro que el peso del factor humano en el coste se reduce, en pro de un aumento del peso del factor tecnológico.
La experiencia nos va demostrando que algunos oficios humanos han cambiado mucho, y ciertos trabajos de tipo artesanal clásico son actualmente ‘impagables’. Es muy posible que la fabricación de hélices tenga una trayectoria acelerada en la dirección de las tecnologías modernas.

10. Conclusiones.

Se puede decir que la fabricación aditiva aplicada a las hélices marinas es un campo nuevo, incipiente, pero en el cual ya hay actores industriales punteros trabajando.

Las nuevas tecnologías que se están implementando, como las máquinas CNC para realizar trabajos de pulido y acabado final de hélices (logran el alisado y afinado de las superficies, por medio mecánico y programado, con el conociendo de la geometría de la hélice), están sustituyendo a personal especializado en la industria naval, mejorando el rendimiento productivo y la calidad final. A la vez, esta nueva maquinaria también están abriendo nuevos campos de trabajo, para personal especializado no solo en su mantenimiento y manejo si no en el campo del diseño y modelización.

La implementación de nuevas tecnologías está logrando grandes avances en el desarrollo de hélices. Suponen una disminución de costes para investigación y poder producir un mayor número de prototipos con un coste económico más bajo. Este nuevo sistema también permite probar nuevos diseños de hélices a escala real en buque y comprobar la eficiencia de las mismas.

Este trabajo fue importante, a nivel personal, para satisfacer las inquietudes en relación a la impresión 3D. Así se ha conseguido relacionar un hobby particular con las materias impartidas en la universidad. En todo caso, ha sido una experiencia gratificante, en la que he ampliado conocimientos.

11. Bibliografia.

11.1. Libros

[1] M.W:e Oosurveld and P. Van Oossanen. July 1975. Farther Compuert Analysis On Wageninghe. Rotterdam Holland.

[2] Mark F. Nittel. 3 July 1989. Marine technology Vol 26, No. 3, 202-209.

[3] John Carlton. July 2012. Marine Propellers And Propulsion. Editorial Butterworth-Heinemann

[4] Resistance & Propulsion (I) Mar 2010, Propeller geometry & Basic Definitions. Schol of Marine Science and Technology.

11.2. Paginas Web

[5] Ultimaker. **https://ultimaker.com/en/products/ultimaker-cura**: [Consultado en Agosto 2017]

[6] Wikipidia. **https://es.wikipedia.org/wiki/Estereolitograf%C3%ADa: [Consultada en Agosto 2017]**

[7] Wikipidia. https://es.wikipedia.org/wiki/Modelado_por_deposici%C3%B3n_fundida [Consultada en Agosto 2017]

[8] BBC. **http://www.bbc.com/mundo/noticias/2016/03/160315_atala_impresora_organos_am [Consultada en Agosto 2017]**

[9] Borjaroca Wordpress. **https://borjaroca.files.wordpress.com/2014/12/impresora-laser-3d.jpg [Consultada en Agosto 2017]**

[10] Casusopropellers. http://www.casusopropellers.com/ desarrollo-y-produccion [Consultada en Agosto 2017]

[11] Port Of Rotterdam https://www.portofrotterdam.com/en/news-and-press-releases/ramlab-prints-first-ships-propeller [Consultada en Agosto 2017]

12. Anexos

Anexo 1 Farther compuert analysis on wageninghe. M.W.e. OOSURVELD and P. VAN OOSSANEN

FURTHER COMPUTER-ANALYZED DATA OF THE WAGENINGEN B-SCREW SERIES

by

M.W.C. OOSTERVELD and P. VAN OOSSANEN

Publication No. 479 of the N.S.M.B.

Reprinted from

INTERNATIONAL SHIPBUILDING PROGRESS
SHIPBUILDING AND MARINE ENGINEERING MONTHLY
ROTTERDAM - HOLLAND

Vol. 22 - No. 251 - July 1975

FURTHER COMPUTER-ANALYZED DATA OF THE WAGENINGEN B-SCREW SERIES

by

M.W.C. OOSTERVELD and P. VAN OOSSANEN *)

Summary

In this paper the open-water characteristics of the Wageningen B-series propellers are given in polynomials for use in preliminary ship design studies by means of a computer. These polynomials were obtained with the aid of a multiple regression analysis of the original open-water test data of the 120 propeller models comprising the B-series. All test data was corrected for Reynolds effects by means of an 'equivalent profile' method developed by Lerbs. For this Reynolds number effect additional polynomials are given. Criteria are included to facilitate the choice of expanded blade area and blade thickness. Finally, a number of new type of diagrams are given with which the optimum diameter and optimum RPM can easily be determined.

1. Introduction

In preliminary ship design studies in which the ship size, speed, principal dimensions and proportions are to be determined, the application of computers is rapidly increasing. Here, the hydrodynamic aspects, including resistance data, wake and thrust deduction data and the propeller characteristics are of importance.

In this paper the characteristics of screw propellers are given in a form suitable for use in preliminary design problems. These characteristics are obtained from open-water test results with the Wageningen B-screw series [1]**). B-series propellers are frequently used in practice and possess satisfactory efficiency and adequate cavitation properties. At present about 120 screw models of the B-series have been tested.

Some years ago the fairing of the B-screw series test results was started by means of a regression analysis. In addition, the test results were corrected for Reynolds number effects by using a method developed by Lerbs [2]. Preliminary results of these investigations were given by Van Lammeren et al [3] and by Oosterveld and Van Oossanen [4].

The fairing of the B-screw series test results has now been completed. The thrust and torque coefficients K_T and K_Q of the screws are expressed as polynomials in the advance ratio J, the pitch ratio P/D, the blade-area ratio A_E/A_O, and the blade number Z. In addition, the effect of Reynolds number and of the thickness of the blade profile at a characteristic radius is taken into account in the polynomials. As such the following relations have been determined:

$$\left.\begin{aligned} K_T &= f_1(J, P/D, A_E/A_O, Z, R_n, t/c) \\ K_Q &= f_2(J, P/D, A_E/A_O, Z, R_n, t/c) \end{aligned}\right. \qquad (1)$$

2. Geometry of B-series screws

A systematic screw series is formed by a number of screw models of which only the pitch ratio P/D is varied. All other characteristic screw dimensions such as the diameter D, the number of blades Z, the blade-area ratio A_E/A_O, the blade outline, the shape of blade sections, the blade thicknesses and the hub-diameter ratio d/D are the same. These screw series now comprises models with blade numbers ranging from 2 to 7, blade area ratios ranging from 0.30 to 1.05 and pitch ratios ranging from 0.5 to 1.4.

Table 1 gives the overall geometric properties of the original Wageningen B-series. The required coordinates of the profiles can be calculated by means of formulas, analogous to the formulas given by Van Gent and Van Oossanen [5] and Van Oossanen [6], viz:

$$\left.\begin{aligned} y_{face} &= V_1(t_{max} - t_{t.e.}) \\ y_{back} &= (V_1 + V_2)(t_{max} - t_{t.e.}) + t_{t.e.} \end{aligned}\right\} \text{for } P \leq 0 \qquad (2)$$

and

*) Netherlands Ship Model Basin, Wageningen, the Netherlands.

**) Numbers in brackets refer to the list of references at the end of this paper.

Table 1
Dimensions of Wageningen B-propeller series.

Dimensions of four-, five-, six- and seven bladed B-screw series.					
r/R	$\frac{c_r}{D} \cdot \frac{Z}{A_E/A_O}$	a_r/c_r	b_r/c_r	$s_r/D=A_r-B_rZ$	
				A_r	B_r
0.2	1.662	0.617	0.350	0.0526	0.0040
0.3	1.882	0.613	0.350	0.0464	0.0035
0.4	2.050	0.601	0.351	0.0402	0.0030
0.5	2.152	0.586	0.355	0.0340	0.0025
0.6	2.187	0.561	0.389	0.0278	0.0020
0.7	2.144	0.524	0.443	0.0216	0.0015
0.8	1.970	0.463	0.479	0.0154	0.0010
0.9	1.582	0.351	0.500	0.0092	0.0005
1.0	0.000	0.000	0.000	0.0030	0.0000
Dimensions of three-bladed B-screw series.					
r/R	$\frac{c_r}{D} \cdot \frac{Z}{A_E/A_O}$	a_r/c_r	b_r/c_r	$s_r/D=A_r-B_rZ$	
				A_r	B_r
0.2	1.633	0.616	0.350	0.0526	0.0040
0.3	1.832	0.611	0.350	0.0464	0.0035
0.4	2.000	0.599	0.350	0.0402	0.0030
0.5	2.120	0.583	0.355	0.0340	0.0025
0.6	2.186	0.558	0.389	0.0278	0.0020
0.7	2.168	0.526	0.442	0.0216	0.0015
0.8	2.127	0.481	0.478	0.0154	0.0010
0.9	1.657	0.400	0.500	0.0092	0.0005
1.0	0.000	0.000	0.000	0.0030	0.0000

$A_r B_r$ = constants in equation for S_r/D

a_r = distance between leading edge and generator line at r

b_r = distance between leading edge and location of maximum thickness

c_r = chord length of blade section at radius r

s_r = maximum blade section thickness at radius r

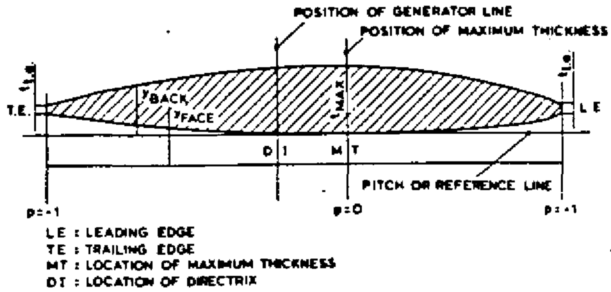

Figure 1. Definition of geometric blade section parameters of Wageningen B- and BB-series propellers.

$$\left.\begin{aligned} y_{face} &= V_1(t_{max} - t_{l.e.}) \\ y_{back} &= (V_1 + V_2)(t_{max} - t_{l.e.}) + t_{l.e.} \end{aligned}\right\} \text{for } P > 0 \tag{3}$$

From Figure 1 it follows that:

y_{face}, y_{back} = vertical ordinate of a point on a blade section on the face and on the back with respect to the pitch line,

t_{max} = maximum thickness of blade section,

$t_{t.e.}$, $t_{l.e.}$ = extrapolated blade section thickness at the trailing and leading edges,

V_1, V_2 = tabulated functions dependent on r/R and P,

P = non-dimensional coordinate along pitch line from position of maximum thickness to leading edge (where P=1), and from position of maximum thickness to trailing edge (where P = -1).

Values of V_1 and V_2 are given in Tables 2 and 3. The values of $t_{l.e.}$ and $t_{t.e.}$ are usually chosen in accordance with rules laid down by classification societies or in accordance with manufacturing requirements. In conjunction with the geometry of this propeller series, it is remarked that at the Netherlands Ship Model Basin modified B-series propellers are now used and designed, which have a slightly wider blade contour near the blade tip. These propellers are denoted as 'BB' propellers. For the sake of completeness, Table 4 is included which gives the particulars of this series. The performance characteristics of these BB-series propellers may be considered identical with the original B-series propellers.

Table 2

Values of V_1 for use in equations 2 and 3.

r/R \ P	-1.0	-.95	-.9	-.8	-.7	-.6	-.5	-.4	-.2	0
.7-1.0	0	0	0	0	0	0	0	0	0	0
.6	0	0	0	0	0	0	0	0	0	0
.5	.0522	.0420	.0330	.0190	.0100	.0040	.0012	0	0	0
.4	.1467	.1200	.0972	.0630	.0395	.0214	.0116	.0044	0	0
.3	.2306	.2040	.1790	.1333	.0943	.0623	.0376	.0202	.0033	0
.25	.2598	.2372	.2115	.1651	.1246	.0899	.0579	.0350	.0084	0
.2	.2826	.2630	.2400	.1967	.1570	.1207	.0880	.0592	.0172	0
.15	.3000	.2824	.2650	.2300	.1950	.1610	.1280	.0955	.0365	0

r/R \ P	+1.0	+.95	+.9	+.85	+.8	+.7	+.6	+.5	+.4	+.2	0
.7-1.0	0	0	0	0	0	0	0	0	0	0	0
.6	.0382	.0169	.0067	.0022	.0006	0	0	0	0	0	0
.5	.1278	.0778	.0500	.0328	.0211	.0085	.0034	.0008	0	0	0
.4	.2181	.1467	.1088	.0833	.0637	.0357	.0189	.0090	.0033	0	0
.3	.2923	.2186	.1760	.1445	.1191	.0790	.0503	.0300	.0148	.0027	0
.25	.3256	.2513	.2068	.1747	.1465	.1008	.0669	.0417	.0224	.0031	0
.2	.3560	.2821	.2353	.2000	.1685	.1180	.0804	.0520	.0304	.0049	0
.15	.3860	.3150	.2642	.2230	.1870	.1320	.0920	.0615	.0384	.0096	0

Table 3

Values of V_2 for use in equations 2 and 3.

r/R \ P	-1.0	-.95	-.9	-.8	-.7	-.6	-.5	-.4	-.2	0
.9-1.0	0	.0975	.19	.36	.51	.64	.75	.84	.96	1
.85	0	.0975	.19	.36	.51	.64	.75	.84	.96	1
.8	0	.0975	.19	.36	.51	.64	.75	.84	.96	1
.7	0	.0975	.19	.36	.51	.64	.75	.84	.96	1
.6	0	.0965	.1885	.3585	.5110	.6415	.7530	.8426	.9613	1
.5	0	.0950	.1865	.3569	.5140	.6439	.7580	.8456	.9639	1
.4	0	.0905	.1810	.3500	.5040	.6353	.7525	.8415	.9645	1
.3	0	.0800	.1670	.3360	.4885	.6195	.7335	.8265	.9583	1
.25	0	.0725	.1567	.3228	.4740	.6050	.7184	.8139	.9519	1
.2	0	.0640	.1455	.3060	.4535	.5842	.6995	.7984	.9446	1
.15	0	.0540	.1325	.2870	.4280	.5585	.6770	.7805	.9360	1

r/R \ P	+1.0	+.95	+.9	+.85	+.8	+.7	+.6	+.5	+.4	+.2	0
.9-1.0	0	.0975	.1900	.2775	.3600	.51	.6400	.75	.8400	.9600	1
.85	0	.1000	.1950	.2830	.3660	.5160	.6455	.7550	.8450	.9615	1
.8	0	.1050	.2028	.2925	.3765	.5265	.6545	.7635	.8520	.9635	1
.7	0	.1240	.2337	.3300	.4140	.5615	.6840	.7850	.8660	.9675	1
.6	0	.1485	.2720	.3775	.4620	.6060	.7200	.8090	.8790	.9690	1
.5	0	.1750	.3056	.4135	.5039	.6430	.7478	.8275	.8880	.9710	1
.4	0	.1935	.3235	.4335	.5220	.6590	.7593	.8345	.8933	.9725	1
.3	0	.1890	.3197	.4265	.5130	.6505	.7520	.8315	.8920	.9750	1
.25	0	.1758	.3042	.4108	.4982	.6359	.7415	.8259	.8899	.9751	1
.2	0	.1560	.2840	.3905	.4777	.6190	.7277	.8170	.8875	.9750	1
.15	0	.1300	.2600	.3665	.4520	.5995	.7105	.8055	.8825	.9760	1

Table 4
Particulars of BB-series propellers.

r/R	$\frac{c_r}{D} \cdot \frac{Z}{A_E/A_O}$	a_r/c_r	b_r/c_r
0.200	1.600	0.581	0.350
0.300	1.832	0.584	0.350
0.400	2.023	0.580	0.351
0.500	2.163	0.570	0.355
0.600	2.243	0.552	0.389
0.700	2.247	0.524	0.443
0.800	2.132	0.480	0.486
0.850	2.005	0.448	0.498
0.900	1.798	0.402	0.500
0.950	1.434	0.318	0.500
0.975	1:122	0.227	0.500

a_r = distance between leading edge and generator line at r

b_r = distance between leading edge and location of maximum thickness at r

c_r = chord length at r

3. Analysis of model test data

The open-water test results of B-series propellers are given in the conventional way in the form of the thrust and torque coefficients K_T and K_Q, expressed as a function of J and the pitch ratio P/D, where:

$$K_T = \frac{T}{\rho n^2 D^4} \tag{4}$$

$$K_Q = \frac{Q}{\rho n^2 D^5} \tag{5}$$

$$J = \frac{V_A}{nD} \tag{6}$$

in which

T = propeller thrust,
Q = propeller torque,
ρ = fluid density,
n = revolutions of propeller per second,
D = propeller diameter,
V_A = velocity of advance.

The open-water efficiency is defined as:

$$\eta_o = \frac{J}{2\pi} \frac{K_T}{K_Q} \tag{7}$$

The effect of a Reynolds number variation on the test results has been taken into account by using the method developed by Lerbs [2], from the characteristics of equivalent blade sections. This method has been followed also in References 7, 8, 9 and 10.

In the Lerbs equivalent profile method the blade section at 0.75R is assumed to be equivalent for the whole blade. At a specific value of the advance coefficient J, the lift and drag coefficient C_L and C_D and the corresponding angle of attack α, for the blade section, are deduced from the K_T- and K_Q -values from the open-water test.

Reynolds number effects are only considered to influence the drag coefficient of the equivalent profile. It is furthermore assumed that this influence is in accordance with a vertical shift of the C_D-curve, equal to the change in the minimum value of the drag coefficient. This minimum value is for thin profiles composed of mainly frictional resistance, the effect of the pressure gradient being small.

According to Hoerner [11], the minimum drag coefficient of a profile is:

$$C_{D_{min.}} = 2C_f\left(1 + 2\frac{t}{c_{0.75R}}\right) \tag{8}$$

in which;

$$C_f = \frac{0.075}{[0.43429 \ln(R_{n_{0.75R}}) - 2]^2} \tag{9}$$

where;

$$R_{n_{0.75R}} = \frac{c_{0.75R}\sqrt{V_A^2 + (0.75\pi nD)^2}}{\nu} \tag{10}$$

C_f is the drag coefficient of a flat plate in a turbulent flow and the term $1 + 2\frac{t}{c_{0.75R}}$ represents the effect of the pressure gradient; $c_{0.75R}$ is the chord length at 0.75R and ν the kinematical viscosity.

On setting out the minimum value of the drag coefficient as obtained from the polar curve for each propeller on a base of Reynolds number, a large scatter is apparent as shown in Figure 2. When this minimum value of the drag coefficient

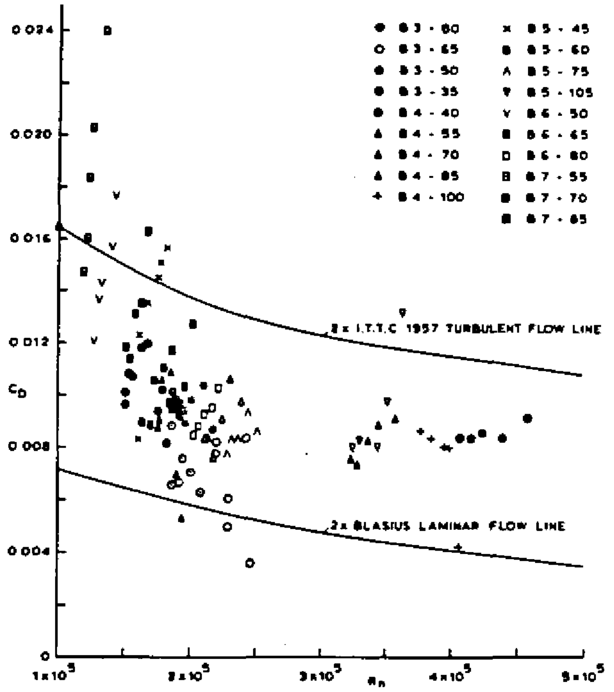

Figure 2. Uncorrected value of minimum drag coefficient of equivalent profile of B-series propellers.

is set out against $\frac{A_E/A_O}{Z}$ for each pitch-diameter ratio, it is seen that below a specific value of the blade area-blade number ratio an increase in the $C_{D_{min.}}$ value occurs. For a pitch-diameter ratio equal to 1.0, this is shown in Figure 3. The existence of such a correlation of the $C_{D_{min.}}$ value with propeller geometry points to the fact that the scatter in Figure 2 is not entirely due to Reynolds number effects and experimental errors. It is obvious that the drag coefficient is influenced by a three-dimensional effect. It is necessary, therefore, before correcting for Reynolds number according to the given equations, to subtract this three-dimensional effect from the $C_{D_{min.}}$ value. An estimation of this effect was obtained by applying regression analysis of which the results are given by Van Oossanen [6].

The thus obtained lift and drag coefficients were each expressed as a function of blade number, blade area ratio, pitch-diameter ratio and angle of attack in polynomials by means of a multiple regression analysis method. By applying this process in reverse, thrust and torque coefficient values were then calculated. The basis for this reverse process was formed by calculating C_L and C_D coefficients from the C_L and C_D polynomials for specific combinations of Z, A_E/A_O, P/D, α and R_n. The resulting values formed the input for the development of a thrust coefficient and a torque coefficient polynomial. The thrust and torque coefficients were then expressed as polynomials in the advance coefficient J, pitch ratio P/D, blade area ratio A_E/A_O and blade number Z and with the aid of a multiple regression analysis method the significant terms of the polynomials and the values of the corresponding coefficients were determined. For $R_n = 2x10^6$ the polynomials obtained in this way are given in Table 5. The choice of a Reynolds number value of $2x10^6$ for the characteristics on the model scale followed from the fact that the corresponding $C_{D_{min.}}$ values is an average of all model $C_{D_{min.}}$ values.

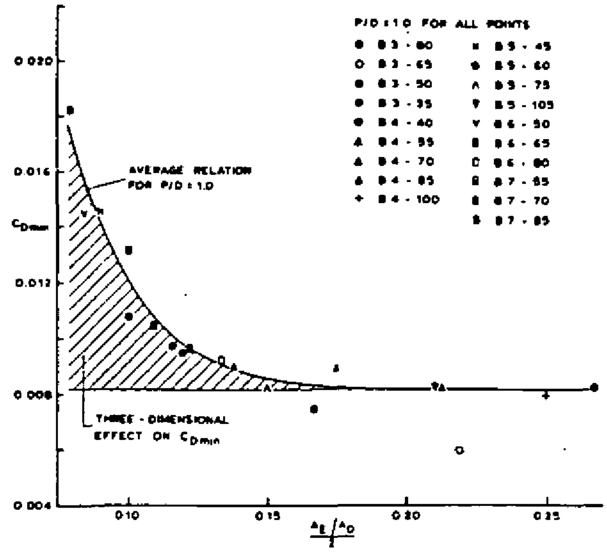

Figure 3. Three-dimensional effect on minimum drag coefficient of equivalent profile of B-series propellers.

4. Reynolds number effect on propeller chararacteristics

In formulating the minimum value of the drag coefficient as a function of the Reynolds number (see equation 8), it is possible to calculate thrust and torque values valid for full-scale by correcting this C_D-value.

This was performed for Reynolds numbers equal to $2x10^7$, $2x10^8$ and $2x10^9$ for a selected grid of J, P/D, A_E/A_O and Z-values. Together with the values for $R_n = 2x10^6$, these K_T and K_Q values formed the input for the determination of a K_T and K_Q polynomial for the additional Reynolds number effect above $2x10^6$. These polynomials are given in Table 6. The actual value to be substituted into these polynomials is the common logarithm of the actual Reynolds number. Thus if $R_n = 2x10^7$, the value to be substituted is 7.3010.

To demonstrate how the Reynolds number effect is dependent on the number of propeller blades, the blade area ratio, the pitch-diameter ratio and the advance coefficient, diagrams have been prepared each of which gives the effect of one of these parameters on K_T and K_Q with increasing Reynolds number. The effect of the number of blades is shown in Figure 4 while the effect of the expanded blade area ratio is shown in Figure 5. Figure 6 gives the effect of the pitch-diameter ratio and Figure 7 shows the effect of the advance coefficient J. The results shown are for the propellers grouped around the B5-75 ($Z = 5$, $A_E/A_O = 0.75$) propeller with a pitch-diameter ratio of 1.0, working at an advance coefficient equal to 0.5.

Table 5

Coefficients and terms of the K_T and K_Q polynomials for the Wageningen B-screw Series for $R_n = 2x10^6$.

$$\begin{matrix} K_T \\ K_Q \end{matrix} = \sum_{s,t,u,v} \begin{bmatrix} C_{s,t,u,v} \cdot (J)^s \cdot (P/D)^t \cdot (A_E/A_O)^u \cdot (z)^v \\ C_{s,t,u,v} \cdot (J)^s \cdot (P/D)^t \cdot (A_E/A_O)^u \cdot (z)^v \end{bmatrix}$$

K_T: $C_{s,t,u,v}$	s (J)	t (P/D)	u (A_E/A_O)	v (z)	K_Q: $C_{s,t,u,v}$	s (J)	t (P/D)	u (A_E/A_O)	v (z)
+0.00880496	0	0	0	0	+0.00379368	0	0	0	0
−0.204554	1	0	0	0	+0.00886523	2	0	0	0
+0.166351	0	1	0	0	−0.032241	1	1	0	0
+0.158114	0	2	0	0	+0.00344778	0	2	0	0
−0.147581	2	0	1	0	−0.0408811	0	1	1	0
−0.481497	1	1	1	0	−0.108009	1	1	1	0
+0.415437	0	2	1	0	−0.0885381	2	1	1	0
+0.0144043	0	0	0	1	+0.188561	0	2	1	0
−0.0530054	2	0	0	1	−0.00370871	1	0	0	1
+0.0143481	0	1	0	1	+0.00513696	0	1	0	1
+0.0606826	1	1	0	1	+0.0209449	1	1	0	1
−0.0125894	0	0	1	1	+0.00474319	2	1	0	1
+0.0109689	1	0	1	1	−0.00723408	2	0	1	1
−0.133698	0	3	0	0	+0.00438388	1	1	1	1
+0.00638407	0	6	0	0	−0.0269403	0	2	1	1
−0.00132718	2	6	0	0	+0.0558082	3	0	1	0
+0.168496	3	0	1	0	+0.0161886	0	3	1	0
−0.0507214	0	0	2	0	+0.00318086	1	3	1	0
+0.0854559	2	0	2	0	+0.015896	0	0	2	0
−0.0504475	3	0	2	0	+0.0471729	1	0	2	0
+0.010465	1	6	2	0	+0.0196283	3	0	2	0
−0.00648272	2	6	2	0	−0.0502782	0	1	2	0
−0.00841728	0	3	0	1	−0.030055	3	1	2	0
+0.0168424	1	3	0	1	+0.0417122	2	2	2	0
−0.00102296	3	3	0	1	−0.0397722	0	3	2	0
−0.0317791	0	3	1	1	−0.00350024	0	6	2	0
+0.018604	1	0	2	1	−0.0106854	3	0	0	1
−0.00410798	0	2	2	1	+0.00110903	3	3	0	1
−0.000606848	0	0	0	2	−0.000313912	0	6	0	1
−0.0049819	1	0	0	2	+0.0035985	3	0	1	1
+0.0025983	2	0	0	2	−0.00142121	0	6	1	1
−0.000560528	3	0	0	2	−0.00383637	1	0	2	1
−0.00163652	1	2	0	2	+0.0126803	0	2	2	1
−0.000328787	1	6	0	2	−0.00318278	2	3	2	1
+0.000116502	2	6	0	2	+0.00334268	0	6	2	1
+0.000690904	0	0	1	2	−0.00183491	1	1	0	2
+0.00421749	0	3	1	2	+0.000112451	3	2	0	2
+0.0000565229	3	6	1	2	−0.0000297228	3	6	0	2
−0.00146564	0	3	2	2	+0.000269551	1	0	1	2
					+0.00083265	2	0	1	2
					+0.00155334	0	2	1	2
					+0.000302683	0	6	1	2
					−0.0001843	0	0	2	2
					−0.000425399	0	3	2	2
					+0.0000869243	3	3	2	2
					−0.0004659	0	6	2	2
					+0.0000554194	1	6	2	2

$R_n = 2 \times 10^6$

Table 6

Polynomials for Reynolds number effect (above $R_n = 2x10^6$) on K_T and K_Q.

$$
\begin{aligned}
\Delta K_T = \ & 0.000353485 \\
& -0.00333758(A_E/A_O)J^2 \\
& -0.00478125(A_E/A_O)(P/D)J \\
& +0.000257792(\log R_n-0.301)^2 \cdot (A_E/A_O)J^2 \\
& +0.0000643192(\log R_n-301)(P/D)^6 \cdot J^2 \\
& -0.0000110636(\log R_n-0.301)^2 (P/D)^6 J^2 \\
& -0.0000276305(\log R_n-0.301)^2 z(A_E/A_O)J^2 \\
& +0.0000954(\log R_n-0.301) z(A_E/A_O)(P/D)J \\
& +0.0000032049(\log R_n-0.301) z^2(A_E/A_O)(P/D)^3 J
\end{aligned}
$$

$$
\begin{aligned}
\Delta K_Q = \ & -0.000591412 \\
& +0.00696898(P/D) \\
& -0.0000666654\, z(P/D)^6 \\
& +0.0160818(A_E/A_O)^2 \\
& -0.000938091(\log R_n-0.301)(P/D) \\
& -0.00059593(\log R_n-0.301)(P/D)^2 \\
& +0.0000782099(\log R_n-0.301)^2 (P/D)^2 \\
& +0.0000052199(\log R_n-0.301) z(A_E/A_O)J^2 \\
& -0.00000088528(\log R_n-0.301)^2 z(A_E/A_O)(P/D)J \\
& +0.0000230171(\log R_n-0.301) z(P/D)^6 \\
& -0.00000184341(\log R_n-0.301)^2 z(P/D)^6 \\
& -0.00400252(\log R_n-0.301)(A_E/A_O)^2 \\
& +0.000220915(\log R_n-0.301)^2 (A_E/A_O)^2
\end{aligned}
$$

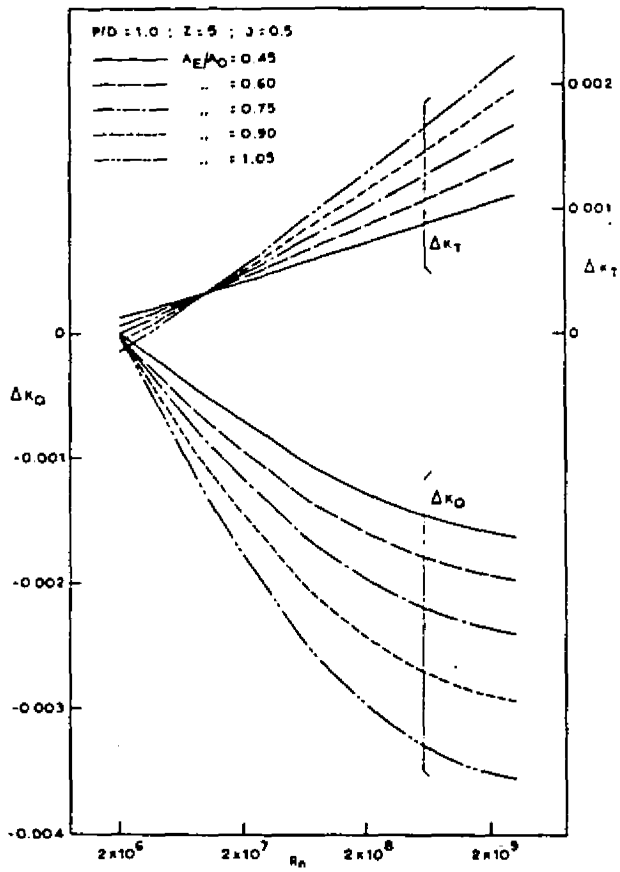

Figure 5. Influence of blade area ratio on Reynolds number effect on thrust and torque coefficients.

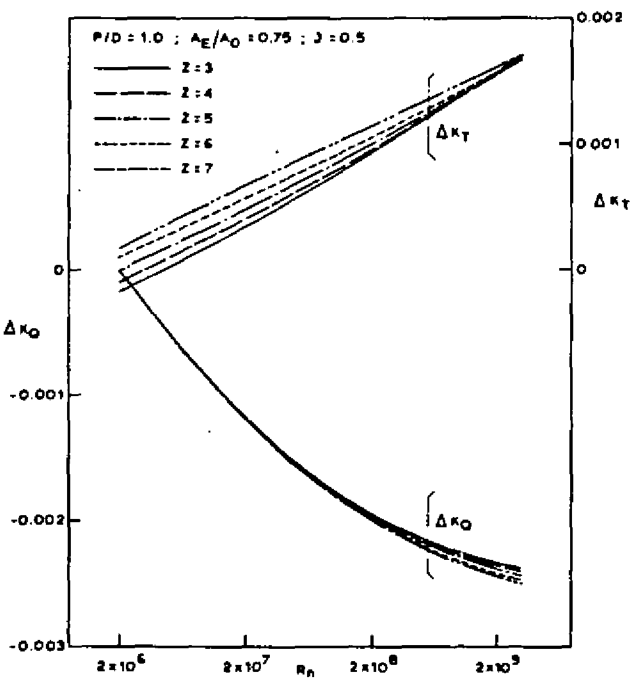

Figure 4. Influence of number of blades on Reynolds number effect on thrust and torque coefficients.

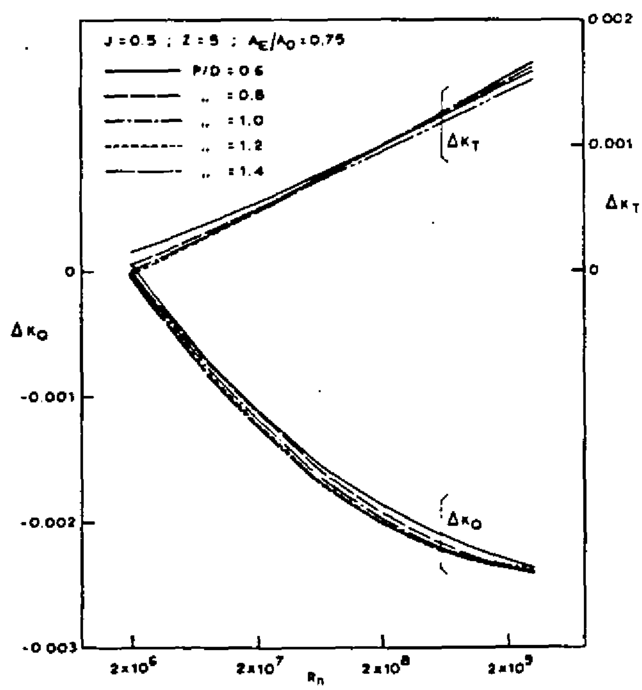

Figure 6. Influence of pitch-diameter ratio on Reynolds number effect on thrust and torque coefficients.

It should be noticed that the increment in K_T (ΔK_T) and the increment in K_Q (ΔK_Q) presented in Figures 4 to 7 are relative to a Reynolds number value of $2x10^6$. The value of the Reynolds number is determined by equation 10. Strictly, therefore, the ΔK_T and ΔK_Q values for a Reynolds number equal to $2x10^6$ should equal zero. As shown in Figures 4 to 7, this is not the case. This is due to the difficulty in multiple regression analysis methods to prescribe that the resulting relation must have a specific value for a particular combination of values for the independent variables.

5. Effect of variation in blade thickness on propeller characteristics

The effect of blade thickness on the thrust and torque coefficients can be determined in an analogous manner as used to determine the effect of Reynolds number as described in section 4. A change in the t/c-value of the equivalent propeller blade section at 0.75R is again only considered to influence the value of the minimum drag coefficient. Thus, as was the case in analysing the effect of Reynolds number, the drag coefficient of the equivalent blade section as a function of angle of attack (or advance ratio) is shifted vertically upwards or downwards in accordance with the change in the value of the minimum drag coefficient $C_{D_{min}}$. This situation, therefore, leads to the idea that the effect of a specific change in the t/c-value at 0.75R can be represented by a specific change in Reynolds number.

The polynomials given in Tables 5 and 6 are for a blade thickness-chord length ratio equal to:

$$t/c_{0.75R} = \frac{(0.0185 - 0.00125Z)Z}{2.073\, A_E/A_O} \qquad (11)$$

By rearranging equation 8, 9 and 10 a change in this value of t/c can be shown to correspond to a new value of the Reynolds number given by:

$$R^1_{n0.75R} = \exp\left[4.6052 + \sqrt{\frac{1+2(t/c)_{0.75R}}{1+2(t/c)^1_{0.75R}}} \cdot (\ln R_{n0.75R} - 4.6052)\right] \qquad (12)$$

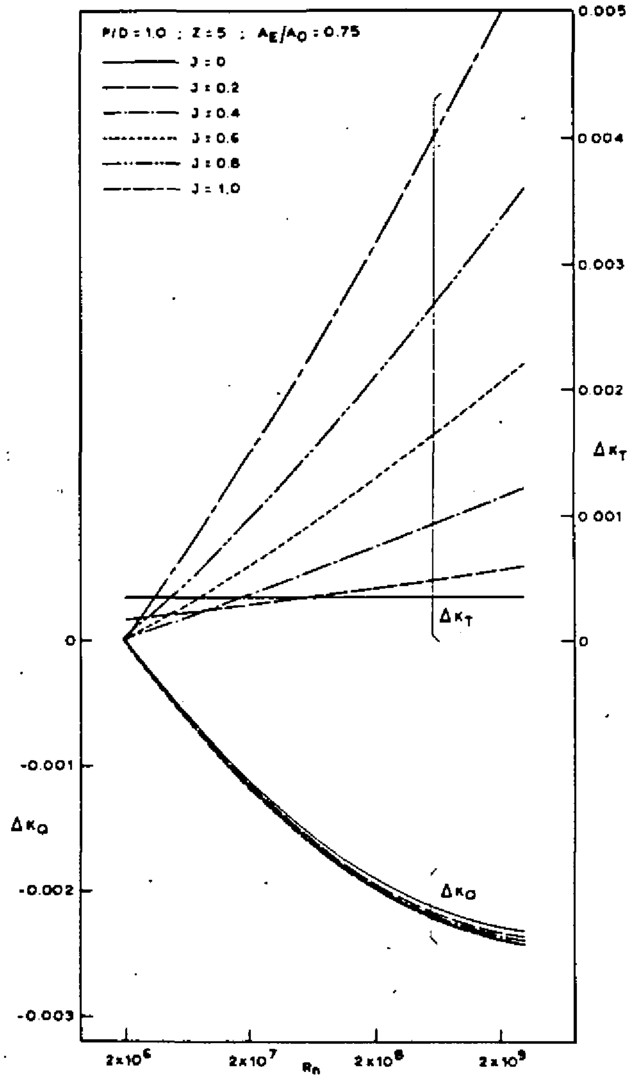

Figure 7. Influence of advance ratio on Reynolds number effect on thrust and torque coefficients.

where

$R^1_{n0.75R}$ = effective Reynolds number for a change in $(t/c)_{0.75R}$

and

$(t/c)^1_{0.75R}$ = new t/c value at 0.75R.

Thus, when it is assumed that an increase or decrease in blade section thickness (relative to equation 11) does not influence the effective camber and pitch, the effect on thrust and torque can be ascertained by calculating an effective new value for the Reynolds number according to equation 12 and then determining, by means of the polynomials presented in Table 5 and Table 6, the associated values of K_T and K_Q.

6. Choice of blade area ratio based on cavitation criteria

A reasonable indication as to the required blade area ratio of fixed pitch propellers can be obtained by means of a formula given by Keller [12], viz:

$$\frac{A_E}{A_O}=\frac{(1.3+0.3Z)T}{(P_o-P_V)\cdot D^2}+K \tag{13}$$

where

$\frac{A_E}{A_O}$ = expanded blade area ratio,

Z = number of blades,

T = propeller thrust in kg,

P_o = static pressure at centre line of propeller shaft in kg/m^2,

P_V = vapour pressure in kg/m^2,

K = constant which can be put equal to 0 for fast twin-screw ships,

K = 0.10 for other twin-screw ships,

K = 0.20 for single-screw ships.

7. Choice of characteristic thickness chord length ratio based on cavitation criteria and strength

In a number of previous studies [13, 5], it is shown that the minimum allowable blade section thickness based on strength criteria does not give the largest margin against cavitation when operating in a non-uniform velocity field. In a propeller design the proper compromise between the conflicting characters of thick blade sections (having a large cavitation-free angle of attack range) and thin blade sections (being free of cavitation at low cavitation numbers at shock-free entry of the flow) must be made.

For every type of thickness and camber distribution used, there is only one optimum t/c-value for a specific value of the cavitation number. For propeller blade sections with an elliptic type of thickness distribution the optimum t/c-value, giving the largest cavitation-free lift coefficient range, can be approximately given by:

$$(t/c)_{opt}=0.3\sigma-0.012 \tag{14}$$

where

σ = cavitation number of the blade section in the vertical upright blade position.

Relation 14 is only valid for small blade section cambers and values of the cavitation number between 0.1 and 0.6. A handy formula for the value of the cavitation number of the blade section at 0.75R in the vertical upright blade position is:

$$\sigma=\frac{200+20(h-0.375D)}{V_A^2+(0.04ND)^2} \tag{15}$$

in which

h = distance in meter of propeller shaft to effective water surface,

V_A = velocity of advance of propeller in m/sec.,

N = revolutions per minute,

D = propeller diameter in meter.

The resulting thickness-chord length ratio of the equivalent blade section at 0.75R must also possess satisfactory strength properties. Many methods have been devised to determine the minimum acceptable value of the blade thickness at various propeller radii. However, in this preliminary design stage, in which the only interest of the naval architect is focussed on a parametric study to determine overall propeller parameters, it is quite sufficient to use a very simple formula to ensure that the chosen t/c-value is not too small. In this regard it should be noticed that for normal merchant ships equation 14 always leads to larger t/c-values than, e.g., the t/c-value for the B-series according to equation 11.

A simple formula for the minimum blade thickness at 0.75R can be derived from Saunders [14], viz:

$$t_{min_{0.75R}}=D\left[0.0028+0.21\sqrt[3]{\frac{(2375-1125P/D)P_S}{4.123ND^3\left(S_c+\frac{D^2N^2}{12.788}\right)}}\right] \tag{16}$$

where

$t_{min_{0.75R}}$ = minimum blade thickness at 0.75R in feet,

D = propeller diameter in feet,

P_S = shaft horsepower per blade,

N = revolutions per minute,

S_c = maximum allowable stress in pounds per square inch (psi).

In this formula the bending moment due to the centrifugal force effect is neglected, which is correct only for propellers with zero rake. The additional formula for the chord length for determining the minimum value of t/c at 0.75R is:

$$C_{0.75R} = \frac{2.073 A_E/A_O \cdot D}{Z} \qquad (17)$$

8. Diagrammatical representation of polynomials: determination of optimum diameter and optimum propeller revolutions

For many purposes, it is still useful to have at one's disposal diagrams giving the characteristics of open-water tests. It was, therefore, decided to make a new set of diagrams for the B-series based on the K_T and K_Q polynomials given in Tables 5 and 6.

Figure 8 gives the K_T-K_Q-J diagram of the B5-75 propeller for a Reynolds number of 2×10^6. For the case that the optimum propeller diameter is to be calculated when the power, the rotative propeller speed and the advance velocity is specified, use is generally made of the variables B_{p_1}, and δ defined as:

$$B_{p_1} = N \cdot P^{1/2} \cdot V_A^{-5/2} \qquad (18)$$
$$\delta = N \cdot D \cdot V_A^{-1}$$

in which

N = number of propeller revolutions per minute,
P = shaft horsepower in british units (1HP = 76kgm/sec.),
D = propeller diameter in feet,
V_A = advance velocity of propeller in knots.

Since the value of B_{p_1} and δ are dependent on the system of units used, it is appropriate to replace these variable by the non-dimensional variables $K_Q^{1/4} \cdot J^{-5/4}$ and J^{-1} respectively, such that:

$$0.1739\sqrt{B_{p_1}} = K_Q^{1/4} \cdot J^{-5/4}$$

and (19)

$$0.009875\delta = J^{-1}$$

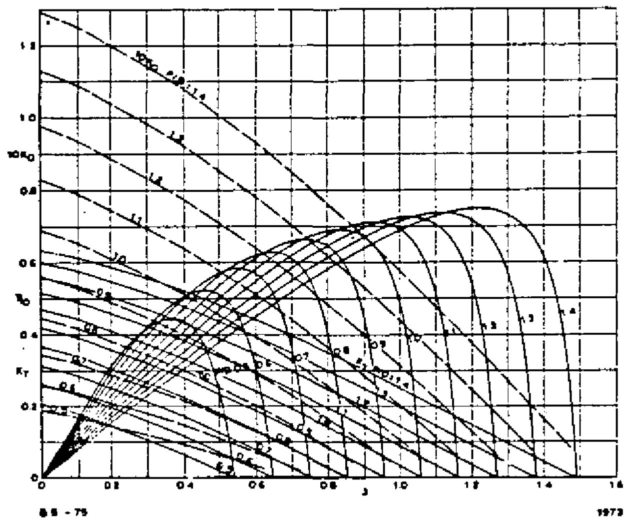

Figure 8. K_T-K_Q-J diagram of B5-75 propeller according to polynomials given in Table 5 ($R_n = 2 \times 10^6$).

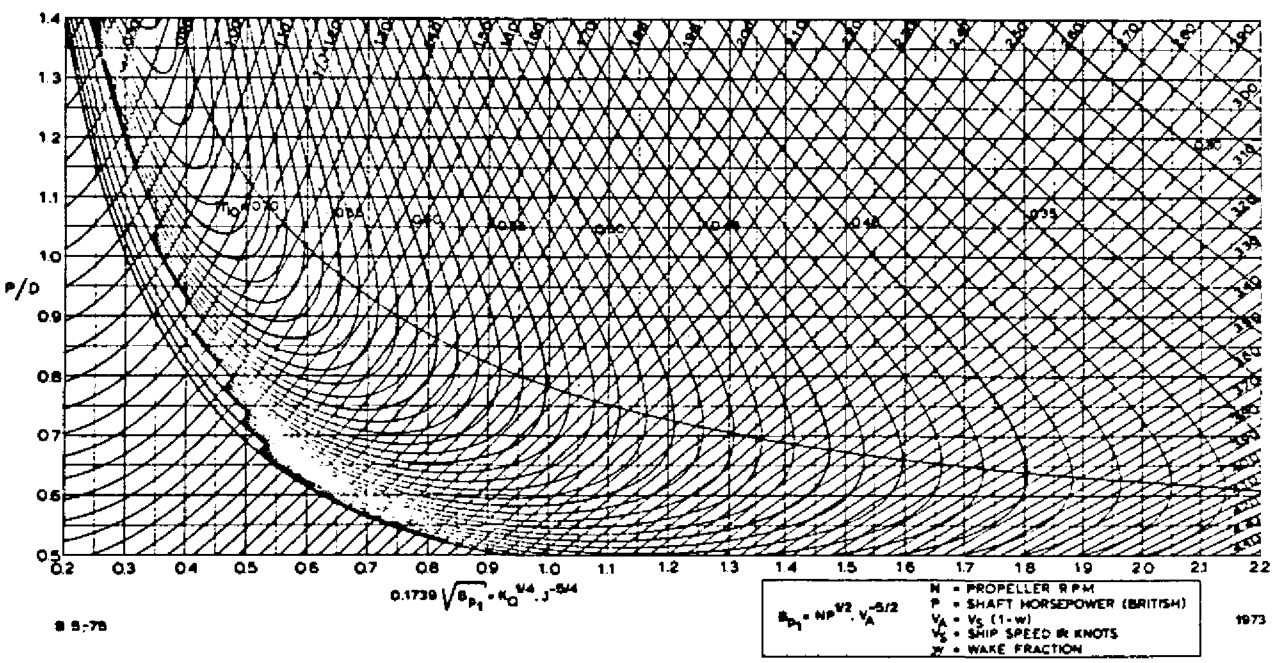

Figure 9. $K_Q^{1/4} \cdot J^{-5/4} - J^{-1}$ diagram of B5-75 propeller according to polynomials given in Table 5 ($R_n = 2 \times 10^6$) for determination of optimum diameter.

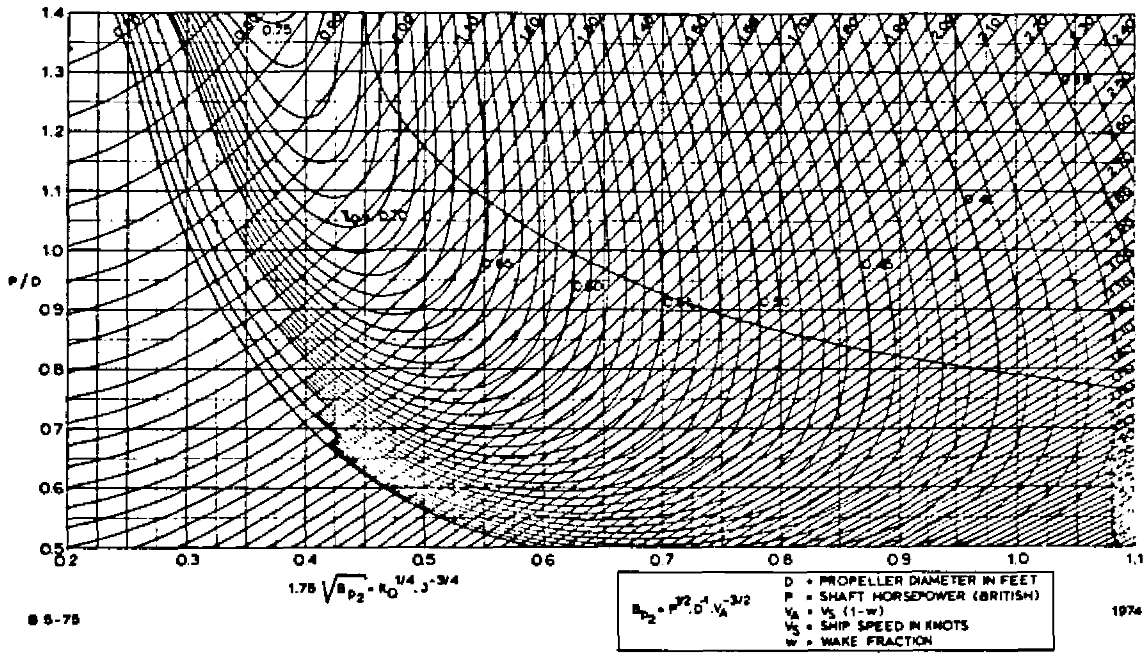

Figure 10. $K_Q^{1/4} . J^{-3/4} - J^{-1}$ diagram of B5-75 propeller according to polynomials given in Table 5 ($R_n = 2 \times 10^6$) for determination of optimum diameter.

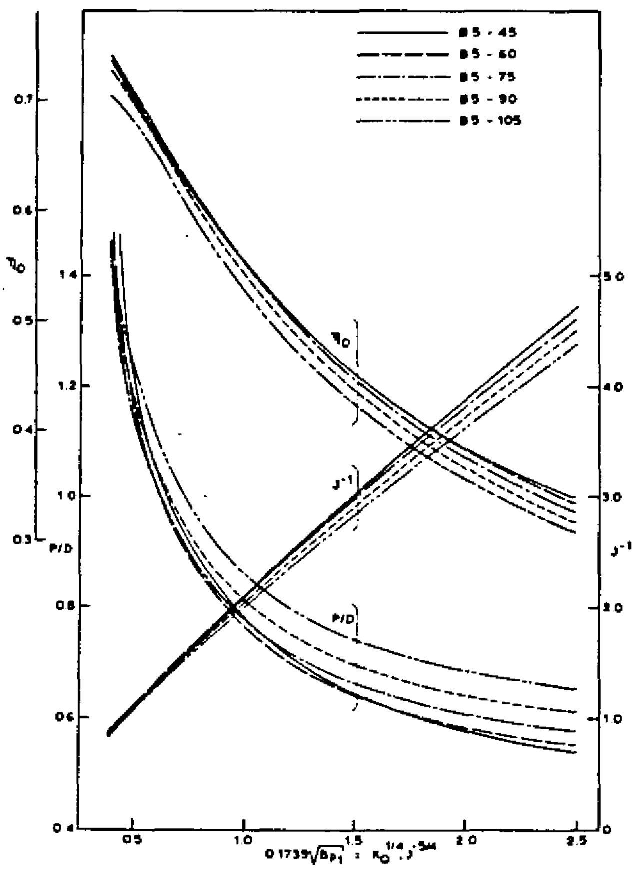

Figure 11. Values of pitch-diameter ratio and J^{-1} corresponding to optimum diameter (based on $K_Q^{1/4} . J^{-5/4}$).

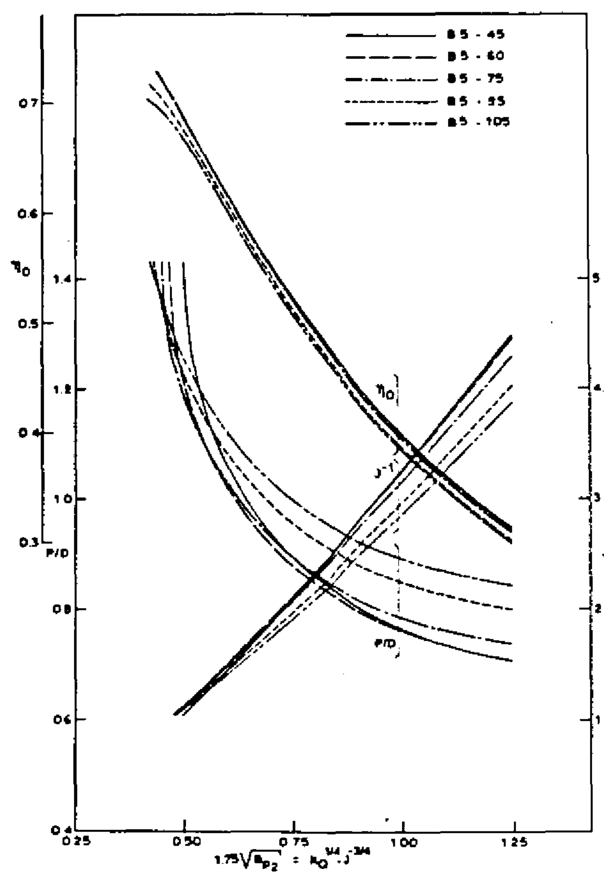

Figure 12. Values of pitch-diameter ratio and J^{-1} corresponding to optimum RPM (based on $K_Q^{1/4} . J^{-3/4}$).

The square root of B_{p_1} is adopted since then a linear scale can be used in the resulting diagrams for this variable. Figure 9 shows the result for the B5-75 propeller for a Reynolds number of $2x10^6$.

In the case that the optimum propeller speed is to be determined when the power, the propeller diameter and the advance velocity is specified, use can be made of the power constant B_{p_2}, defined as:

$$B_{p_2} = P^{1/2} \cdot D^{-1} \cdot V_A^{-3/2} \tag{20}$$

in which the variables P, D and V_A are defined as in equations 18. This power constant can be replaced by the non-dimensional expression $K_Q^{1/4} \cdot J^{-3/4}$ as follows:

$$1.75\sqrt{B_{p_2}} = K_Q^{1/4} \cdot J^{-3/4} \tag{21}$$

Here also the square root of B_{p_2} is adopted since then a linear scale on the horizontal axis can be used in the resulting diagram. Figure 10 shows the result for the B5-75 propeller for a Reynolds number of $2x10^6$. At the Netherlands Ship Model Basin, diagrams of the type shown in Figures 9 and 10 have been prepared for all B-series propellers for a Reynolds number value of $2x10^6$.

A diagram giving the values of the pitch-diameter ratio P/D, the open-water efficiency η_0 and J^{-1}, corresponding to the value of the optimum diameter, based on $K_Q^{1/4} \cdot J^{-5/4}$, is given in Figure 11. Figure 12 gives the analogous diagram for the value of the optimum number of revolutions. Both diagrams are for the 5-bladed B-series propellers.

9. References

1. Troost, L., 'Open-water tests with modern propeller forms', Trans. NECI, 1938, 1940 and 1951.
2. Lerbs, H.W., 'On the effect of scale and roughness on free running propellers', Journal ASME, 1951.
3. Lammeren, W.P.A. van, Manen, J.D. van and Oosterveld, M.W.C., The Wageningen B-screw series', Trans. SNAME, 1969.
4. Oosterveld, M.W.C. and Oossanen, P. van, 'Recent developments in marine propeller hydrodynamics', Jubilee Meeting of NSMB, 1972.
5. Gent, W. van and Oossanen, P. van, 'Influence of wake on propeller loading and cavitation', Paper presented at 2nd Lips Propeller Symposium; May 1973. International Shipbuilding Progress, 1973.
6. Oossanen, P. van, 'Calculation of performance and cavitation characteristics of propellers including effects of non-uniform flow and viscosity'. Doctor's thesis, Delft University of Technology, 1974: Netherlands Ship Model Basin, Publication No. 457, 1974.
7. Lindgren, H., 'Model tests with a family of three and five bladed propellers', Publication No. 47, SSPA, 1961.
8. Lindgren, H. and Bjarne, E., 'The SSPA standard propeller family open-water characteristics', Publication No. 60, SSPA, 1967.
9. Newton, R.N. and Rader, H.P., 'Performance data of propellers for high-speed craft', Trans. RINA, 1961.
10. Schmidt, D., 'Einfluss der Reynoldzahl und der Rauhigkeit auf die propeller-characteristik, berechnet nach der Methode des äquivalenten Profils', Schiffbauforschung 11, 1972.
11. Hoerner, S.F., 'Fluid dynamic drag', Published by the author, 1971.
12. Keller, J. auf'm, 'Enige aspecten bij het ontwerpen van scheepsschroeven', Schip en Werf, No. 24, 1966.
13. Oossanen, P. van, 'A method for minimizing the occurrence of cavitation on propellers in a wake', International Shipbuilding Progress, Vol. 18, No. 205, 1971.
14. Saunders, H.E., 'Hydrodynamics in ship design', Vol. 2, page 620, published by the Society of Naval Architects and Marine Engineers, 1957.

Anexo 2. A Rational Approach to propeller geometry. J. Klein, Member, Bird-Jhonson Company, Walpole, Massachusetts.

THE SOCIETY OF NAVAL ARCHITECTS AND MARINE ENGINEERS
74 Trinity Place, New York, N.Y. 10006
Paper to be presented at Propellers 75, Philadelphia, Pa., July 22-23, 1975

A Rational Approach to Propeller Geometry

No. 11

J. Lester Klein, Member,
Bird-Johnson Company, Walpole, Massachusetts

ABSTRACT

A system of geometry definition and resulting mathematical relationships is presented for describing propeller blades as "ordinary" three-dimensional bodies. Topics discussed include coordinate system characteristics, foil section geometry, pitch helix relationships, calculation of coordinates, interpolation methods, surface normals, and planar sections. Applications and examples discussed include stress analysis, numerically controlled machining, pattern construction, and dimensional checking of blades.

NOMENCLATURE

- A = chord station designation
- A_D = developed area
- A_E = expanded area
- A_P = projected area
- A_T = true surface area
- B = chord station designation
- c = chord length
- D = propeller diameter, $2R_O$
- F = force
- g = subscript denoting center of gravity
- h = value of x_R at blade root
- $\bar{i}$ = unit vector along X-axis
- $\bar{j}$ = unit vector along Y-axis
- K = midchord station designation
- $\bar{k}$ = unit vector along Z-axis
- LE = leading edge
- LEFR = leading edge fairing radius
- LER = leading edge radius
- ℓ = direction cosine, $\bar{u}\cdot\bar{i}$
- M = moment, generally
- m = direction cosine, $\bar{u}\cdot\bar{j}$
- n = direction cosine, $\bar{u}\cdot\bar{k}$
- O = origin
- $\overline{OR}$ = radius vector from origin
- P = local pitch
- R = cylindrical coordinate distance
- R_O = propeller radius, D/2
- r = radius in X-Z plane
- S = skew
- T = blade section thickness
- $\bar{T}$ = vector tangent to a space curve
- TE = trailing edge
- t = time
- $\bar{t}$ = unit vector tangent to a space curve
- $\bar{u}$ = unit vector in space, generally
- W = mass
- X = Cartesian, cylindrical, and expanded view coordinate axis
- x = distance from origin along X-axis
- x_C = fractional chord length
- x_K = X-coordinate of pitch helix midchord
- x_R = fractional radius, R/R_O
- Y = Cartesian coordinate axis
- Y_{PF} = pressure face offset
- Y_{SF} = suction face offset
- Y_T = total section "thickness", $Y_{SF}-Y_{PF}$
- y = distance from origin along Y-axis
- Z = Cartesian coordinate axis
- $\tilde{Z}$ = expanded view coordinate axis
- z = distance from origin along Z-axis
- $\tilde{z}$ = distance from origin along $\tilde{Z}$-axis, $R\theta$
- $\tilde{z}_K$ = $\tilde{Z}$ coordinate of midchord, $R\theta_K$
- γ = arctan (x/z)
- θ = cylindrical coordinate angle, arctan (z/y)
- θ_K = theta-coordinate of pitch helix midchord
- ρ = rake
- ϕ = geometric pitch angle, arctan $(P/(2\pi R))$
- Ω = pitch change rotation angle, $\Delta\gamma$
- ω = angular velocity

INTRODUCTION

In 1971, Bird-Johnson Company contracted to supply controllable reversible pitch propellers for the U.S. Navy's new Spruance Class (DD963) destroyer fleet (1,2) to the Ingalls Shipbuilding Division of Litton Industries. To achieve the accuracy and uniformity in propeller blade geometry considered necessary to meet the specifications, it was decided to machine "all surfaces of the blade castings" completely to final dimensions (within 0.002 to 0.003 inch of final size) by the use of numerically controlled (NC) machines. In a manner of speaking, numerically controlled machines do only what they are told to do, i.e., they can carry out only those motions for which they receive a command. Since the command "FAIR", a word commonly found on propeller blade drawings, is not a legal word in NC programming languages, and since the words "all surfaces of the blade castings" include the flange, faces, tip detail, leading edge detail, chisel trailing edge, fillet-flange interface areas, and Prairie air passageways, it became necessary to specify the entire blade geometry in precise and self-consistent mathematical terms. Also, the requirements for detailed stress analyses, vibration analyses, and a blade static load shop-test emphasized the need for a suitable mathematical definition of the propeller blades.

Relatively few organizations are engaged in the design, manufacture, and analysis of marine propeller blades. In the manufacturing of most marine propellers, the blade faces, edges, and fillets are "machined" from the as-cast surface to final dimensions by hand grinding at the foundries where they are cast. Therefore, to carry out the analysis, manufacturing, and testing steps for the DD963 blades, it became necessary to subcontract with organizations and people having little or no previous experience with propeller blade geometry or technology, as well as with "old-timers" in the field. As an additional complication in specifying blade geometry, the DD963 blade has a relatively complex shape, with an appreciable amount of skew and rake.

In view of the above considerations, it was decided that the then existing practices and conventions used for specifying propeller blade geometry were not wholly satisfactory for the tasks and people involved. Accordingly, revisions to the existing systems of establishing and specifying propeller blade geometry were developed by Bird-Johnson Company to accommodate the needs of the DD963 program. The resulting geometry system is also being used for the Guided Missile Frigate (FFG-7 class, formerly PF109) propeller blade (1,9). In brief, the system consists of specifying all points on or in the blade in terms of their Cartesian coordinates and the direction cosines of the surface normals at these points. Such a means of specification is widely understood, especially in the aerospace industry, where the skills are available for much of the software and tooling required. It also turns out that this system of specification is being readily accepted and used by people in less sophisticated industries, such as model makers and pattern makers. The following sections of this paper present the methods used to convert the hydrodynamicist's basic blade design data into a coordinate system and the resulting propeller blade drawing. Although the discussion applies specifically to separable blades (controllable pitch and built-up propellers), most of the material is believed to be applicable to monobloc propellers as well.

INPUT PARAMETERS

From the standpoint of geometry considerations, a separable propeller blade can be treated as consisting of three parts: (a) the blade section, which interacts with the water to provide thrust; (b) the blade flange, which provides the means of attaching the blade section to the hub; and (c) a transition region (fillet area) between the blade section and the flange. Although the methods for establishing a suitable hydrodynamic design for the blade section will not be discussed in detail here, a brief explanation of the design basis is considered desirable.

Almost any three-dimensional body can be described graphically by a combination of outline views and cross-sections. Oftentimes the cross-sections portray parallel planar cuts. With such cuts, the three-dimensional body can be "constructed" from drawings of the cross-sections by "stacking" the cross-sections, one above the other, at a suitable distance apart. Propeller blades are designed on the basis of "sections" of constant radius (a constant radius section is formed by the intersection of the propeller blade with a cylinder coaxial with the shaft axis). A propeller blade can be thought of as being built up of a series of coaxial (constant radius) sections suitably stacked and oriented with respect to each other. A smooth transition is assumed over the interval between each pair of given sections.

The input parameters and information required for a complete geometric description of a propeller blade are summarized as follows: (a) a definition of a series of sections of constant radius and the orientation in space of these sections; (b) a drawing of the hub so that a blade flange can be designed; (c) criteria for the configuration of the fillet transition region between blade and flange; (d) details such as trailing edge design and tip shape; and (e) special features, such as Prairie air passageways.

DEFINITIONS AND COORDINATE SYSTEMS

Unless otherwise stated, the following conditions prevail:

1. Propeller blade is in the "up" position.
2. The observer is standing aft, looking forward.
3. Blade is right hand--leading edge is on observer's right, and the sense of blade rotation is clockwise from observer's viewpoint.
4. Blade is set at design pitch.
5. The hub to which the blade is attached has blade ports machined so that the blade spindle axis is precisely located (the blade spindle axis is the axis about which the blade pivots during pitch changes).

Cartesian Coordinates (X, Y, Z)

As shown in Figure 1, the Cartesian coordinate axes have the following meanings: the X-axis is coincident with the propeller shaft axis; the Y-axis is coincident with the blade spindle axis, the Z-axis is in the athwartships direction, and therefore mutually perpendicular to the X and Y axes; the origin is at the common intersection of the X, Y, and Z axes. Sign conventions for a right hand blade are as follows: values of x are positive forward of the origin, negative aft of the origin; values of y are always positive; values of z are positive to the right of the origin (towards the leading edge), negative to the left of the origin (towards the trailing edge).

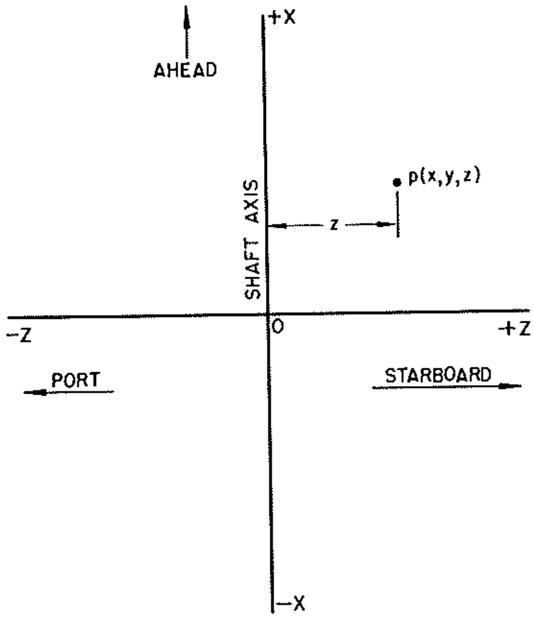

(a) Plan View

where $\bar{i}$, $\bar{j}$, and $\bar{k}$ are the unit vectors along the X, Y and Z axes, respectively. Conversely, for a left hand blade, $\bar{i} \times \bar{j} = -\bar{k}$, $\bar{j} \times \bar{k} = -\bar{i}$, and $\bar{k} \times \bar{i} = -\bar{j}$, which is consistent with a left hand coordinate system. Such use of mathematically consistent systems reduces the chances for error in stress analysis computations, computer programming, and generating software for NC machining.

Quantities such as tangents to curves and normals to surfaces are specified in terms of unit vectors, i.e., $\bar{u} = \alpha\bar{i} + \beta\bar{j} + \gamma\bar{k}$, where $\alpha^2 + \beta^2 + \gamma^2 = 1$. Here $\bar{u}$ is a unit vector specifying a direction in space; $\bar{i}$, $\bar{j}$ and $\bar{k}$ have the meaning specified above; α, β, and γ are the components of the vector along the X, Y, and Z axes, respectively (α, β, and γ are also equivalent to the direction cosines commonly designated as ℓ, m, and n, respectively).

Cylindrical Coordinates (X, R, θ)

Cylindrical coordinates, used for specifying pitchometer measurements, are also convenient for purposes of derivation and computation. As shown in Figure 1, the radius R for any point is the perpendicular distance from the X-axis to that point (note that R is not the distance from the origin to the point). A true view of R is obtained in the Y-Z plane or any plane parallel thereto. Theta is the angle between R and the Y-axis, and is measured in the Y-Z plane (θ is expressed in radians unless otherwise specified). The sign of R is always plus; θ is positive when R is rotated clockwise from the Y-axis, negative when R is rotated counterclockwise.

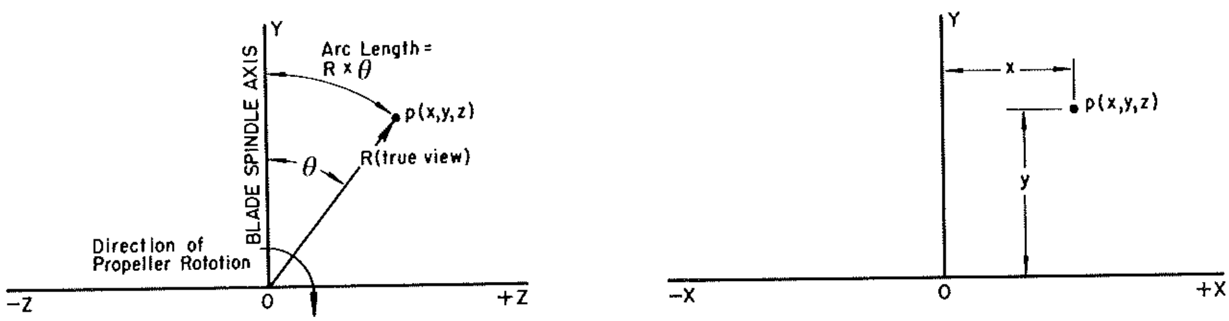

(b) Transverse Elevation

(c) Longitudinal Elevation

Figure 1. Cartesian and cylindrical coordinate system for a right hand blade in the up position in true space.

For a left hand blade, the only change is that z is positive to the left of the origin (still towards the leading edge).

It should be noted that for a right hand blade, a right hand coordinate system is used, i.e., in vector notation $\bar{i} \times \bar{j} = \bar{k}$, $\bar{j} \times \bar{k} = \bar{i}$, and $\bar{k} \times \bar{i} = \bar{j}$,

X has the same meaning as it does for Cartesian coordinates.

For a left hand blade, θ is the only cylindrical coordinate that changes sign.

Expanded View Coordinates (X, $\tilde{Z}$)

If the surface of a cylinder co-axial with the X-axis is flattened as shown in Figure 2, a plane surface results. Lines drawn in such a plane are called expanded views, and distances measured in the plane are sometimes expressed in units of "expanded inches". For convenience, the plane is herein designated the X-$\tilde{Z}$ plane; any point p in the plane has the coordinates (x_p, $\tilde{z}_p$), where x_p has the same value as in Cartesian or cylindrical coordinates, and $\tilde{z}_p = R\theta_p$.

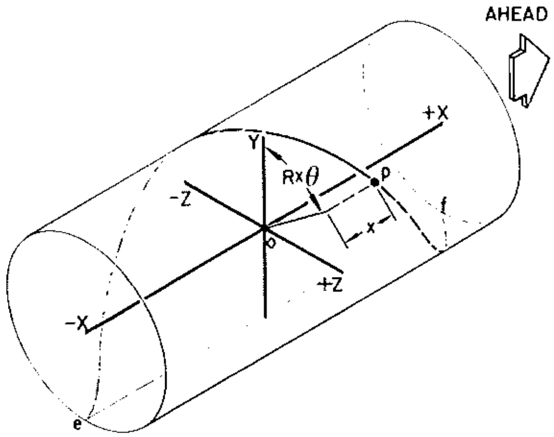

(a) Isometric view of cylindrical surface in true space.

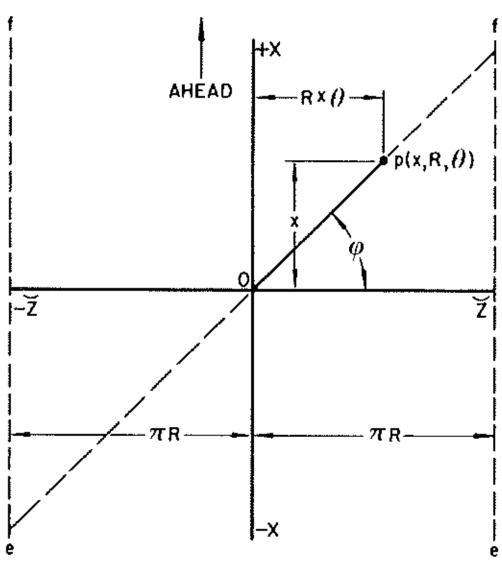

(b) Cylindrical surface after slitting along line e-f and flattening (expanded view)--the X-$\tilde{Z}$ plane.

Figure 2. Development of the X-$\tilde{Z}$ plane from a cylindrical surface.

The following characteristics of points and lines in the X-$\tilde{Z}$ plane are noteworthy:

1. An expanded view is not a true space view.
2. All points in the X-$\tilde{Z}$ plane are at the same radius.
3. As discussed below, a space curve that is a helix in true space becomes a straight line in the X-$\tilde{Z}$ plane. Conversely, any straight line in the X-$\tilde{Z}$ plane is a helix in true space; as limiting cases, the $\tilde{Z}$-axis can be thought of as a pitch helix having zero pitch and the X-axis as a pitch helix having infinite pitch. Line $\overline{Op}$ in Figure 2b represents a typical pitch helix, with a pitch angle equal to ϕ.

Coordinate Relationships

As is evident from Figures 1 and 2, the following relationships exist among the three coordinate systems:

$$y = R \cos \theta \tag{1}$$

$$z = R \sin \theta \tag{2}$$

$$z/y = \tan \theta \tag{3}$$

$$y^2 + z^2 = R^2 \tag{4}$$

$$\tilde{z} = R\theta \tag{5}$$

$$z = \frac{\sin \theta}{\theta} \cdot \tilde{z} \tag{6}$$

Rotation About Spindle Axis

Changing pitch is accomplished by rotating the blade about its spindle axis. This condition is illustrated in Figure 3 for a positive rotation, i.e., one that causes an increase in pitch. The magnitude of the rotation is measured by the angle Ω. A point on the blade originally at location p(x,y,z) will be found at p'(x',y',z') after the rotation. Since the radius r in the X-Z plane remains fixed (see Figure 3),

$$x'_p = r \sin (\gamma + \Omega) \tag{7}$$

$$= x \cos \Omega + z \sin \Omega$$

$$y'_p = y_p \tag{8}$$

$$z'_p = r \cos (\gamma + \Omega) \tag{9}$$

$$= z \cos \Omega - x \sin \Omega$$

$$R'_p = (y_p{}^2 + z'_p{}^2)^{0.5} \tag{10}$$

$$\theta'_p = \arctan (z'_p/y) \tag{11}$$

Note that the rotation causes a change in radius and therefore moves point p out of its original X-$\tilde{Z}$ plane, since (in the general case) a rotation causes a change in the value of z without causing a change in y, and therefore

$R'_p \neq R_p$ (refer to equations 4 and 10).

For rotation in the opposite sense (i.e., to lesser pitch), the sign of the angle Ω becomes negative in equations (7) and (9). The relationships given yield correct algebraic signs for all four quadrants in the X-Z plane.

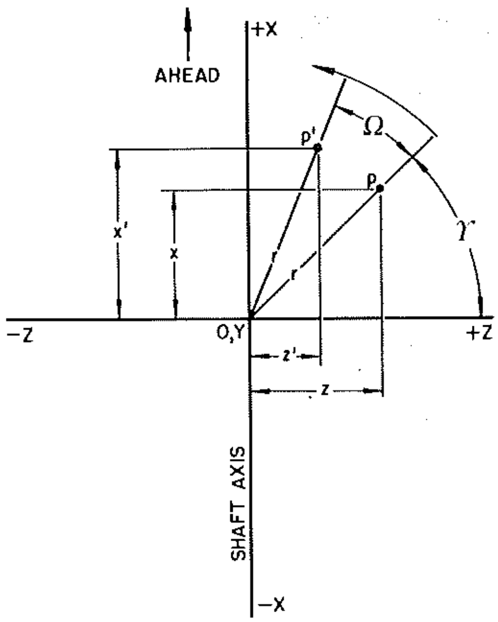

Figure 3. Rotation of blade about Y (spindle) axis.

FOIL SECTION GEOMETRY

As stated earlier, a major item of input for specifying blade geometry is the definition of "sections" at constant radius. The sections used for modern marine propeller blades are basically modified NACA airfoils (3,4), based on forms designated as either NACA 66 (Mod) or NACA 16 (Mod)[1]. Henceforth such shapes will be called simply "foils" or "sections". The steps in achieving suitable foil shapes at a constant radius are shown schematically in Figure 4.

Figure 4a depicts a NACA basic thickness form. This section is symmetrical about the straight line $\overline{LE\text{-}A\text{-}TE}$ joining the leading edge and trailing edge. Line $\overline{U\text{-}A\text{-}L}$ is a typical line perpendicular to $\overline{LE\text{-}A\text{-}TE}$; note that distance $\overline{AU}$ equals distance $\overline{AL}$, with each distance being half the total thickness T corresponding to station A.

Figure 4b shows the same section after "cambering". Line $\overline{LE\text{-}A\text{-}TE}$ is now a curved line, called the camber line; since line $\overline{U\text{-}A\text{-}L}$ is still perpendicular to line $\overline{LE\text{-}A\text{-}TE}$, it is no longer perpendicular to the (straight) nose-tail line, $\overline{LE\text{-}B'\text{-}B\text{-}TE}$.

Figures 4a and 4b represent sections in true space. When Figure 4b is replotted on X-$\breve{Z}$ coordinates, as shown in Figure 4c, the desired constant radius "section" for a propeller blade is obtained. Since the nose-tail line (henceforth designated the chord) in Figure 4c is a straight line on an X-$\breve{Z}$ plot, the chord is a helix in true space, as noted earlier.

The labelling and dimensioning of Figure 4c are intended to include most of the items typically necessary for a complete specification of the geometry of a constant radius section. The camber line, although of great interest to the hydrodynamicist, is not usually shown[2]. A particularly convenient reference point, the midchord, is designated as station "K". Dimensions measured perpendicular to the chord in the X-$\breve{Z}$ plane are called offsets. At station B', for example, distance Y_{SF} is the suction face ("upper") offset, and distance Y_{PF} is the pressure face ("lower") offset. Offsets above the chord are positive, those below the chord are negative; therefore, because of the algebraic sign of Y_{PF}, the total thickness is given as $Y_T = Y_{SF} - Y_{PF}$.

It should be noted that since the offset line $\overline{U'\text{-}B'\text{-}L'}$ in Figure 4c is a straight line on an X-$\breve{Z}$ plot, line $\overline{U'\text{-}B'\text{-}L'}$ is a helix in true space; therefore, the straight line distance between points U' and L' in true space is not exactly equal to the value Y_T shown in Figure 4c.

The information usually given as specification data for each constant radius section, as depicted in X-$\breve{Z}$ plots (expanded views), includes the following items:

1. Chord length, c.
2. Pitch, P, which enables calculation of pitch angle, ϕ.
3. Information which permits calculation of x_K and $\breve{z}_K$, the coordinates of the midchord. Rake and skew, not identified in Figure 4c but discussed below, constitute the additional information required for calculation of x_K and $\breve{z}_K$.

[1] NACA, the National Advisory Committee for Aeronautics, was the predecessor of NASA, the National Administration for Space and Aeronautics.

[2] In the absence of information regarding the basis for the camber line shape, attempts to reconstruct the line can be quite laborious, and the results may be inexact. Camber line information on a propeller blade drawing would be very useful information in some cases.

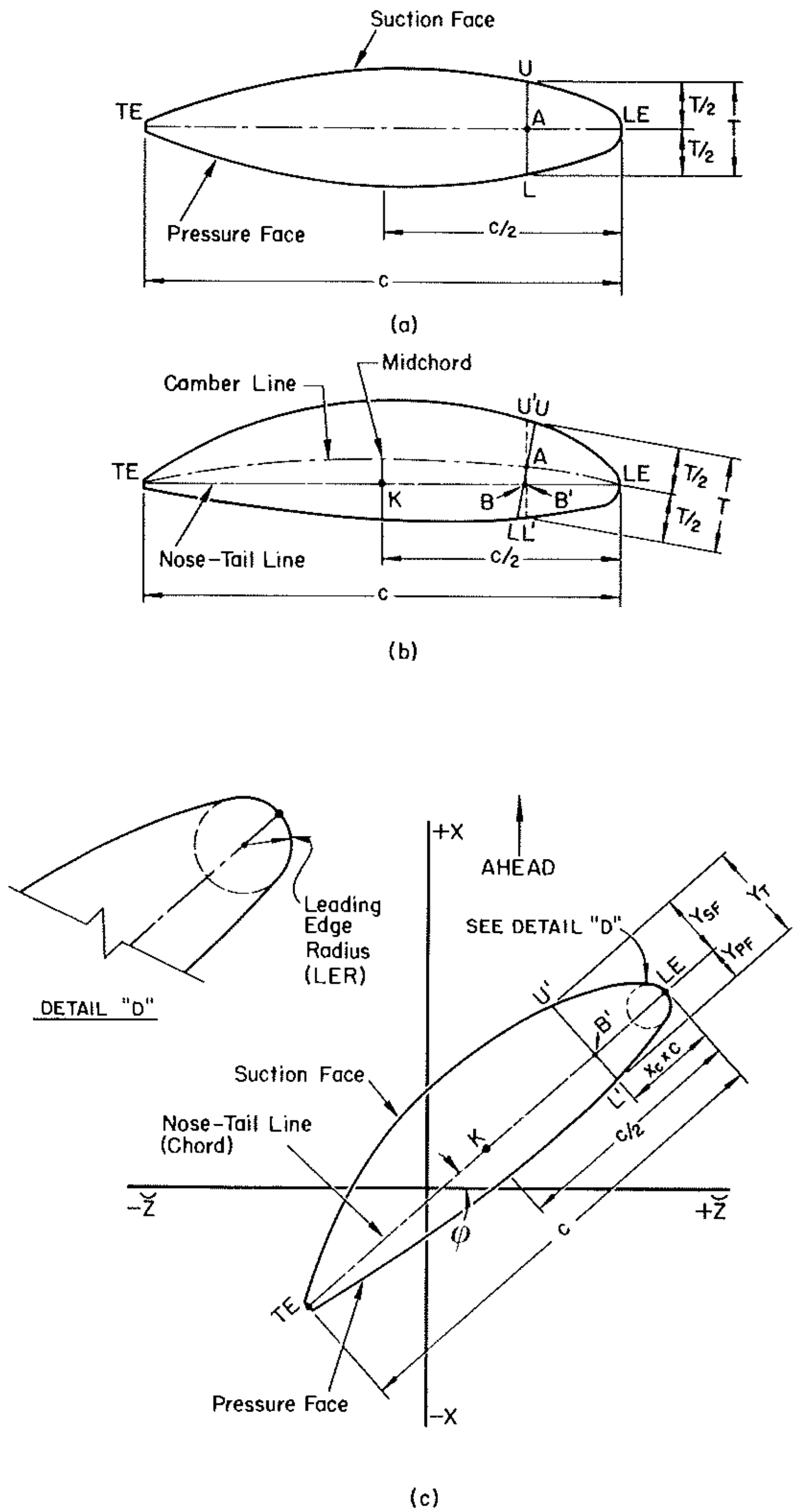

Figure 4. Conceptual steps in achieving a constant radius section in the X-$\breve{Z}$ plane.

4. Offsets for the suction and pressure face contours at stations corresponding to various positions along the chord as distances from the leading edge; these stations are referenced as fractional chord distances, x_C, expressed in percent. For commercial blades, typical stations for offset specifications are as follows, in percent of chord: 0, 2.5, 5, 10, 20, 30, 40, 50, 60, 70, 80, 90, and 100. U. S. Navy drawings give additional stations, especially at the leading and trailing edges. Sections derived from the basic NACA 16 foil shape have their maximum thickness (Y_T) at 50% chord, while those derived from the basic NACA 66 foil shape have their maximum thickness at 45% chord.

5. Leading edge radius (LER). Other details, such as leading edge fairing radius (LEFR) and special trailing edge details, are sometimes given.

THE PITCH HELIX

Basic Relationships

Refer to Figure 2a. Consider the space curve generated by a point p on a line under the following conditions: (a) the distance from the X axis to point p on the line is R; (b) at time t = 0 the line is coincident with the Y axis; (c) starting at time t = 0 the line rotates at a constant angular velocity about the X-axis, while at the same time the line undergoes a translation motion at constant velocity along the X-axis. In terms of cylindrical coordinates (X, R, θ), the coordinates of p at t = 0 are (0, R, 0), and at some later time t the coordinates are (x, R, θ). If C_1, C_2, C_3, and C_4 are constants, then

$$x = C_1 t \tag{12a}$$

$$\theta = C_2 t \tag{12b}$$

and $$x/\theta = C_1/C_2 = C_3 \tag{12c}$$

further $$x/R\theta = C_3/R = C_4 \tag{12d}$$

or $$x/R\theta = \tan\phi \text{ in the X-}\overline{Z}\text{ plane} \tag{12e}$$

Equation 12e can also be written in the form

$$x/\overline{Z} = \tan\phi \tag{12f}$$

The curve generated by point p is a pitch helix; it can be thought of as being traced on the surface of an imaginary cylinder of radius R[3]. Equations 12d and 12f show that in an X-$\overline{Z}$ (expanded) view, the slope, $C_4 = \tan\phi$, of the pitch helix curve is constant, and therefore a pitch helix is a straight line in an X-$\overline{Z}$ plot.

By definition, when $\theta = 2\pi$ (one complete revolution), the point on the line has advanced the distance x = P, equal to the pitch. At that time the coordinates of point p are (P, R, 2π), and equation 12e becomes

$$\tan\phi = P/(2\pi R) \tag{13a}$$

In terms of the dimensionless quantities P/D (local pitch divided by propeller diameter) and fractional radius $x_R = R/R_O$ (local radius divided by propeller radius), the relationship becomes

$$\tan\phi = \frac{P/D}{\pi x_R} \tag{13b}$$

Equations 12e and 13a can be combined into the following useful form for a pitch helix that intersects the Y axis

$$\theta = \frac{2\pi}{P}\,x \tag{14}$$

In the general case, the pitch helix does not intersect the Y axis, and it is necessary to rewrite equation 14 in more general terms (equations 13a and 13b are true for all cases). It is convenient to express the relationship by reference to the cylindrical coordinates of the midchord, (x_K, R, θ_K), as follows:

$$(\theta - \theta_K) = \frac{2\pi}{P}\,(x - x_K) \tag{15}$$

Equations 1-6, 13, and 15 can be combined to give y and z as a function of x as follows:

$$y = R\cos\left(\frac{2\pi x}{P} - \frac{2\pi x_K}{P} + \theta_K\right) \tag{16}$$

$$z = R\sin\left(\frac{2\pi x}{P} - \frac{2\pi x_K}{P} + \theta_K\right) \tag{17}$$

If equation 17 is differentiated to give dz/dx, and the reciprocal, dx/dz, combined with equation 13a, the following relationship is obtained:

$$dx/dz = \tan\phi \cdot \frac{1}{\cos\left(\frac{2\pi x}{P} - \frac{2\pi x_K}{P} + \theta_K\right)} \tag{18}$$

From equations 16 and 4, equation 18 may be written in the forms

---

[3] Exactly the same curve would be scratched on the surface of a real cylinder of radius R if point p were a needle, the line to which p is attached merely translated at the same linear velocity and did not rotate, and the cylinder (instead of the line) rotated at the same angular velocity--in other words, like cutting a screw thread on a lathe.

$$dx/dz = \frac{R}{y} \cdot \tan \phi \qquad (19)$$

and

$$dx/dz = \frac{R}{(R^2 - z^2)^{0.5}} \cdot \tan \phi \qquad (20)$$

The foregoing results lead to the following conclusions regarding the appearance of views of a pitch helix in true space:

1. A projection on the X-Y plane (longitudinal view) is a cosine curve (equation 16).
2. A projection on the X-Z plane (plan view) is a sine curve (equation 17). The tangent to this curve has a slope equal to tan ϕ only when $z = 0$; everywhere else the slope of the curve in the plan view is greater than tan ϕ (equation 20). These attributes of a pitch helix will be germane in the subsequent discussion of the "developed" blade outline.
3. A projection on the Y-Z plane (transverse view) is, of course, a circle.

Rake, Skew and Midchord Location

Much of the terminology used to describe the geometry of marine propeller blades originated at a time when blades were much simpler in geometry than modern designs. Consider a line joining the midchord position of the pitch helix at each radius (this line will henceforth be designated as the "midchord line" or "skew line"). One of the simplest blade geometries occurs when the midchord line is a straight line coincident with the blade spindle axis (Y axis)--such a blade is said to have neither rake nor skew. If the midchord line is rotated about the Z axis, the blade is said to have rake. Since rotation in which the blade tip is moved aft (a negative X motion) was considered "good" from a ship design standpoint, the magnitude of tip motion aft was preceded by a plus sign; conversely, a movement of the tip in the positive X direction was assigned a minus sign.

Movement of the midchord line in the Z (athwartship) direction is related to a quantity called skew. Again, movement in a negative Z direction has been customarily called positive skew, and vice-versa.

The complexity of modern blade geometries often does not permit specifying the midchord line location in space merely by giving the position of the blade tip with respect to some other point, such as the midchord of the blade root section. As stated earlier, a means that is both adequate and convenient from a mathematical standpoint is to give the cylindrical coordinates (x_K, R, θ_K) of the midchord for each constant radius section.

For the purposes of this paper, rake and skew are defined as follows:

Rake, ρ, at a given radius is $(-1) \cdot x_\rho$ for the point (x_ρ, R, 0) on the pitch helix. Percent rake is equal to $-100x_\rho/R$.

Skew, S, at a given radius, is the curvilinear (true) length of pitch helix between the midchord point (x_K, R, θ_K) on the pitch helix, and the point (x_ρ, R, 0) that is either on the pitch helix or on an extension thereof (the true length of a pitch helix is shown, of course, in an X-$\bar{Z}$ plot). The sign of skew is opposite that of θ_K[4].

Examples of combined rake and skew are shown in Figure 5 for chords drawn on the X-$\bar{Z}$ plane. Note that in Figure 5c it has been necessary to extend the chord beyond the leading edge to dimension the skew.

The coordinates of the midchord can be readily calculated from rake, ρ, and skew, S, as follows (see Figure 5 and refer to equations 13 and 13b):

$$x_K = -(S \cdot \sin \phi + \rho) \qquad (21a)$$

or

$$x_K = -\left(\frac{S(P/D)}{[(P/D)^2 + (\pi x_R)^2]^{0.5}} + \rho\right) \qquad (21b)$$

and

$$\theta_K = -S \cdot \cos \phi/R \text{ (radians)} \qquad (22a)$$

or

$$\theta_K = -\frac{2\pi(S/D)}{[(P/D)^2 + (\pi x_R)^2]^{0.5}} \text{ (radians)} \qquad (22b)$$

Tangent to Pitch Helix

For various reasons, such as defining fillet geometry, it is necessary

---

[4] The definition of rake given here has its drawbacks. For example, a blade that has midchord coordinates of (0, R, 0) at every radius would be said to have zero rake and zero skew. Yet, the same blade, when every section is moved aft one inch with respect to the blade spindle axis, would have midchord coordinates of the form (-1, R, 0), and the blade would be said to have a constant rake at each radius of plus one inch, and zero skew.

The choices of algebraic sign used here for rake and skew represent concessions to custom. For computer programming purposes, it is considered more convenient by the author to reverse the signs.

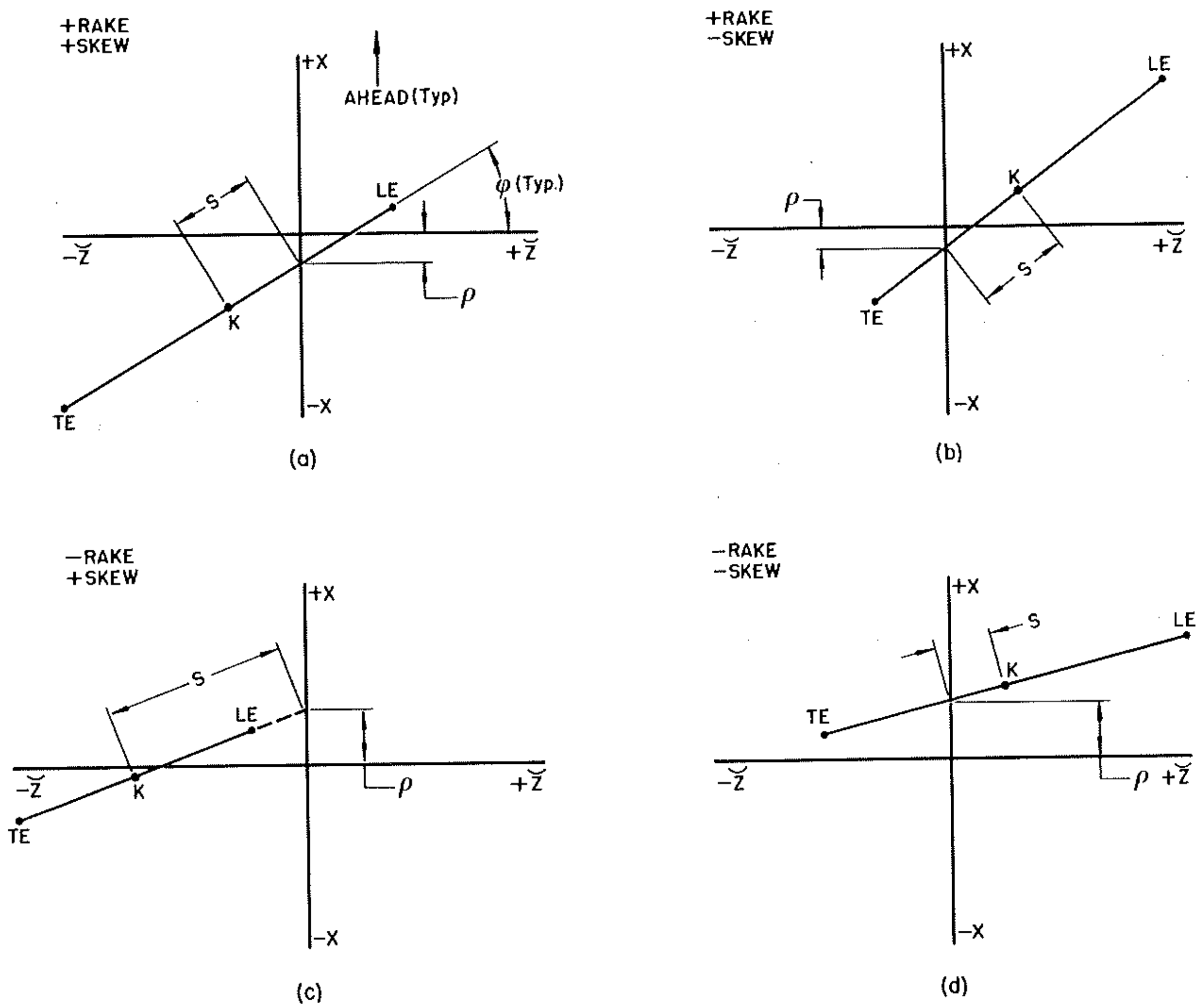

Figure 5. Examples of combined rake and skew.

to specify a plane perpendicular to a pitch helix at a particular point on the helix, i.e., a plane whose normal is the tangent to the pitch helix. In general terms, the tangent $\bar{T}$ to a space curve is the vector defined as

$$\bar{T} = dx\bar{i} + dy\bar{j} + dz\bar{k} \tag{23}$$

From equations 15, 1 and 2, the necessary relationships are obtained:

$$dx = \frac{P}{2\pi}\, d\theta \tag{24}$$

$$dy = -\, R \sin \theta d\theta \tag{25}$$

and

$$dz = R \cos \theta d\theta \tag{26}$$

The unit vector tangent to the pitch helix $\bar{t}$ is given as

$$\bar{t} = \alpha_t\bar{i} + \beta_t\bar{j} + \gamma_t\bar{k} \tag{27}$$

where α_t, β_t, and γ_t are the direction cosines of the unit tangent vector.

$$\bar{t} = \bar{T}/(\bar{T} \cdot \bar{T})^{0.5} \tag{28}$$

and

$$\bar{T} \cdot \bar{T} = (dx\bar{i} + dy\bar{j} + dz\bar{k}) \cdot (dx\bar{i} + dy\bar{j} + dz\bar{k}) \tag{29}$$

or

$$(\bar{T} \cdot \bar{T})^{0.5} = \left[\left(\frac{P}{2\pi}\right)^2 + R^2\right]^{0.5} d\theta \tag{30}$$

Equations 24-30, along with equation 13a, can be combined to give the following results for the direction cosines of the unit vector tangent to a pitch helix at any point (x, R, θ):

$$\alpha_t = \sin \phi \tag{31a}$$

$$\beta_t = -\sin\theta\cos\phi \tag{31b}$$

$$\gamma_t = \cos\theta\cos\phi \tag{31c}$$

Since the relationships of equation 31 are expressed in terms of the pitch angle ϕ, they can be rewritten in terms of pitch or P/D if desired (see equation 13). It should be noted that α_t is a constant for all points on the pitch helix. Also, the tangent for the projection of the pitch helix in the X-Z plane is given by α_t/γ_t; dividing equation 31a by equation 31c and substituting R/y for 1/cos θ leads to the same result as equation 19.

CALCULATION OF COORDINATES

Assume that the following information is available for a constant radius section: radius (R), pitch (P), chord length (c), rake (ρ), skew (S), and offsets (Y_{SF} and Y_{PF}) at known distances from the leading edge. Based on the discussion above, the pitch angle ϕ and midchord coordinates (x_K, R, θ_K) can be calculated, and an expanded view drawn on an X-$\breve{Z}$ plot. A portion of such a plot is shown in Figure 6.

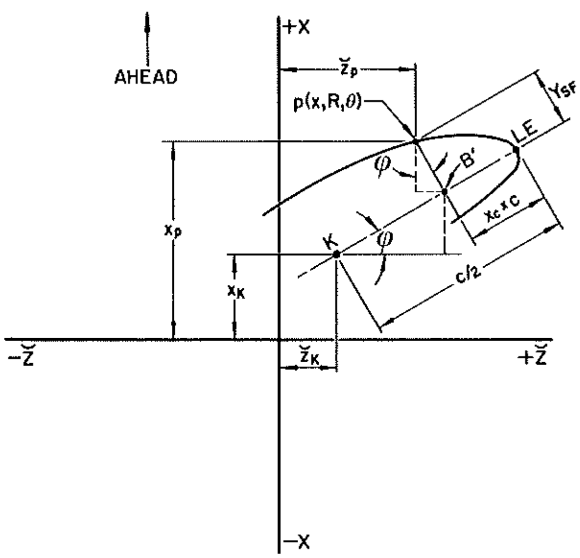

Figure 6. Geometric construction for deriving relationship between values in X-$\breve{Z}$ plane and cylindrical coordinates.

By inspection of Figure 6, the following relationships are seen to be true for a point p (X, R, θ) on the suction face (x_c is the fractional distance along the chord from the leading edge):

$$x_p = x_K + c(0.5 - x_c)\sin\phi + Y_{SF}\cos\phi \tag{32}$$

$$\breve{z}_p = \breve{z}_K + c(0.5 - x_c)\cos\phi - Y_{SF}\sin\phi \tag{33a}$$

or

$$\theta_p = \theta_K + \frac{c(0.5 - x_c)\cos\phi}{R} - \frac{Y_{SF}\sin\phi}{R} \quad \text{(radians)} \tag{33b}$$

$$Y_p = R\cos\theta_p \tag{34}$$

$$Z_p = R\sin\theta_p \tag{35}$$

These equations, plus equation 13 (pitch angle), equation 21 (x_K), and equation 22 (θ_K) give the cylindrical and Cartesian coordinates for any point on the blade surface for which the basic input data have been given. Also, points on the pitch helix are obtained for any percent chord merely by setting the offset Y_{SF} equal to zero.

For the pressure face, the quantity Y_{SF} is replaced by Y_{PF} in equations 32 and 33, i.e.:

$$x_p = x_K + c(0.5 - x_c)\sin\phi + Y_{PF}\cos\phi \tag{36}$$

and

$$\theta_p = \theta_K + \frac{c(0.5 - x_c)\cos\phi}{R} - \frac{Y_{PF}\sin\phi}{R} \tag{37}$$

The sign convention for offsets discussed earlier must be maintained; for example, the offsets for the pressure face of the section illustrated in Figure 4c will have a negative sign, and the product of the terms Y_{PF} and $\cos\phi$ will be negative in equation 36. The relationships presented give correct algebraic signs for all four quadrants of the X-$\breve{Z}$ plane.

INTERPOLATION METHODS

The hydrodynamically-based input data are usually supplied as a series of discreet numbers, rather than as continuous functions that describe the entire surfaces of the blade. When applied only to the input data, the methods described above yield spatial coordinates only at discreet points. Interpolation methods are therefore necessary for obtaining values at intermediate locations.

Approaches

In principle, there are three philosophically-based approaches that can be used. Each approach yields a different set of values for the spatial coordinates at the interpolated locations. Although the differences are usually small, they can be significant.

1. Direct spatial coordinate basis. After the input data have been converted to spatial coordinates (X, Y, Z), all

interpolation is done on the basis of treating each of the coordinates as a function of a suitable variable, such as chord length or radius. The resulting hydrodynamically-related geometry characteristics such as pitch and offsets can be computed at intermediate locations by working "backwards" with equations 32-37, 22, 21, and 13.

2. Physical basis. In this approach, the input data--pitch, rake, skew, offsets, etc.--are interpolated first, and then the resulting spatial coordinates at the intermediate locations computed by working "forwards" with equations 13, 21, 22 and 32-37.

3. Mixed basis. This approach is simply a mixture of the approaches described above.

The first approach is usually most economical from the standpoint of computer execution time, especially when planar sections are required. The second approach has the highest probability of maintaining the hydrodynamic design philosophy throughout the blade--this method is the one used to define all blade surfaces as part of the NC machining effort for the DD963 and FFG-7 blades. The "mixed basis" approach is usually the most convenient one to use from the standpoints of either computer programming or graphical interpolation, but such an approach can lead to inconsistencies.

Graphical Methods

In the absence of access to a computer, graphical methods are a necessity. The deficiencies associated with graphical interpolation usually become rapidly apparent to the practitioner, if not to others.

Analytical Methods

A large amount of literature describing analytical interpolation methods and associated routines is available (see, for example, references 5-7). A brief discussion of the application of some of the methods in defining propeller blade geometry is presented below.

Single Function Representation

Although it is sometimes possible to represent a blade geometry attribute for a given blade design by a single function for the entire blade (e.g., skew versus radius), other important attributes such as offset versus chord length are not well represented by a single function. Accordingly, blade geometry is best described by piecewise functions, which are applicable to any blade design.

Piecewise Function Representation

Piecewise functions connecting input points can be categorized by the continuity of their derivatives and by their usefulness in calculating properties of the propeller blade.

1. Piecewise linear. A piecewise linear approximation for a propeller blade is the simplest and crudest approximation of all. A blade whose surface contours actually conformed to a piecewise linear approximation would be considered hydrodynamically unsuitable. However, piecewise linear representations of a blade are surprisingly good when used for integration (trapezoidal rule), e.g., computing weight, center of gravity, centrifugal forces, and associated moments.

2. Piecewise parabolic, continuous position. Consider a series of n input points designated 1, 2, 3, 4, ...n. If one parabola is passed through points 1, 2, 3, a second through points 3, 4, 5, a third through points 5, 6, 7, etc., the result is a piecewise parabolic representation of a curve connecting all the points. Such a curve is discontinuous in first derivative (slope), and therefore unsuitable for NC machining applications. However, use of piecewise parabolic functions for integration (weight, force, moments, etc.) gives results that are very close to those obtained from the more elaborate procedures described below.

3. Piecewise parabolic, continuous slope. If, in the example above, only the first parabola is passed through three points, and all the others (except the last) through only two points, we can require the parabolas to match slopes where they join each other. This type of interpolation is useful for some NC machining applications.

4. Continuous cubic. Continuous cubic interpolation, also known as "cubic spline" or "chain of cubics" consists of a chain of third degree polynomials of the form $y = a(x - x_i)^3 + b(x - x_i)^2 + c(x - x_i) + d$, where (x_i, y_i) and (x_{i+1}, y_{i+1}) are input points, and y is the calculated interpolated value between y_i and y_{i+1} (7). Continuous cubics give continuous first and second derivatives, a very useful property in connection with 5-axis machining.

Conic Functions

The parabolic and cubic interpolation functions described above cannot provide an infinite slope, such as is required to describe the blade contour at the leading edge. This problem can be overcome by interchanging x and y and by other mathematical manipulations. A very good way of providing for infinite slopes is the use of a generalized conic function of the form $ax^2 + by^2 + cxy + dx + ey + f = 0$. Such functions are used for specification of leading edge, fillets, and tip contours.

Interpolation vs. Fairing

In all of the above discussion on interpolation methods, it has been tacitly assumed that a smooth curve, free of wiggles, hollows, and bumps, can be passed through all of the input points, i.e., no fairing is needed. If a combination of fairing and interpolation is required, the method and computer program given in reference 8 can be adapted.

LENGTH OF SPACE CURVES

In some applications, such as calculating pressure drops in Prairie air channels, it is necessary to know the distance along a space curve associated with a propeller blade. For purposes of computing length, a space curve can be approximated as closely as desired by a piecewise linear curve.

The straight line distance ℓ between any two points in space is given exactly by the expression

$$\ell = [(x_2 - x_1)^2 + (y_2 - y_1)^2 + (z_2 - z_1)^2]^{0.5} \qquad (38)$$

The interpolation routines discussed above are used to generate the Cartesian coordinates of a number of points along the space curve, and the distances between adjoining points are computed and summed. The number of points is then doubled, the length recalculated, and the procedure repeated until the sum has converged to a number having the desired precision. This approach is practical only with the use of a computer or a very good desk calculator.

In the graphical method, a pair of dividers is used to "step off" the curve as shown in the developed view (discussed below). The graphical method does not necessarily converge to a precise curve length, since there can be a cumulative error in the setting of the dividers.

SURFACE NORMALS

The orientation (or "attitude") of a surface at any point is specified by the direction cosines of the unit vector normal to the surface at this point. Surface normals are of importance in stress analysis, experimental load simulation, and NC machining. Three methods--two analytical and one graphical--are presented below for establishing unit vector surface normals. Coordinate mapping is defined first.

Coordinate Mapping

Figure 7a is a schematic three-dimensional plot of a blade face (either suction or pressure). Lines labelled R_1 and R_3 are curves connecting points (x, y, z) on the blade face at input radii R_1 and R_3. Line R_2 is a similar line connecting only interpolated points. Lines C_1 and C_3 connect points whose (x, y, z) coordinates were computed from input data for a common value of chord fraction x_C in equations 36 and 37. Line C_2 is a similar line connecting only interpolated points.

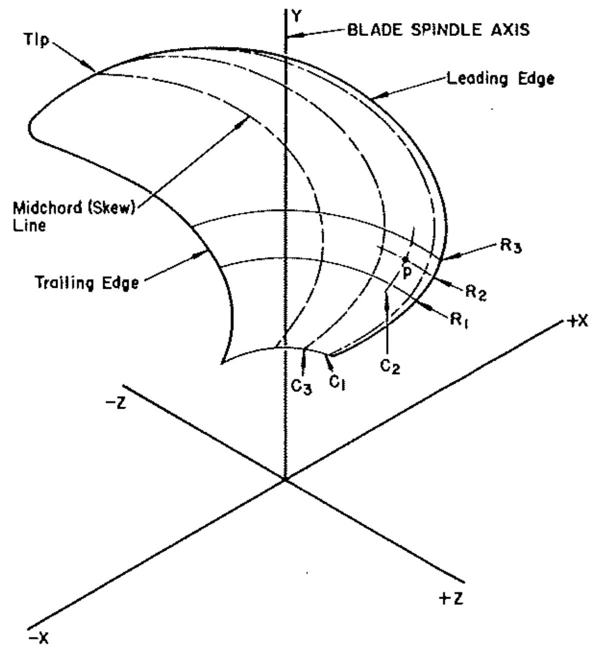

(a) Coordinate Mapping of a Blade Surface Based on Input Points.

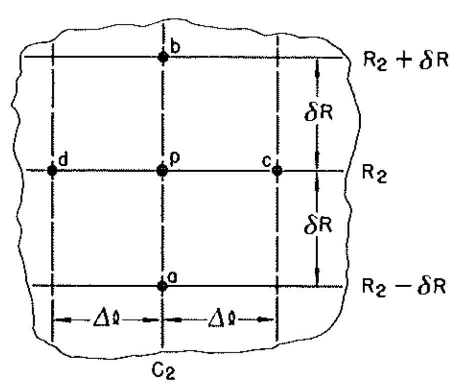

(b) Enlarged View of Blade Surface in Vicinity of Point "p".

Figure 7. Computation of surface normals.

Lines such as R_1 will henceforth be called "iso-R" lines, and lines such as C_1 called "iso-x_C" lines. Figure 7a is a schematic representation of coordinate mapping. Proper coordinate mapping requires two views of the iso-R lines and/or iso-x_C lines, such as the Y-Z view and Y-X views shown in Figure 10. This subject will be discussed further in the section on graphical methods for obtaining planar sections through the blade.

Analytical Methods

In both analytical methods described below, lines R_2 and C_2 in Figure 7a are derived entirely by interpolation functions, as described earlier. A procedure for computing surface normals at point p, the intersection of lines R_2 and C_2 in Figure 7a, then becomes a general method.

Direct differentiation. If the "direct spatial coordinate basis" of interpolation has been used (see section entitled INTERPOLATION METHODS), and if the interpolation functions provide accurate first derivatives, then it is possible to calculate values of dx/dx_C, dy/dx_C and dz/dx_C along line R_2 (i.e., at constant x_R); corresponding values of dx/dx_R, dy/dx_R, and dz/dx_R can be calculated along line C_2 (at constant x_C). The derivatives are then manipulated in a fashion similar to that described in the subsection entitled "Tangent to Pitch Helix" to give at point p the unit vectors $\vec{t}_R$ and $\vec{t}_C$ tangent to lines R_2 and C_2, respectively. The vector cross product $\vec{t}_C \times \vec{t}_R$ then gives the unit vector normal to the blade surface at point p.

Neighboring points. Figure 7b illustrates the basis for the "neighboring points" method of computing surface normals. This method is completely general, and can therefore be used in conjunction with any reliable interpolation method. The interpolation functions are used to compute the (x, y, z) coordinates of points labelled a, b, c and d in the neighborhood of point p. It is important that points a and b be equidistant from p, as measured along the radius or along the Y axis, and that points c and d are also equidistant from point p. It is not necessary that the dimension labelled "$\Delta\ell$" in Figure 7b be equal to that labelled "δR". The normalized cross-product of the vector connecting points a and b with that connecting points c and d in Figure 7b then gives a unit vector normal to the blade surface at point p. The choice of suitable values for $\Delta\ell$ and δR in Figure 7b depends on local blade curvature; care must also be exercised in computer programming to avoid loss of significant figures.

Graphical Methods

A subsequent section of this paper entitled PLANAR SECTIONS describes graphical methods for obtaining planar sections. These methods can be used to construct constant X, constant Y, and constant Z section contours of the blade faces. Graphical construction of normals to the contours through point p of Figure 7 in any two of the mutually perpendicular true views thus obtained allows direct scaling of the vector components of the surface normal.

BLADE OUTLINES AND AREAS

Blade outlines and conventional surface areas are computed on the basis of setting all blade section offsets equal to zero, i.e., a blade of zero thickness all over.

Expanded Outline

An expanded "outline" is not a blade outline in any physical sense; rather it is a plot of radius versus negative skew and radius versus chord length, as shown in Figure 8, which depicts the expanded outline for the FFG-7 blade (9). In the expanded outline the pitch helix is depicted merely as a horizontal line connecting points of constant radius on the leading edge, skew line, and trailing edge.

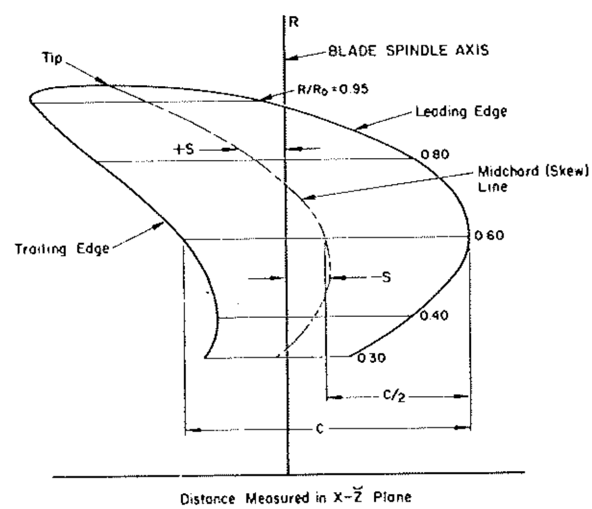

Figure 8. Expanded "outline" of FFG-7 blade.

True Space Outlines

True space outlines are X-Z, Y-Z, and Y-X plots of the blade outline, as shown in Figure 9, a, b, and c for the FFG-7 blade. The coordinates of the points for such plots are obtained from equations 13, 21, 22 and 32-37 for each radius by setting y_{SF} and y_{PF} equal to zero, and selecting the values of x_c (0.0, 0.5, and 1.0) for leading edge, skew line, and midchord. It is also desirable to plot the entire chord (pitch helix) for several values of fractional radius; the points for such plots are obtained simply by choosing a suitable series of values for x_c in equations 32-37. The calculations for such plots can be made quite simply and rapidly with a modern desk calculator.

The outline view in the X-Z plane is not given in most blade drawings. However, this view can be very useful, since it provides the basis for an obvious rapid graphical method for rotation about the Y axis (changing pitch).

Developed Outline

A developed outline represents an

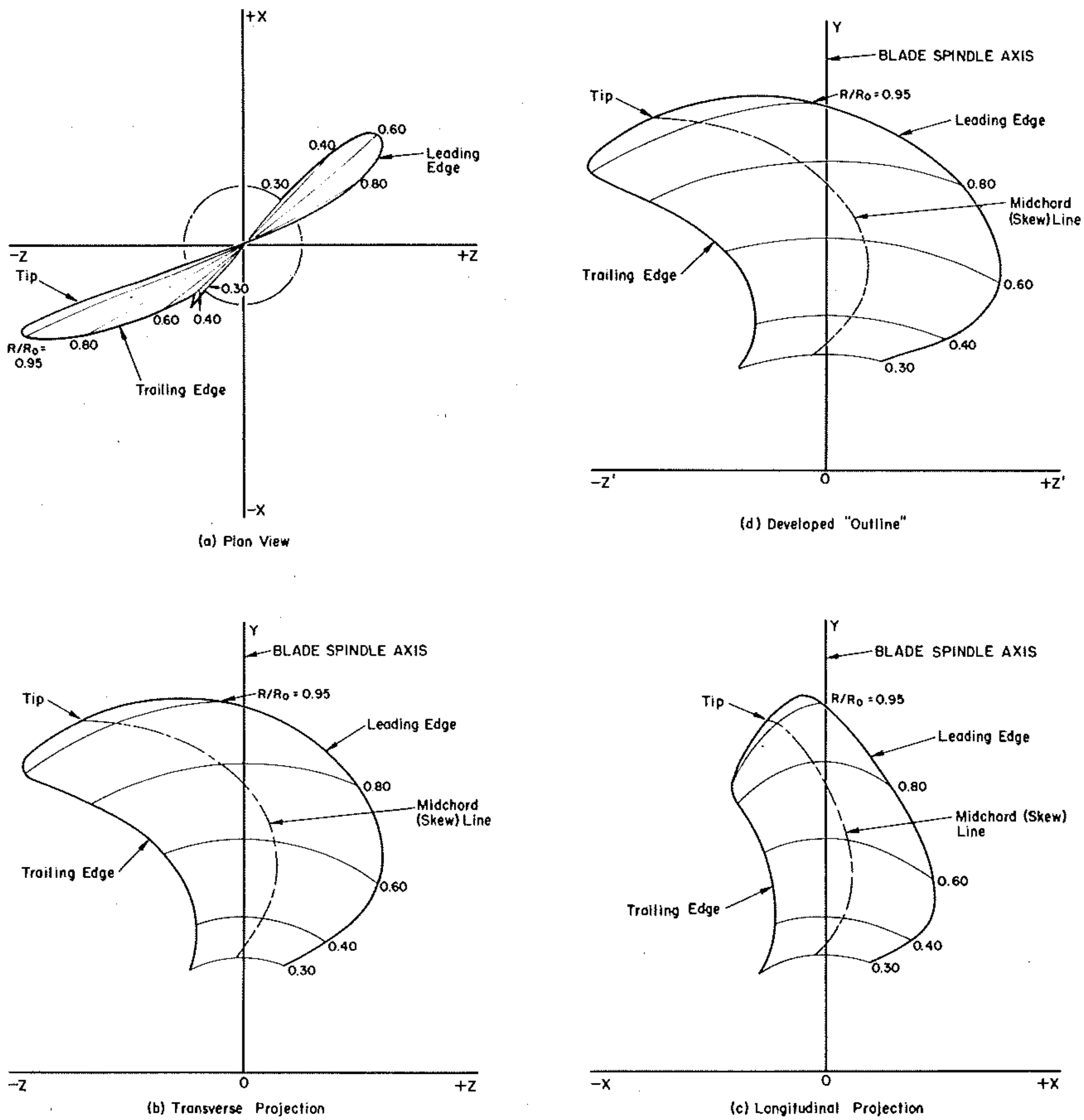

Figure 9. Views of blade outline, midchord, and pitch helices.

attempt to portray the shape of the two-dimensional body that would be obtained if it were possible to flatten a blade having uniformly zero thickness into a planar figure. The developed outline is obtained by rotating each pitch helix about the Y axis an amount equal to the pitch angle for that helix, i.e., by applying equations 7-9 to the (x, y, z) coordinates obtained for the true space outlines described above and plotting Y versus Z' as shown in Figure 9d. A value of the angle Ω equal to the pitch angle ϕ for each radius is used. For the reasons cited in the previous discussion of the basic geometric properties of the pitch helix, the values of X' obtained by this method are not constant for a set of coordinate points that represent a constant radius at design pitch.

Dimensions measured a relatively short distance from any point within a developed outline are approximately equal to true point-to-point dimensions. The developed outline is therefore useful for applications such as piecewise linear approximations of the lengths of space curves (such as the leading edge), and showing the location and dimensions of weld repair areas.

Propeller Areas

Several indices of the surface area (one side only) of a propeller blade can be calculated. In keeping with convention in the following discussions, the area per blade is multiplied by the number of blades Z to give the total propeller-related area in each case.

Expanded area. The expanded area A_E is the surface area of a blade contained within expanded outline, or, equivalently, the area under the curve of total chord length versus radius. In terms of chord length c, fractional radius x_R, and the value of x_R for the blade root radius h,

$$A_E = ZR_O \int_h^{1.0} c\,dx_R \tag{39}$$

or $$A_E = ZR_O \int_{0.0}^{1.0} [(x_R)_2 - (x_R)_1]\,c\,dx_C \tag{40}$$

where $(x_R)_2$ and $(x_R)_1$ are the bounds of vertical lines within the expanded outline (Figure 8). It is readily apparent that equation 39 is much simpler to evaluate analytically than equation 40, since chord length is always a single valued function of radius, whereas radius is a double valued function of chord length. In general, double valued functions should be avoided, if possible, in analytical evaluations of propeller blade geometry.

Projected area. The projected area is that area contained within the transverse projection outline, Figure 9b. Since each line of constant radius is an arc of a circle in this outline, the analytical expression for projected area can be written as

$$A_P = 2ZR_O{}^2 \int_h^{1.0} (\theta_{LE} - \theta_K)\,x_R\,dx_R \tag{41}$$

where θ_{LE} is the value of theta at the leading edge.

From Figure 5 it is also apparent that an equivalent expression for projected area is

$$A_P = ZR_O \int_h^{1.0} c \cos\phi \, dx_R \tag{42}$$

Developed area. The developed area A_D is that area contained within the developed outline, Figure 9d. As a consequence of the definitions used in each case, the value of developed area is slightly less than that of expanded area; for most purposes it suffices to set $A_D \simeq A_E$. If a more precise value of developed area is required, a method similar to that described below for calculating the true surface area can be used.

True surface area. All of the blade areas discussed above have been for blade shapes whose geometry has been simplified by setting the blade section offsets equal to zero, i.e., blades of zero thickness all over. True surface areas, which will not be the same for the suction and pressure faces of a blade, are evaluated by integrating the length of the space curve representing the locus of points at constant radius on the blade surface with respect to radius. The steps in the procedure are as follows (LE = leading edge, TE = trailing edge):

1. Use a suitable interpolation routine (preferably continuous cubics) to generate a dense array of Cartesian coordinates for points on the blade surface at each input (design) radius.
2. Use equation 38 to calculate each value of ℓ_{ij}, the distance between points j and j + 1 on the ith radius.
3. For each radius compute

$$L_i = \sum_{j=LE}^{j=TE} \ell_{ij}$$

4. Compute the true area of the surface in question (times the number of blades) as

$$A_T = ZR_O \int_h^{1.0} L_i\,dx_R \tag{43}$$

BLADE PASSING

When a propeller having a high blade area ratio is specified, the possibility exists that the leading edge of one blade may interfere with the trailing edge of an adjacent blade during pitch changes (9). Such potential interference during blade passing is usually of concern only at radii near the root. It should be noted that if the blade has skew at the root radii, interferences during blade passing (if they exist) will occur between leading and trailing edge points that are at <u>different</u> radii when the blades are set at design pitch.

A rapid, approximate method for assessing the probability of interference during blade passing is to make a layout of two adjacent developed outlines on a propeller hub. For a five-bladed propeller, for example, the spindle axes of the two developed outlines are placed 72 degrees apart. This method is inexact, since the developed outline presents near-maximum values of R' for leading and trailing edges for all radii simultaneously.

The analytical criteria for interference during blade passing may be formulated in terms of the cylindrical coordinates of the leading and trailing edges after blade rotation about the spindle axis by the angular amount Ω. Consider a pair of points (X'_{LE}, R'_{LE}, θ'_{LE}) and (x'_{TE}, R'_{TE}, θ'_{TE}) (see equations 7-11). If there exists any pair of points for any value of Ω such that

(a) $x'_{LE} = x'_{TE}$

and (b) $R'_{LE} = R'_{TE}$

and (c) $\theta'_{TE} + \dfrac{2\pi}{Z(\text{no. blades})} \leq \theta'_{LE}$

there will be interference during blade passing. A convenient method of applying the above criterion is to plot θ'_{LE} and $(\theta'_{TE} + 2\pi/Z)$ versus R' for a series of values of Ω, where $\Omega \simeq -\phi_{ROOT}$.

MASS, CG, FORCES AND MOMENTS

Basis

The computation procedures described in the following discussion are intended to be applicable to a blade set at any pitch rather than just design pitch.

Consider some attribute of the blade associated with its geometry, such as tipping and twisting moments resulting from centrifugal forces. At any point in the blade, the contribution of an elemental volume to the effect being calculated depends on the coordinates of that point (x', y', z'). If the attribute in question is denoted by the letter U, then in mathematical terms U is a function of the off-design pitch position coordinates x', y', z', as well as other parameters. However, since the off-design pitch position coordinates are related to the design pitch coordinates by continuous functions (equations 7-11), it is proper to compute the numerical value of the quantity $\delta^2U/(\delta x_R \delta x_C)$ at each point as a function of x', y', z' and perform a double numerical integration along the original (unprimed) chord lengths and radii to obtain the desired answer.

The steps for carrying out this procedure are given in general terms as follows:

1. For each input constant radius section, and at each input station on that section, calculate the primed coordinates associated with Y_{SF} and Y_{PF}, the suction and pressure face offsets for that station.
2. Evaluate (numerically) the quantity $\delta^2U/(\delta x_R \delta x_C)$ at each point.
3. Use numerical integration methods (preferably based on the interpolation routines discussed earlier) to evaluate

$$\frac{\delta U}{\delta x_R} = \int_{0.0}^{1.0} \left(\frac{\delta^2 U}{\delta x_R \delta x_C}\right) dx_C$$

for each input radius.
4. Use numerical integration methods to evaluate

$$U = \int_{h}^{1.0} \frac{\delta U}{\delta x_R}\, dx_R$$

where h is the value of x_R at the blade root.

Mass

An elemental volume of the blade is obtained by forming the product $(Y_{SF} - Y_{PF}) \cdot (c\,dx_C) \cdot (R_O dx_R)$. The expression for mass then becomes

$$W = \rho R_O \int_{h}^{1.0}\int_{0.0}^{1.0} c(Y_{SF} - Y_{PF}) dx_C dx_R \qquad (44)$$

where ρ is the mass density. Mass is, of course, independent of pitch setting.

Center of Gravity

In the discussion below, the subscripts s and p denote coordinates calculated from suction and pressure face offsets, respectively. By definition and from equations 44 and 10, the coordinates of the center of gravity are given as

$$(x')_g = \frac{\rho R_O}{W} \int_{h}^{1.0}\int_{0.0}^{1.0} c(Y_{SF} - Y_{PF}) \cdot \left(\frac{x'_s + x'_p}{2}\right) dx_C dx_R \qquad (45)$$

$$(y')_g = \frac{\rho R_O}{W} \int_h^{1.0}\int_{0.0}^{1.0} c(Y_{SF} - Y_{PF}) \cdot \left(\frac{y's + y'p}{2}\right) dx_C dx_R \qquad (46)$$

$$(z')_g = \frac{\rho R_O}{W} \int_h^{1.0}\int_{0.0}^{1.0} c(Y_{SF} - Y_{PF}) \cdot \left(\frac{z's + z'p}{2}\right) dx_C dx_R \qquad (47)$$

$$(R')_g = [(y')_g^2 + (z')_g^2]^{0.5} \qquad (48)$$

Since the center of gravity does not change its position with respect to the blade during pitch changes, the center of gravity can be calculated at design pitch and then simply rotated with the blade during pitch changes.

Centrifugal Force

Since the centrifugal force can be calculated on the basis of having the entire mass concentrated at the center of gravity, equations 44-48 provide the basis for all of the computations required; therefore, the magnitudes of the forces are given as

$$F_{Y'} = W\omega^2 (y')_g \qquad (49)$$

$$F_{Z'} = W\omega^2 (z')_g \qquad (50)$$

and $$F_{R'} = W\omega^2 (R')_g \qquad (51)$$

There is, of course, no component of centrifugal force in the X direction.

Centrifugal Force Moments

Since the moments associated with centrifugal force cannot be treated as though the force acts at the center of gravity, the contribution of each elemental volume must be computed and summed. In formulating the required equations, which form the basis for subsequent computer program statements, care must be exercised to obtain proper algebraic signs for the contribution of each elemental volume. Use of the formal vector cross product definition of moment in a right hand coordinate system satisfies the requirement. In terms of the radius vector from the origin $\overline{OR}$ and the element of force $d\overline{F}_{R'}$, the moment is given by

$$d\overline{M} = \overline{OR} \times d\overline{F}_{R'} \qquad (52)$$

where $$\overline{OR} = \frac{x's + x'p}{2}\,\overline{i} + \frac{y's + y'p}{2}\,\overline{j} + \frac{z's + z'p}{2}\,\overline{k} \qquad (53)$$

and $$d\overline{F}_{R'} = dF_{Y'}\overline{j} + dF_{Z'}\overline{k} \qquad (54)$$

Carrying out the multiplication we find

$$d\overline{M}_X = \left[\frac{(y's + y'p)}{2}\, dF_{Z'} - \frac{(z's + z'p)}{2}\, dF_{Y'}\right]\overline{i} \qquad (55)$$

$$d\overline{M}_Y = -\frac{(x's + x'p)}{2}\, dF_{Z'}\overline{j} \qquad (56)$$

$$d\overline{M}_Z = \frac{(x's + x'p)}{2}\, dF_{Y'}\overline{k} \qquad (57)$$

A complete expression for the magnitude of $\overline{M}_Y$ the (twisting) moment about the blade spindle axis is

$$M_Y = -\omega^2 \rho R_O \int_h^{1.0}\int_0^{1.0} c(Y_{SF} - Y_{PF}) \cdot \frac{(z's + z'p)}{2} \cdot \frac{(x's + x'p)}{2}\, dx_C dx_R \qquad (58)$$

Similar expressions can be written for M_X and M_Z, the (upsetting) moments about the X and Z axes, respectively.

PLANAR SECTIONS

Planar sections through the blade are necessary and/or desirable for many applications. Examples of such applications include determination of section modulus in stress calculations, establishing a meaningful basis for fillet and tip details, layout of Prairie air channels, design of support tooling for NC machining, and building patterns for castings. After the spatial coordinates of the blade surfaces have been determined (equations 32-37), either analytical or graphical methods can be used to establish the contours of a planar section.

Sectioning Plane Definition

A useful form for the definition of a plane is the equation

$$ax + by + cz + d = 0 \qquad (59)$$

where the coefficients a, b and c are the direction cosines of the unit vector normal to the plane. The quantity d is determined by requiring the plane to pass through a point whose coordinates are known or can be calculated.

For graphical work a sectioning plane is shown in a given view by the trace of the intersection of the sectioning plane with the viewing plane. The trace is readily constructed by passing a straight line through two axis intercepts. From equation 59 it is evident that the X-axis intercept = -d/a, the Y-axis intercept = -d/b, and the Z-axis intercept = -d/c.

Analytical Methods

All analytical methods consist of finding a series of unique (x, y, z) coordinate points on each blade surface that satisfy the equation for the defining plane. In the general case, a plane can be required to pass through a maximum of three input points; therefore, essentially all points representing the intersection of the sectioning plane and the blade surfaces are interpolation points. Consequently, as a practical matter, analytical methods require the use of a computer.

A straightforward method (albeit "brute force") for finding the points of intersection consists of a converging trial and error approach. In this method, the unknown point is located in an interval somewhere between two known boundaries. The interval is divided into two halves, and a test applied to establish in which half the unknown point lies. Repeated application of this procedure locates the unknown point within any precision desired.

If the "direct spatial coordinate basis" of interpolation is used (see INTERPOLATION METHODS), quadratic or cubic interpolation equations can be solved directly for the answer as soon as the location of the point in question has been narrowed down to a particular set of interpolation equations.

Graphical Methods

Under the section entitled SURFACE NORMALS, a procedure for coordinate mapping was described. The graphical method of obtaining planar sections consists simply of determining the intersection in two views of the traces of the sectioning plane with either the iso-R lines, or the iso-x_c lines, or both. It will be recalled that the points for the iso-R and iso-x_c lines derived from the input points can be readily computed with a modern desk calculator.

An illustration of the graphical method of obtaining planar sections is given in Figure 10, which shows some of the iso-x_c lines for the FFG-7 blade pressure face. The points for the iso-R lines are shown for some of the radii, but these points are not connected, since iso-R lines are not required for the example illustrated. The sectioning plane has the simple equation Y = H (the value for H is 66.0 inches in Figure 10), i.e., a constant Y plane. For each intersection point a-g the Z and X coordinates are read from Figures 10a and 10b, respectively. Figure 10c shows the resulting constant Y pressure face contour--the suction face contour is also shown as a matter of interest.

Reference Lines

If the sectioning plane is not perpendicular to one of the coordinate axes, it is desirable to define a reference line in the sectioning plane. The blade contours on the section can then be specified in terms of offset distances from the reference line, as well as by the spatial coordinates of points on the contours. The basis for choosing the location of the reference line is often somewhat arbitrary.

FILLET AND TIP DETAILS

Since fillet and tip details are not usually defined in terms of constant radius "sections", it is necessary to specify these details in terms of true planar sections.

Fillets

From a structural integrity standpoint, a reasonable basis for specifying the defining planes for fillet details is to require that they be perpendicular to the root pitch helix. For a point f on the root pitch helix having the coordinates (x_f, y_f, z_f), it follows from equations 1, 2 and 31 that the equation for a plane normal to the pitch helix and passing through the point (x_f, y_f, z_f) may be written as

$$(\sin \phi_h) \cdot (x - x_f) - \frac{z_f}{R_f}(\cos \phi_h)y + \frac{Y_f}{R_f}(\cos \phi_h)z = 0 \qquad (60)$$

where ϕ_h is the pitch angle for the root pitch helix.

Fillets are usually specified in terms of a compound radius, such as a 3T and T/3 blend, where $T = (Y_{SF})_f - (Y_{PF})_f$. The blade contours and fillet radii must lie in a plane such as that defined by equation 60 for the fillet specification to have physical meaning. The use of a compound radius leads to a discontinuity in second derivative at the three tangency points--blade-to-3T, 3T-to-T/3, and T/3-to-flange. Consequently, for purposes of 5-axis NC machining, the compound radius is replaced by a closely matching conic section, as discussed earlier.

Tip Details

The tip must be specified and dimensioned in true space coordinates, i.e., the details must be shown on a true planar section. A reasonable defining plane is one that passes through the tip and is perpendicular to the pitch helix at the tip. The equation for this plane is the same as equation 60, except that the subscript f

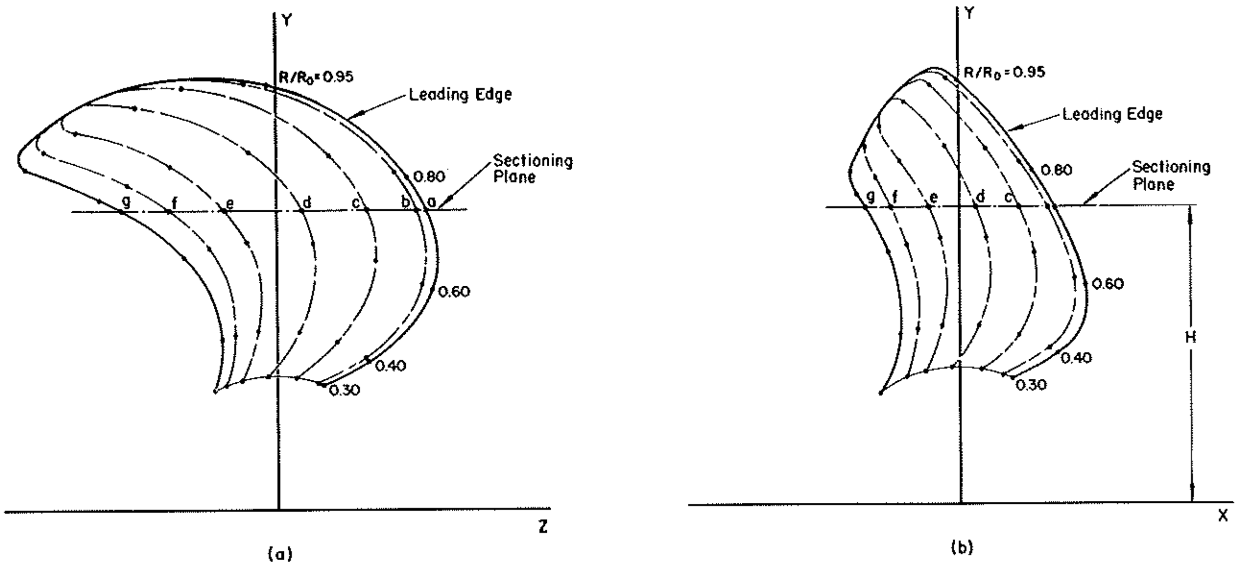

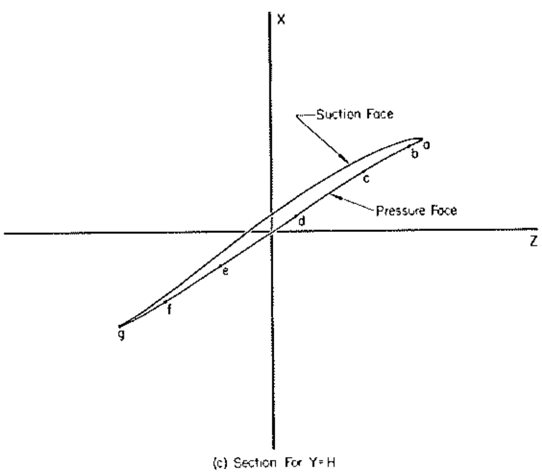

Figure 10. Use of coordinate mapping to construct constant Y planar section.

now refers to the tip.

OTHER APPLICATIONS

The concepts discussed above concerning the defining of propeller blade geometry in terms of coordinate systems have led to other applications in blade technology. A brief discussion of three of these applications follows.

Blade Flange Layout

For centering the blade root sections with respect to the bolt circle in the flange, constant Y sections near the root can be overlaid on a drawing (X-Z view) of the flange.

Pattern Construction

Wooden patterns to be used for foundry work can be made fairly simply by the following procedures.

1. Each suction face offset in the table of offsets is increased by the cleanup allowance; the pressure face offsets are decreased algebraically the same amount (because of the difference in algebraic sign between Y_{SF} and Y_{PF}). Although this procedure leads to errors in cleanup allowance, the error is rather small everywhere except at the leading edge where it may be as much as 10 or 20 percent of the cleanup allowance. However, most patterns are made deliberately oversize near the edges, eliminating the problem.

2. Spatial coordinates are calculated based on the revised offsets.

3. Constant Y sections are determined at, say, two-inch intervals of Y.

4. The pattern is assembled from flat lumber cut to the constant Y sections that have been laid out with a shrink rule.

5. The pattern can be assembled and checked at an off-design pitch setting, which makes the pattern more accessible than one constructed at design pitch.

Dimensional Checking

Model propeller blades, full size castings in the as-cast condition, and finish machined blades can be accurately checked dimensionally without the use of a pitchometer or cylindrical template gages. To achieve high accuracy, the blade is rotated to a suitable off-design setting (zero pitch at the 0.7 radius works very well), and the measured (x', y', z') coordinates compared with the computed theoretical coordinates.

ACKNOWLEDGMENTS

The author wishes to express his appreciation to John A. Norton of Bird-Johnson Company, and Tim Schauermann, Ken Bakke, and Fred Kernbach of Boeing Computer Services, for their helpful discussions and ideas.

REFERENCES

1. D. E. Ridley and R. C. Case, "Controllable Pitch Propellers in the DD-963; A Status Report", presented at the ASME Gas Turbine Conference and Products Show, Zurich, Switzerland, March 30 - April 4, 1974.

2. Dean A. Rains, "DD963 Power Plant", Marine Technology, January, 1975.

3. I. H. Abbott and A. E. Von Doenhoff, Theory of Wing Sections, New York, Dover Publications, Inc., 1959.

4. Terry Brockett, "Minimum Pressure Envelopes for Modified NACA-66 Sections with NACA a = 0.8 Camber and Buships Type I and Type II Sections", DTMB Report 1780, February, 1966.

5. B. Carnahan, H. A. Luther, and J. O. Wilkes, Applied Numerical Methods, New York, John Wiley & Sons, Inc., 1969.

6. G. Forsythe and C. B. Moller, Computer Solution of Linear Algebraic Systems, Englewood Cliffs, New Jersey, Prentice-Hall, 1967.

7. Curtis F. Gerald, Chapter 13, Applied Numerical Analysis, Reading, Massachusetts, Addison-Wesley Press, 1970.

8. A. H. Fowler and C. W. Wilson, "Cubic Spline, A Curve Fitting Routine", Union Carbide Corporation Nuclear Division, Y-12 Plant Report Y-1400, Revision 1, June, 1966, (available from National Technical Information Service, Springfield, Virginia, 22151).

9. S. B. Denny, H. A. Themak, and J. J. Nelka, "Hydrodynamic Design Considerations for the Controllable-Pitch Propeller for the Guided Missile Frigate", Naval Engineers Journal, April, 1975.

DISCUSSION PAPER No. 11

J. K. WILLIAMS, CDR, USN (Philadelphia Naval Shipyard): I would like to beg Mr. Klein's indulgence, as I intend to deviate somewhat from the written discussion which I mailed to him, because I've learned a lot in the last two days. Also, I represent those two invidious groups mentioned periodically during the symposium - the manufacturer and the operator, and I appreciate the opportunity to present comments from those viewpoints.

There have been two underlying themes throughout the symposium -

> We can't define the load, and we can't define the geometry.

Messrs. Tsakonas and Jacobs presented an excellent approach to the first of these problems yesterday afternoon.

Mr. Klein's paper is a most significant and most welcome approach to the specification of propeller geometry. Since April 1972, Philadelphia Naval Shipyard has had a five-axis numerically controlled propeller profiler, and has wrestled with exactly the same problems discussed in this paper - compounded by the fact that Philadelphia has been manufacturing integral casting N-bladed propellers. This further complicates the problem in that collisions between the cutting tool and blades adjacent to the blade being machined must be prevented, either by mathematical modeling or by trial and error when tool motions are programmed. Also, as Mr. Klein points out, standard propeller definition leaves many undefined areas - such as blending fillets and edge and tip details - the blending is done by the manufacturer.

Since commencing numerically controlled manufacture of propellers, Philadelphia has been a proponent of closed form mathematical modeling of propellers - piecewise continuous, if need be - but eliminating the use of offsets as the defining element. David Watson Taylor Naval Ship Research and Development Center and Philadelphia Naval Shipyard are now working on a complete propeller definition, but it <u>follows</u> propeller design rather than <u>precedes</u> it. In these days of higher transcendental functions, infinite series and ultra sophisticated computers, we feel that it is not unreasonable to ask that the designer consider modernized techniques, which will facilitate not only manufacture, but stress and hydrodynamic analysis. We have seen many approaches to finite element analysis recently. The reason there are so many methods is the same as the reason there are so many techniques of doing numerical integrals and numerical integration of differential equations - none of them are any good. If there were only one generally applicable method, everybody would be using it. With an analytically and completely defined geometry, everyone benefits - not only can the designer perform his structural analyses, he could use cathode ray tube computer graphics to actually display his product in varying orientations and detect cusps and discontinuities himself, rather than have them pointed out by a mechanic or parts programmer. The mathematical model could be sliced or sectioned in any way desired, leading to reduced manufacturing costs by providing pitchometer readings in R, θ, and X, which can be compared digitally to readings on the actual hardware, rather than laborious layouts and hand sculpting to fitted gages. Blueprints and gage plans for repair activities not having N/C or computer capabilities could be produced at minimal cost.

Speaking of costs, to digress for a moment, I would like to commend all the previous authors for their concern about computer costs and program efficiency - however, I think you gentlemen are looking through the wrong end of the telescope - the major costs are in manufacturing and operation. If a 200% increase in design costs leads to a 2% reduction in manufactuing cost, the increase will more than pay for itself. Gentlemen, I am beginning to suspect that we, the manufacturer, spend more undoing what the designer did in order to be able to make a propeller than the designer spends designing it in the first place.

As an operator, let me tell you that <u>one docking</u> to replace a broken, damaged, or poorly designed propeller costs more than 100 times the few seconds of computer time in question in comparisons of the various finite element methods.

Admittedly, much of this could be done using the present methods of propeller definition - if you, the designer, are content to let us, the manufacturer, select the interpolation and fairing techniques which will describe over 99% of the blade surface.

Mr. Klein is to be highly commended for his original publication of this method. It should serve as a catalyst for designers to transfer their conceptual design to detail design for manufacture, because it provides the mathematical framework upon which propeller design engineers can build closed form models of propellers.

I would like to present a call to action to SNAME that a committee be formed to continue the efforts begun in this paper because of the many benefits that it offers to all of us.

The tools are there, gentlemen, and we at Philadelphia feel that the time has come for the propeller designer to use them to specify completely his design intent in a way that provides for a minimum order of error when it is translated into hardware at a reduced production cost.

TERRY BROCKETT (Naval Ship Research and Development Center): The screw propeller is one of the most complex shapes of engineering interest known to man. Its design geometry is specified in a helical reference framework with non-orthogonal coordinates. This complex geometry has caused a significant delay in application of fundamental principles to design and analysis of propellers. Curiously, to date there has been no paper devoted exclusively to propeller geometry. The author is to be congratulated on filling this void with a timely, well-written paper which obviously reflects extensive practical application of the general results presented.

At the Naval Ship Research and Development Center, we are currently developing a capability of propeller blade-surface definition similar to that described in the paper. We are also convinced the "Physical Basis" of interpolation described by the author best preserves the designer's intent and are using this throughout our work. We use cubic splines to represent the radial variations of chord length, pitch, total rake, skew angle, and maximum thickness-to-chord and camber-to-chord ratios. Our blade-section shapes are currently composed of mean-line and thickness forms for which analytical specification exists. Hence our dependence on numerical techniques is somewhat less than described by the author. We have also found small but potentially measurable differences in the coordinates at interpolated points depending on which radial variable is used for the interpolation, e.g., skew back vs skew angle.

Our major problem to date has been in specification of blade edge details. The analytic functions for section shape include rounded leading edges but the trailing-edge and blade-tip details are often arbitrary decisions and reflect conflicting criteria. Further discussion of how the author handled the merging of these edge details would be a welcome addition to the paper.

The results of our investigation will be used by the Philadelphia Naval Shipyard (PNSY) to aid in the N-C manufacture of propellers. Since PNSY already has an outstanding capability to manufacture propellers by hand, a prime motivation of N-C machining is to decrease the cost of manufacture. Personnel at PNSY tell us it is not cost effective to machine the blade to final size by N-C methods. Perhaps the author would relate some of his experience with the cost of final machining vs machining to a point which requires only minor hand work to grind the surfaces smooth and shape the leading edge.

As a final point of discussion, we point out a minor error in the paper: the determination of surface areas. Equation (40) of the paper is difficult to interpret and equation (43) is incomplete. The element of surface area may be obtained by taking the absolute value of the vector cross product of two tangent vectors to the surface obtained by differentiation of the position vector of points on the surface. The two differential elements of length are along the independent coordinates. Using the author's notation one finds:

$$A = z \int_h^{1.0} dx_R \int_0^{1.0} \left| \bar{t}_c \times \bar{t}_R \right| dx_c \qquad (1)$$

Brockett (Ref. 1, eqn 1.10 and 1.11) gives values for $\bar{N} = \bar{t}_c \times \bar{t}_R$ when finite offsets exist and for zero section offsets. For zero offsets, see Equation (2) below.

Using this expression one obtains the developed surface area which is seen to be always greater than or equal to the expanded area since the square root is always greater than or equal to 1. A similar but more complex equation applies to the true surface area.

In conclusion, let me say again that this paper describing the pioneering work done by the author is a welcome addition to the propeller related literature.

Reference:

1. Brockett, T.E., "Propeller Perturbation Problems," Naval Ship R&D Center Report 3880, Oct. 1972.

$$|\bar{N}| = C R_0 \sqrt{1 + \left\{ 2\frac{c}{D}(x_c - 0.5)\frac{d\frac{P}{D}}{dx_R}\frac{\cos^2\phi}{\pi x_R} - \frac{1}{R_0}\frac{dx_K}{dx_R}\cos\phi - x_R\frac{d\theta_K}{dx_R}\sin\phi \right\}} \qquad (2)$$

LYSSIMACHOS VASSILOPOULOS (Marine Vibration Associates): Since the last paper on propeller geometry appears to have been written more than thirty years ago[1], interest on this subject in the intervening period can, at best, be described as dormant. This refreshing paper will therefore be most welcome by propeller theorists, designers and manufacturers as they make increasing use of modern lifting surface theory, finite element techniques and numerically controlled machining. A consistent and unified approach to propeller geometry is badly needed and Mr. Klein is to be congratulated for reviving the subject.

Although we have been using the same coordinate systems as the author[2,3], these are by no means universally adopted, and I therefore believe it would be worthwhile for all those concerned with propellers that a set of well-defined systems be adopted as standard. For example, the most often used (in this country, at least) steady and unsteady lifting surface theories[4,5] make use of different systems, with the result that the user is forced to perform unnecessary coordinate transformations.

I would like to suggest that an ad-hoc panel be formed by the Society to study the standardisation of symbols and terminology of propellers in consultation with classification societies and the International Towing Tank Conference.

The terms rake and skew have been ill-defined for a long time and Mr. Klein's proposals are a step in the right direction. However, since skew and rake are now known to be significant blade attributes in their own right, I feel that blade distortions must be more precisely defined, and I would venture to offer the following:

(a) Rake, at any radius, is the fore-and-aft (or x-coordinate) of the mid-chord point K, positive forward; it is not clear in this paper what point is used to define rake.

(b) Warp, in the sense defined by Nelka[6], is the angular displacement of K in the x=0 plane, measured positive clockwise from the Y-axis; and

(c) Skew is the curvilinear length along the pitch helix, from the Y-axis to K.

With such definitions, a blade can then be thought of as being either raked, or warped or both, i.e. skewed; with Mr. Klein's definitions rake and skew are not independent.

The section on interpolation techniques is useful and we are currently using such techniques in the development of a computer program that will generate automatically the propeller drawing, after the lifting-surface-theory stage of design is completed. In this connection, it is agreed that an x-z view of the blade is very useful and we have included it along with the conventional transverse and elevation views.

Some minor points and questions that come to mind after reading this paper are as follows:

(a) For monobloc propellers the orientation of the blade relative to the Y-axis appears to be arbitrary and should perhaps be standardised. A reasonable convention would be to let the Y-axis (or directrix or blade reference line) pass through O and the mid-chord point K at the "root" section;

(b) Would Mr. Klein care to comment as to where along the hub length the hub radius, r_H is defined?

(c) The assumption $A_D \approx A_E$ is rather crude and should be used only for very rough estimates;

(d) The paper would be enhanced if suitable formulae for the propeller moments and products of inertia about O and along different axes were supplied by Mr. Klein in his reply.

My thanks to the author for a thought-provoking and useful paper!

References:

1. Riddle, A.W., "Modern Screw Propeller Geometry", Association of Engineering and Shipbuilding Draughtsmen, England, 1942.

2. Bradshaw, R.T. and Vassilopoulos, L., "The Propeller Blade Structural Problem and Its Solution by Finite Element Techniques," New England Section, SNAME, 21 January 1972

3. Vassilopoulos, L., "Centrifugal Loads on Propeller Blades," International Shipbuilding Progress, vol. 20, no. 232, December 1973, p. 441

4. Kerwin, J.E., "Computer Techniques for Propeller Blade Section Design," Second Lips Propeller Symposium, Drunen, Holland, May 1973

5. "Techniques for Estimating Vibratory Forces Generated by Propeller," SNAME, Technical & Research Bulletin 1-34, January 1975

6. Nelka, J.J., "Experimental Evaluation of a Series of Skewed Propellers with Forward Rake: Open Water Performance, Cavitation Performance, Field-Point Pressures, and Unsteady Propeller Loading," NSRDC Report 4113, July 1974.

J. LESTER KLEIN (Author): The author wishes to thank Commander Williams, Dr. Brockett, and Mr. Vassilopoulos for their reviews and discussions of his paper.

Commander Williams' comments can perhaps be paraphrased concisely as follows: "We are living in the 1970's, not some earlier age. Let's define, specify, and verify propeller blade geometry accordingly, so that the producer can manufacture propellers conforming to the hydrodynamicist's design by using production methods and procedures that are sensible and economical."

The author, with no effort whatsoever, can recall his own annoyances and frustrations when first attacking the problem of specifying the DD963 propeller blade geometry in terms suitable for all parties concerned with the results of his efforts. It is easy to sympathize with the feelings and opinions expressed by Commander Williams in his discussion, since the author's company has the responsibility for producing the DD963 propeller blades. Commander Williams' call for action to SNAME to continue the efforts begun in this paper is endorsed by the author.

Dr. Brockett has raised several specific points:

1. A request for additional details in defining the geometry of transition areas such as the trailing edge and tip regions.
2. A question concerning the relative costs of NC machining of blades to finish dimensions versus NC machining oversize followed by hand finishing;
3. ambiguity in the meaning of equation 40;
4. lack of completeness in equation 43; and,
5. meaning of developed area.

Dr. Brockett is quite correct in stating that there are some areas of the blade where there are no quantitative hydrodynamic bases for specifying the blade geometry. For hand-made blades, the manufacturer is instructed to make the transition areas "fair," in which case no two blades are precisely the same. For specifying blade geometry for NC machining, the author has adopted the following self-imposed guidelines:

1. Avoid sudden changes in blade shape to reduce the danger of premature cavitation.
2. In the mathematical definition of the transition areas, preserve continuity of the zeroth and first derivative at all times, and preserve continuity in the second derivative whenever possible. For example, the use of conic functions rather than compound radii preserves the continuity of the second derivative -- such continuity is lacking when compound radii are used. Also, avoid wiggles.
3. Be sure that all geometry definitions are programmable.
4. Be sure that the resulting geometry is machinable. Many full scale and enlarged scale computer-generated plots are required to obtain this assurance.

An example of this approach is the treatment used for the trailing edge of the FFG-7 class (Guided Missile Frigate) blade. At the blade root (corresponding to a fractional radius of approximately 0.321 at the trailing edge overhang), the trailing edge is fully rounded (by specification); at the 0.40 fractional radius, the trailing edge is a fully developed chisel edge (by specification). A transition between these two geometries is required. For purposes of geometry definition, the trailing edge was considered to consist of three parts, as portrayed in an expanded view: (1) the chisel edge flat; (2) a fairing radius between the flat and the suction face; and, (3) a fairing radius between the flat and the pressure face.

The chisel edge flat is characterized by two parameters between the 0.321 and 0.40 radii: (a) its length, and (b) the angle between the flat and the tangent to the pressure face contour at a position corresponding to a fractional chord distance of 1.0. For convenience, the angle between the flat and the pitch helix was used as a defining parameter. By specification, the length of flat and angle of the flat with the pitch helix are fixed at the two extremes of the transition region, i.e., the 0.321 radius and the 0.40 radius. For example, at the 0.321 radius the length of flat is 0.000 inch, and the flat makes an angle of 90 degrees with the pitch helix. At the 0.40 radius, the length of flat and angle with the pitch helix turn out to be 2.500 inches and 24.951 degrees, respectively. Arbitrary, smooth functions are then assigned to the length of flat and angle with the pitch helix between the two end points of the transition region.

Correspondingly, arbitrary, smooth functions are also assigned to connect the specified end points for the fairing radii joining the suction and pressure faces to the flat. Finally, the fairing radii are replaced by closely matching conic functions.

The final check is a series of computer-generated plots of the trailing edge at closely spaced intervals of fractional radius. Discontinuities or other problem areas become readily apparent if they exist.

For Dr. Brockett's second question--the relative costs of NC machining to finish dimensions versus NC machining oversize followed by hand finishing -- the author has no firsthand basis for making a comparison, and therefore is unable to answer the question.

Dr. Brockett also points out that equation 40 is difficult to interpret. He is quite correct, since equation 40 is incorrectly stated in the paper. The proper formulation of equation 40 is

$$A_E = 2R_O \int_{0.0}^{c_{max}} [(x_R)_2 - (x_R)_1] dc \qquad (40)$$

where c_{max} is the maximum value of chord length. For most marine propeller blades, c_{max} occurs at a value of x_R less than unity. Equation 39 corresponds to obtaining the area under the curve (suitably bounded) of chord length versus fractional radius, where fractional radius is the abscissa and chord length the ordinate. Equation 40 represents the area for the same plot, except that chord length is now the abscissa and fractional radius the ordinate.

Dr. Brockett is also correct in stating that equation 43 is incomplete for calculating true surface area. A suitable expression for true surface area is

$$A_T = 2R_O \int_h^{1.0} L_i \left(\frac{\delta s}{\delta R}\right)_i dx_R \qquad (43)$$

where the additional factor $\left(\frac{\delta s}{\delta R}\right)_i$ is the ratio (always ≥ 1.0) of the change in length along a line (on the blade surface) of constant percent chord to a change in radius; at each line of constant radius, the quantity $(\delta s/\delta R)_i$ represents an average value along the line of constant radius.

Finally, Dr. Brockett states that his equation shows that the developed area is always greater than or equal to the expanded area, whereas the author states (page 11-15) that the developed area is slightly less than that of the expanded area. The difference in the two statements results from a difference in definition of developed area. In Dr. Brockett's definition of developed area (implicit in his discussion and equations), the developed area is the area of the surface resulting merely by setting all offsets equal to zero; such a surface is non-planar in the general case. In the author's definition (page 11-15), "The developed area A_D is the area contained within the developed outline, Figure 9d.". The author's developed outline, as defined in the paragraph beginning on page 11-14 is a planar surface.

Mr. Vassilopoulos has raised several points, some of which concern terminology, especially the meaning of rake and skew. From the author's standpoint, rake and skew are merely an indirect means (along with pitch) for locating the midchord position of the pitch helix. Rake is defined by the author (top of page 11-8) as ".... (-1) · x_p for the point (x_p, R, 0) on the pitch helix.". Since the point (x_p, R, 0) is a point for which $\theta = 0$ (and, correspondingly, Z = 0), rake has therefore been defined as the negative value of X for the point at which the pitch helix pierces the X-Y plane.

The replies to Mr. Vassilopoulos' other comments and questions are as follows:

1. The hub radius, r_H, is established along the hub at a point where X = 0, i.e., in the Y-Z plane.
2. The author does not agree with Mr. Vassilopoulos' statement that "the assumption $A_D \approx A_E$ is rather crude." For example, in the FFG-7 blade, $A_D = 0.985A_E$.
3. Finally, Mr. Vassilopoulos requests additional formulas comparable to equation 58, which gives the magnitude of $\overline{M}_Y$, the (twisting) moment about the blade spindle axis attributable to centrifugal force. The magnitude of $\overline{M}_X$, the (upsetting) moment about the shaft axis, is obviously zero, since the line of action of the centrifugal force attributable to each elemental mass in the blade must pass through shaft (X) axis (zero moment arm); this result is also readily obtained by evaluating equation 55. However, for purposes of stress analysis it is of importance to compute the upsetting moment about an axis defined by the equations y = a, z = 0, i.e., about an axis in the X-Y plane parallel to the X-axis and displaced from it by a distance "a" along the Y-axis. If we let M_a designate the magnitude of this moment, then

$$M_a = -\omega^2 \rho R_O a \int_h^{1.0}\int_0^{1.0} c(Y_{SF} - Y_{PF}) \frac{(z'_s + z'_p)}{2} dx_c dx_R \qquad (58a)$$

From equation 57,

$$M_Z = \omega^2 \rho R_O \int_h^{1.0}\int_0^{1.0} c(Y_{SF} - Y_{PF}) \cdot \frac{(y'_s + y'_p)}{2} \cdot \frac{(x'_s + x'_p)}{2} dx_c dx_R \qquad (58b)$$

Anexo 3. Marine propellers and propulsión. Extent of the Wageningen B-screw series. John Carlton

muy buen paper, con la geometría de la serie B, y los Kt Kq.

http://teacher.buet.ac.bd/mmkarim/B_Series_Propeller.pdf

Table 6.4 Extent of the Wageningen B-screw series (taken from Reference 6)

Blade number (Z)	*Blade area ratio A_E/A_O*														
2	0.30														
3		0.35			0.50			0.65			0.80				
4			0.40			0.55			0.70			0.85	1.00		
5				0.45			0.60			0.75				1.05	
6					0.50			0.65			0.80				
7						0.55			0.70			0.85			

6.5.1 Wageningen B-screw series

This is perhaps the most extensive and widely used propeller series. The series was originally presented in a set of papers presented by Troost (References 3 to 5) in the late 1940s and, amongst many practitioners, is still referred to as the 'Troost series'. Over the years the model series has been added to so as to provide a comprehensive fixed pitch, non-ducted propeller series. From analysis of the early results it was appreciated that a certain unfairness between the various design diagrams existed and this was considered to result from the scale effects resulting from the different model tests. This led to a complete re-appraisal of the series in which the differences in test procedures were taken into account and the results of this work were presented by van Lammeren *et al.* (Reference 6).

The extent of the series in terms of a blade number versus blade area ratio matrix is shown in Table 6.4 from which it may be seen that the series numbers some 20 blade area–blade number configurations. The geometry of the series is shown in Table 6.5, from which it can be seen that a reasonably consistent geometry is maintained between the members of the series with only a few anomalies; notably the non-constant nature of the face pitch near the root of the four-blade series and the blade outline of the three-bladed propellers. For completeness purposes Figure 6.11 shows the geometric outline of the B5 propeller set. Note that the propellers of this series are generally referred to by the notation $BZ \cdot y$, where B denotes the 'B'-series, Z is the blade number and y is the blade expanded area. The face pitch ratio for the series is in the range 0.6 to 1.4.

The results of the fairing exercise reported by Oosterveld paved the way for detailed regression studies on the performance characteristics given by this model series. Oosterveld and van Oossanen (Reference 7) reported the findings of this work in which the open water characteristics of the series are represented at a Reynolds number 2×10^6 by an equation of the following form:

$$\left.\begin{aligned} K_Q &= \sum_{n=1}^{47} C_n (J)^{S_n} (P/D)^{t_n} (A_E/A_O)^{u_n} (Z)^{v_n} \\ K_T &= \sum_{n=1}^{39} C_n (J)^{S_n} (P/D)^{t_n} (A_E/A_O)^{u_n} (Z)^{v_n} \end{aligned}\right\} \qquad (6.17)$$

where the coefficients are reproduced in Table 6.6.

To extend this work further so that propeller characteristics can be predicted for other Reynolds numbers within the range 2×10^6 to 2×10^9 a set of corrections of the following form was derived:

$$\begin{Bmatrix} K_T(R_n) \\ K_Q(R_n) \end{Bmatrix} = \begin{Bmatrix} K_T(R_n = 2 \times 10^6) \\ K_Q(R_n = 2 \times 10^6) \end{Bmatrix} + \begin{Bmatrix} \Delta K_T(R_n) \\ \Delta K_Q(R_n) \end{Bmatrix} \qquad (6.18)$$

where

$$\begin{aligned} \Delta K_T = {} & 0.000353485 \\ & - 0.00333758\,(A_E/A_O)J^2 \\ & - 0.00478125\,(A_E/A_O)(P/D)J \\ & + 0.000257792(\log R_n - 0.301)^2 \cdot (A_E/A_O)J^2 \\ & + 0.0000643192(\log R_n - 0.301)(P/D)^6 J^2 \\ & - 0.0000110636(\log R_n - 0.301)^2 (P/D)^6 J^2 \\ & - 0.0000276305(\log R_n - 0.301)^2 Z(A_E/A_O)J^2 \\ & + 0.0000954(\log R_n - 0.301)Z(A_E/A_O)(P/D)J \\ & + 0.0000032049(\log R_n - 0.301)Z^2(A_E/A_O) \\ & \quad \times (P/D)^3 J \end{aligned}$$

$$\begin{aligned} \Delta K_Q = {} & -0.000591412 \\ & + 0.00696898(P/D) \\ & - 0.0000666654Z(P/D)^6 \\ & + 0.0160818(A_E/A_O)^2 \\ & - 0.000938091(\log R_n - 0.301)(P/D) \\ & - 0.00059593(\log R_n - 0.301)(P/D)^2 \\ & + 0.0000782099(\log R_n - 0.301)^2(P/D)^2 \\ & + 0.0000052199(\log R_n - 0.301)Z(A_E/A_O)J^2 \\ & - 0.00000088528(\log R_n - 0.301)^2 Z(A_E/A_O) \\ & \quad \times (P/D)J \\ & + 0.0000230171(\log R_n - 0.301)Z(P/D)^6 \\ & - 0.00000184341(\log R_n - 0.301)^2 Z(P/D)^6 \\ & - 0.00400252(\log R_n - 0.301)(A_E/A_O)^2 \\ & + 0.000220915(\log R_n - 0.301)^2(A_E/A_O)^2 \end{aligned}$$

The Wageningen series is a general purpose, fixed pitch, non-ducted propeller series which is used extensively for design and analysis purposes. A variant of the series, designated the BB-series, was introduced, since it was felt that the B-series had tip chord lengths that were not entirely representative of modern practice. Accordingly the BB-series had a re-defined blade outline with wider tips than the parent form. However, the BB-series, of which only a few members exist, has not been widely used.

Table 6.5 Geometry of the Wageningen B-screw series (taken from Reference 7)

Dimensions of four-, five-, six- and seven-bladed propellers

r/R	$\frac{c}{D}\cdot\frac{Z}{A_E/A_O}$	a/c	b/c	$t/D = A_r - B_rZ$	
				A_r	B_r
0.2	1.662	0.617	0.350	0.0526	0.0040
0.3	1.882	0.613	0.350	0.0464	0.0035
0.4	2.050	0.601	0.351	0.0402	0.0030
0.5	2.152	0.586	0.355	0.0340	0.0025
0.6	2.187	0.561	0.389	0.0278	0.0020
0.7	2.144	0.524	0.443	0.0216	0.0015
0.8	1.970	0.463	0.479	0.0154	0.0010
0.9	1.582	0.351	0.500	0.0092	0.0005
1.0	0.000	0.000	0.000	0.0030	0.0000

Dimensions for three-bladed propellers

r/R	$\frac{c}{D}\cdot\frac{Z}{A_E/A_O}$	a/c	b/c	$t/D = A_r - B_rZ$	
				A_r	B_r
0.2	1.633	0.616	0.350	0.0526	0.0040
0.3	1.832	0.611	0.350	0.0464	0.0035
0.4	2.000	0.599	0.350	0.0402	0.0030
0.5	2.120	0.583	0.355	0.0340	0.0025
0.6	2.186	0.558	0.389	0.0278	0.0020
0.7	2.168	0.526	0.442	0.0216	0.0015
0.8	2.127	0.481	0.478	0.0154	0.0010
0.9	1.657	0.400	0.500	0.0092	0.0005
1.0	0.000	0.000	0.000	0.0030	0.0000

A_r, B_r = constants in equation for t/D.
a = distance between leading edge and generator line at r.
b = distance between leading edge and location of maximum thickness.
c = chord length of blade section ar radius r.
t = maximum blade section thickness at radius r

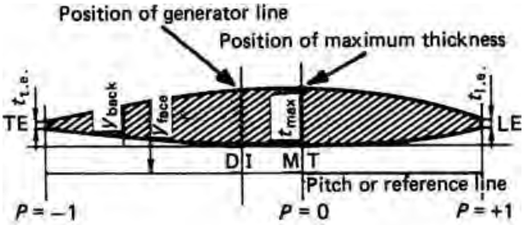

LE = leading edge
TE = trailing edge
MT = location of maximum thickness
DI = location of directrix

$$\left.\begin{aligned} Y_{face} &= V_1(t_{max} - t_{t.e.}) \\ Y_{back} &= (V_1 + V_2)(t_{max} - t_{t.e.}) + t_{t.e.} \end{aligned}\right\} \text{for } P \le 0$$

and

$$\left.\begin{aligned} Y_{face} &= V_1(t_{max} - t_{l.e.}) \\ Y_{back} &= (V_1 + V_2)(t_{max} - t_{l.e.}) + t_{l.e.} \end{aligned}\right\} \text{for } P \ge 0$$

Referring to the diagram, note the following:

Y_{face}, Y_{back} = vertical ordinate of a point on a blade section on the face and on the back with respect to the pitch line.
t_{max} = maximum thickness of blade section.
$t_{t.e.r}, t_{l.e.}$ = extrapolated blade section thickness at the trailing and leading edges.
V_1, V_2 = tabulated functions dependent on r/R and P.
P = non-dimensional coordinate along pitch line from position of maximum thickness to leading edge (where $P = 1$), and from position of maximum thickness to trailing edge (where $P = -1$).

Values of V_1 for use in the equations

r/R P	−1.0	−0.95	−0.9	−0.8	−0.7	−0.6	−0.5	−0.4	−0.2	0
0.7–1.0	0	0	0	0	0	0	0	0	0	0
0.6	0	0	0	0	0	0	0	0	0	0
0.5	0.0522	0.0420	0.0330	0.0190	0.0100	0.0040	0.0012	0	0	0
0.4	0.1467	0.1200	0.0972	0.0630	0.0395	0.0214	0.0116	0.0044	0	0
0.3	0.2306	0.2040	0.1790	0.1333	0.0943	0.0623	0.0376	0.0202	0.0033	0
0.25	0.2598	0.2372	0.2115	0.1651	0.1246	0.0899	0.0579	0.0350	0.0084	0
0.2	0.2826	0.2630	0.2400	0.1967	0.1570	0.1207	0.0880	0.0592	0.0172	0
0.15	0.3000	0.2824	0.2650	0.2300	0.1950	0.1610	0.1280	0.0955	0.0365	0

r/R P	+1.0	+0.95	+0.9	+0.85	+0.8	+0.7	+0.6	+0.5	+0.4	+0.2	0
0.7–1.0	0	0	0	0	0	0	0	0	0	0	0
0.6	0.0382	0.0169	0.0067	0.0022	0.0006	0	0	0	0	0	0
0.5	0.1278	0.0778	0.0500	0.0328	0.0211	0.0085	0.0034	0.0008	0	0	0
0.4	0.2181	0.1467	0.1088	0.0833	0.0637	0.0357	0.0189	0.0090	0.0033	0	0
0.3	0.2923	0.2186	0.1760	0.1445	0.1191	0.0790	0.0503	0.0300	0.0148	0.0027	0
0.25	0.3256	0.2513	0.2068	0.1747	0.1465	0.1008	0.0669	0.0417	0.0224	0.0031	0
0.2	0.3560	0.2821	0.2353	0.2000	0.1685	0.1180	0.0804	0.0520	0.0304	0.0049	0
0.15	0.3860	0.3150	0.2642	0.2230	0.1870	0.1320	0.0920	0.0615	0.0384	0.0096	0

Table 6.5 (cont)

Values of V_2 for use in the equations

r/R P	−1.0	−0.95	−0.9	−0.8	−0.7	−0.6	−0.5	−0.4	−0.2	0
0.9–1.0	0	0.0975	0.19	0.36	0.51	0.64	0.75	0.84	0.96	1
0.85	0	0.0975	0.19	0.36	0.51	0.64	0.75	0.84	0.96	1
0.8	0	0.0975	0.19	0.36	0.51	0.64	0.75	0.84	0.96	1
0.7	0	0.0975	0.19	0.36	0.51	0.64	0.75	0.84	0.96	1
0.6	0	0.0965	0.1885	0.3585	0.5110	0.6415	0.7530	0.8426	0.9613	1
0.5	0	0.0950	0.1865	0.3569	0.5140	0.6439	0.7580	0.8456	0.9639	1
0.4	0	0.0905	0.1810	0.3500	0.5040	0.6353	0.7525	0.8415	0.9645	1
0.3	0	0.0800	0.1670	0.3360	0.4885	0.6195	0.7335	0.8265	0.9583	1
0.25	0	0.0725	0.1567	0.3228	0.4740	0.6050	0.7184	0.8139	0.9519	1
0.2	0	0.0640	0.1455	0.3060	0.4535	0.5842	0.6995	0.7984	0.9446	1
0.15	0	0.0540	0.1325	0.2870	0.4280	0.5585	0.6770	0.7805	0.9360	1

r/R P	+1.0	+0.95	+0.9	+0.85	+0.8	+0.7	+0.6	+0.5	+0.4	+0.2	0
0.9–1.0	0	0.0975	0.1900	0.2775	0.3600	0.51	0.6400	0.75	0.8400	0.9600	1
0.85	0	0.1000	0.1950	0.2830	0.3660	0.5160	0.6455	0.7550	0.8450	0.9615	1
0.8	0	0.1050	0.2028	0.2925	0.3765	0.5265	0.6545	0.7635	0.8520	0.9635	1
0.7	0	0.1240	0.2337	0.3300	0.4140	0.5615	0.6840	0.7850	0.8660	0.9675	1
0.6	0	0.1485	0.2720	0.3775	0.4620	0.6060	0.7200	0.8090	0.8790	0.9690	1
0.5	0	0.1750	0.3056	0.4135	0.5039	0.6430	0.7478	0.8275	0.8880	0.9710	1
0.4	0	0.1935	0.3235	0.4335	0.5220	0.6590	0.7593	0.8345	0.8933	0.9725	1
0.3	0	0.1890	0.3197	0.4265	0.5130	0.6505	0.7520	0.8315	0.8020	0.9750	1
0.25	0	0.1758	0.3042	0.4108	0.4982	0.6359	0.7415	0.8259	0.8899	0.9751	1
0.2	0	0.1560	0.2840	0.3905	0.4777	0.6190	0.7277	0.8170	0.8875	0.9750	1
0.15	0	0.1300	0.2600	0.3665	0.4520	0.5995	0.7105	0.8055	0.8825	0.9760	1

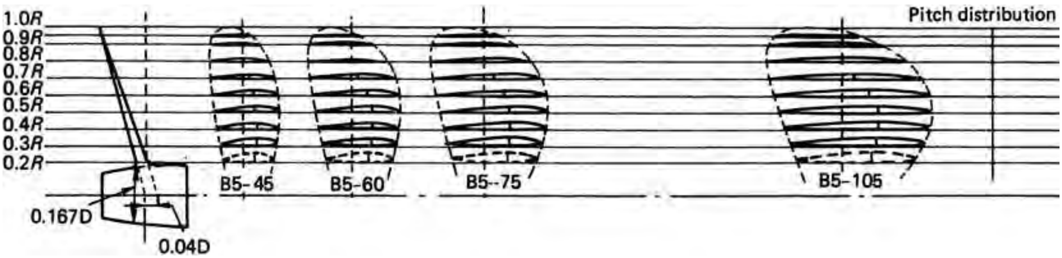

Figure 6.11 General plan of B5-screw series (Reporduced with permission from Reference 6)

6.5.2 Japanese AU-series

This propeller series is many ways complementary series to the Wageningen B-series; however, outside of Japan it has not gained the widespread popularity of the B-series. The series reported by Reference 8 comprises some propellers having a range of blade numbers from four to seven and blade area ratios in the range 0.40 to 0.758. Table 6.7 details the members of the series and Table 6.8, the blade geometry. The propeller series, as its name implies, has AU-type aerofoil sections and was developed from an earlier series having Unken-type sections.

6.5.3 Gawn series

This series of propellers whose results were presented by Gawn (Reference 9) comprised a set of 37 three-bladed propellers covering a range of pitch ratios from 0.4 to 2.0 and blade area ratios from 0.2 to 1.1.

The propellers of this series each had a diameter of 503 mm (20 in.), and by this means many of the scale effects associated with smaller diameter propeller series have been avoided. Each of the propellers has a uniform face pitch; segmental blade sections; constant blade thickness ratio, namely 0.060, and a boss diameter of 0.2D. The developed blade outline was of elliptical form with the inner and outer vertices at 0.1R and the blade tip, respectively. Figure 6.12 shows the outline of the propellers in this series. The entire series were tested in the No. 2 towing rank at A.E.W. Haslar within a range of slip from zero to 100 per cent: to achieve this the propeller rotational speed was in the range 250 to 500 rpm. No cavitation characteristics are given for the series.

Table 6.6 Coefficients for the K_T and K_Q polynomials representing the Wageningen B-screen series for a Reynolds number of 2×10^6 (taken from Reference 7)

Thrust (K_T)						*Torque* (K_Q)					
n	$C_{s,t,u,v}$	$s(J)$	$t(P/D)$	$u(A_E/A_O)$	$v(Z)$	n	$C_{s,t,u,v}$	$s(J)$	$t(P/D)$	$u(A_E/A_O)$	$v(Z)$
1	+0.00880496	0	0	0	0	1	+0.00379368	0	0	0	0
2	−0.204554	1	0	0	0	2	+0.00886523	2	0	0	0
3	+0.166351	0	1	0	0	3	−0.032241	1	1	0	0
4	+0.158114	0	2	0	0	4	+0.00344778	0	2	0	0
5	−0.147581	2	0	1	0	5	−0.0408811	0	1	1	0
6	−0.481497	1	1	1	0	6	−0.108009	1	1	1	0
7	+0.415437	0	2	1	0	7	−0.0885381	2	1	1	0
8	+0.0144043	0	0	0	1	8	+0.188561	0	2	1	0
9	−0.0530054	2	0	0	1	9	−0.00370871	1	0	0	1
10	+0.0143481	0	1	0	1	10	+0.00513696	0	1	0	1
11	+0.0606826	1	1	0	1	11	+0.0209449	1	1	0	1
12	−0.0125894	0	0	1	1	12	+0.00474319	2	1	0	1
13	+0.0109689	1	0	1	1	13	−0.00723408	2	0	1	1
14	−0.133698	0	3	0	0	14	+0.00438388	1	1	1	1
15	+0.00638407	0	6	0	0	15	−0.0269403	0	2	1	1
16	−0.00132718	2	6	0	0	16	+0.0558082	3	0	1	0
17	+0.168496	3	0	1	0	17	+0.0161886	0	3	1	0
18	−0.0507214	0	0	2	0	18	+0.00318086	1	3	1	0
19	+0.0854559	2	0	2	0	19	+0.015896	0	0	2	0
20	−0.0504475	3	0	2	0	20	+0.0471729	1	0	2	0
21	+0.010465	1	6	2	0	21	+0.0196283	3	0	2	0
22	−0.00648272	2	6	2	0	22	−0.0502782	0	1	2	0
23	−0.00841728	0	3	0	1	23	−0.030055	3	1	2	0
24	+0.0168424	1	3	0	1	24	+0.0417122	2	2	2	0
25	−0.00102296	3	3	0	1	25	−0.0397722	0	3	2	0
26	−0.0317791	0	3	1	1	26	−0.00350024	0	6	2	0
27	+0.018604	1	0	2	1	27	−0.0106854	3	0	0	1
28	−0.00410798	0	2	2	1	28	+0.00110903	3	3	0	1
29	−0.000606848	0	0	0	2	29	−0.000313912	0	6	0	1
30	−0.0049819	1	0	0	2	30	+0.0035985	3	0	1	1
31	+0.0025983	2	0	0	2	31	−0.00142121	0	6	1	1
32	−0.000560528	3	0	0	2	32	−0.00383637	1	0	2	1
33	−0.00163652	1	2	0	2	33	+0.0126803	0	2	2	1
34	−0.000328787	1	6	0	2	34	−0.00318278	2	3	2	1
35	+0.000116502	2	6	0	2	35	+0.00334268	0	6	2	1
36	+0.000690904	0	0	1	2	36	−0.00183491	1	1	0	2
37	+0.00421749	0	3	1	2	37	+0.000112451	3	2	0	2
38	+0.0000565229	3	6	1	2	38	−0.0000297228	3	6	0	2
39	−0.00146564	0	3	2	2	39	+0.000269551	1	0	1	2
						40	+0.00083265	2	0	1	2
						41	+0.00155334	0	2	1	2
						42	+0.000302683	0	6	1	2
						43	−0.0001843	0	0	2	2
						44	−0.000425399	0	3	2	2
						45	+0.0000869243	3	3	2	2
						46	−0.0004659	0	6	2	2
						47	+0.0000554194	1	6	2	2

The propeller series represents a valuable data set, despite the somewhat dated propeller geometry, for undertaking preliminary design studies for warships and other high-performance craft due to the wide range of P/D and A_E/A_O values covered. Blount and Hubble (Reference 10) in considering methods for the sizing of small craft propellers developed a set of regression coefficients of the form of equation (6.17) to represent the Gawn series. The coefficients for this series are given in Table 6.9 and it is suggested that the range of applicability of the regression study should be for pitch ratio values from 0.8 to 1.4, although the study was based on the wider range of 0.6 to 1.6. Inevitably, however, some regression formulations of model test data tend to

Anexo 4 Manual Cura en Castellano. Autor Raúl Diosdado.

Manual de usuario

Cura 14.07

Software de Ultimaker para la impresión 3D

Ultimaker

Versión en Español

Zona Maker

En este manual se explica detalladamente el uso, configuración e instalación de CURA, un programa "Open Source" que es utilizado para el laminado e impresión de modelos 3D.

Este manual ha sido confeccionado por Raúl Diosdado usando para ello la siguiente información y recursos:

Manual original de CURA editado por Ultimaker.
https://www.ultimaker.com/spree/uploads/38/original/Cura_User-Manual_v1.0.pdf

Comunidad Ultimaker.
http://umforum.ultimaker.com/

Primera edición publicada en Octuble de 2014

INDICE

Conociendo Cura

Descripción del Software

Cura es un software abierto (Open software) desarrollado por Ultimaker que permite transformar modelos 3D en instrucciones entendibles por la mayoría de impresoras 3D, permitiendo generar un objeto físico a partir de su modelo generado por ordenador.

Existen versiones de cura para las siguientes plataformas:

- Windows XP o superior

-MAC 10.6 o superior

-UNIX Ubuntu 12.10 o superior

Requerimientos mínimos de Hardware

-512 MB de RAM

-200 MB de espacio disponible en el disco duro

-Procesador Pentium 4 o equivalente

Hardware recomendado

-2 GB de RAM

-500 MB de espacio disponible en el disco duro

-Intel Core 2 a 2.0 Ghz o equivalente

Cura es compatible con los siguientes tipos de archivo:

.STL (Este archivo es soportado por la mayoría de programas de diseño 3D)

.OBJ

.DAE

.AMG

Instalación y configuración **inicial**

Instalación

Para instalar Cura en las diferentes plataformas disponibles se procederá de forma similar, encontrándose las diferencias típicas de cada sistema operativo. En este manual se va a explicar detalladamente la instalación sobre windows.

1. Descargar el paquete de instalación de la última versión de CURA correspondiente a vuestro sistema operativo de la página oficial de Ultimaker http://software.ultimaker.com/

2. Ejecutar el instalador

En la primera ventana nos va a aparecer la ruta donde queremos instalar el programa. Podéis indicarle una ruta o dejar la que trae por defecto.

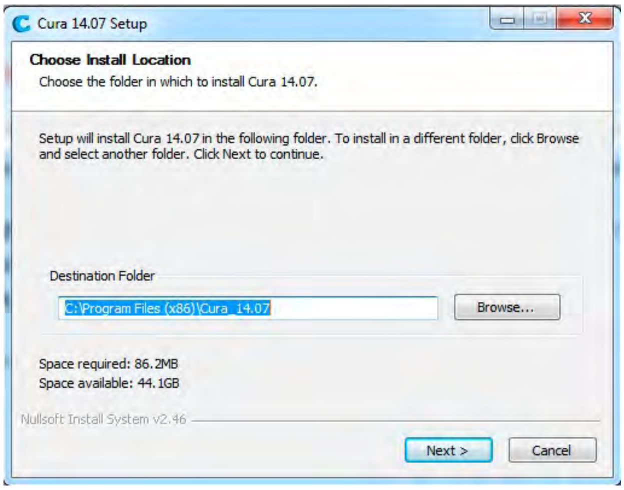

En la siguiente pestaña van a aparecer los componentes que se desean instalar. Además de instalar CURA, el instalador da la opción de instalar los drivers de Arduino y soporte para abrir diferentes formatos. Se recomienda marcar al menos la opción para abrir archivos en formato STL, ya que es el formato más común.

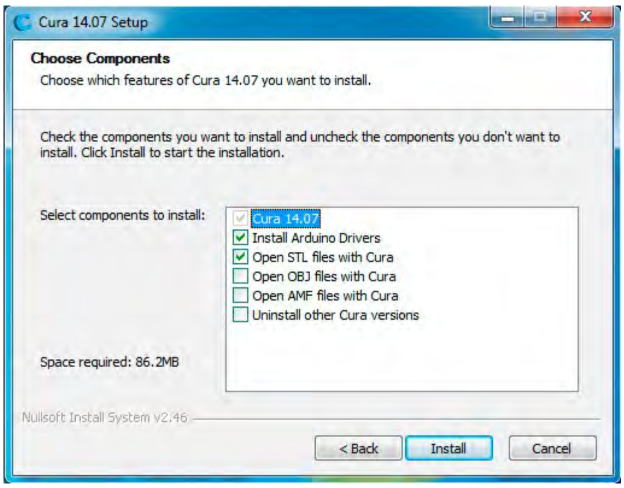

Una vez pulsado el botón instalar, la instalación empezará automáticamente.

Al finalizar, si hemos seleccionado la opción de instalar los drivers de Arduino, se abrirá una ventana que iniciará la instalación de los drivers.

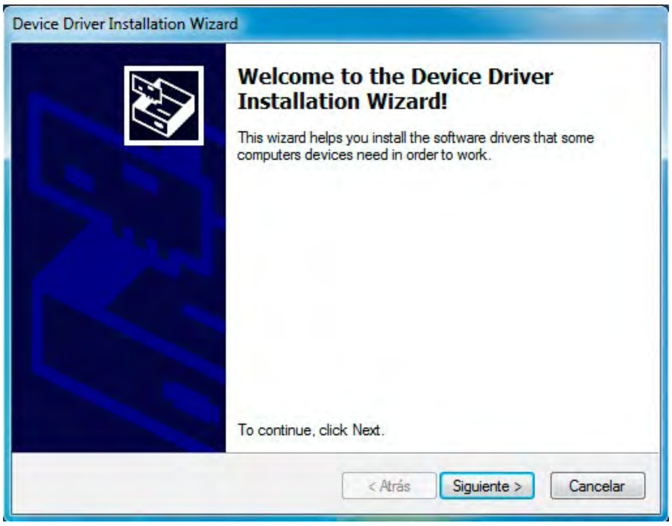

Al terminar con la instalación de los drivers, se abrirá una última ventana que nos indica la finalización del proceso de instalación y nos dará la opción de ejecutar el programa por primera vez.

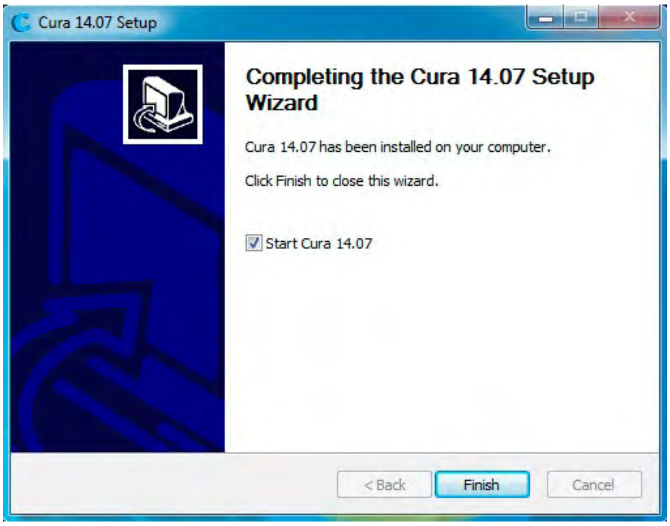

Asistente de configuración inicial (wizard).

Una vez instalado el software, al ejecutarse el programa por primera vez, se va a abrir el asistente de configuración inicial, donde se va a indicar al software parámetros básicos que van a depender del tipo de impresora.

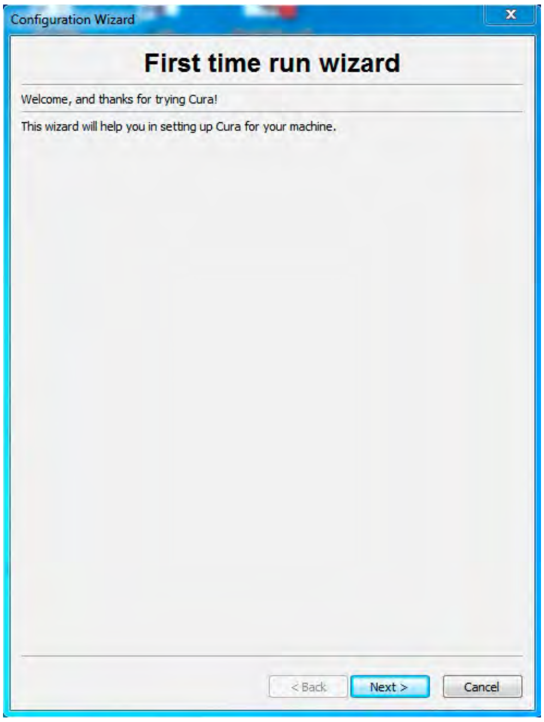

En la segunda pestaña del asistente de configuración, debéis seleccionar el modelo de vuestra impresora. Si vuestra impresora no es una ultimaker o una printbot, seleccionar en "Other" y se abrirá otra ventana con más opciones.

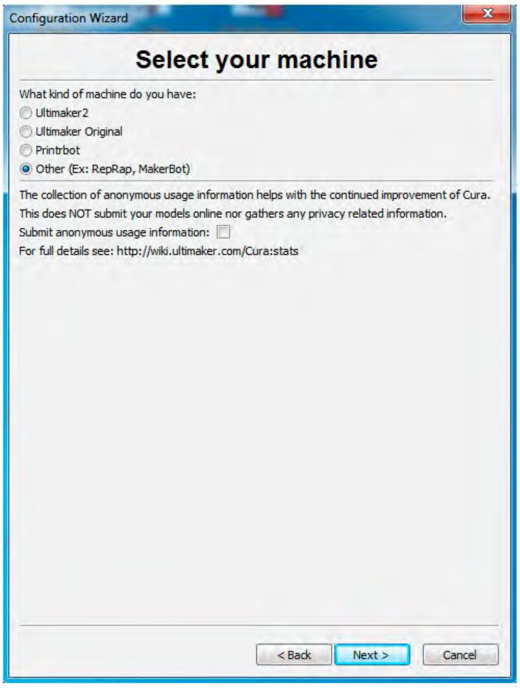

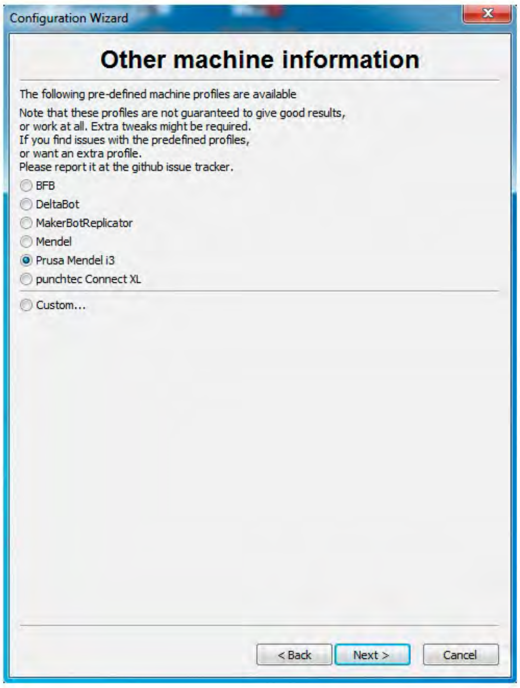

Si vuestro modelo de impresora no se encuentra entre los anteriores, seleccionar "custom" y se abrirá una pestaña donde debéis de indicar los parámetros básico de vuestra máquina, como el volumen de impresión, el tamaño de la boquilla del HotEnd o si posee cama caliente o no.

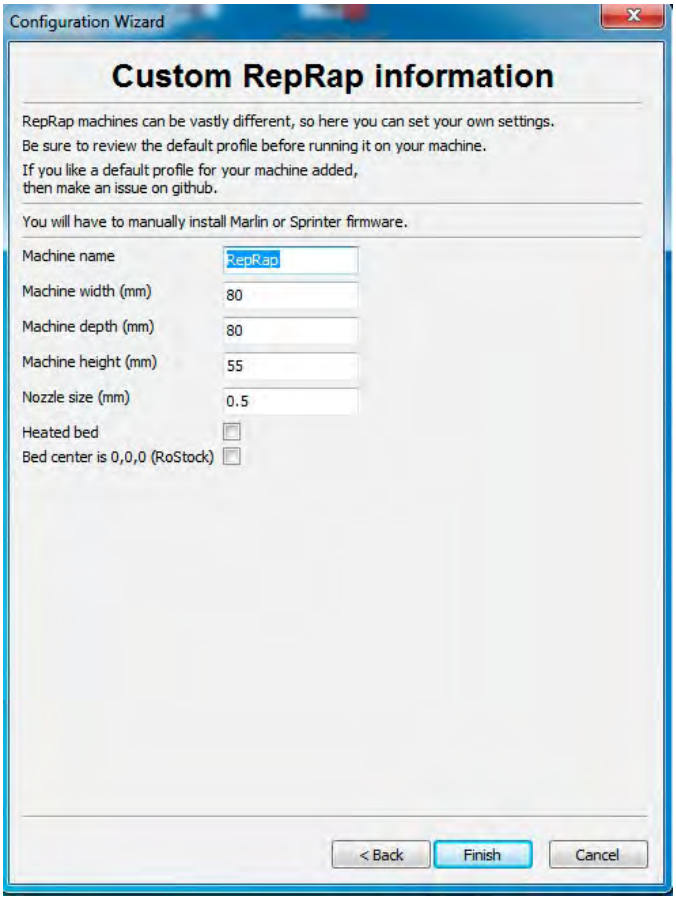

Una vez completado el asistente de configuración, ya tendréis CURA totalmente operativo.

Entorno de Programa

Cuando iniciamos CURA, si ya hemos rellenado los parámetros básicos del asistente de configuración, nos va a aparecer la siguiente pantalla.

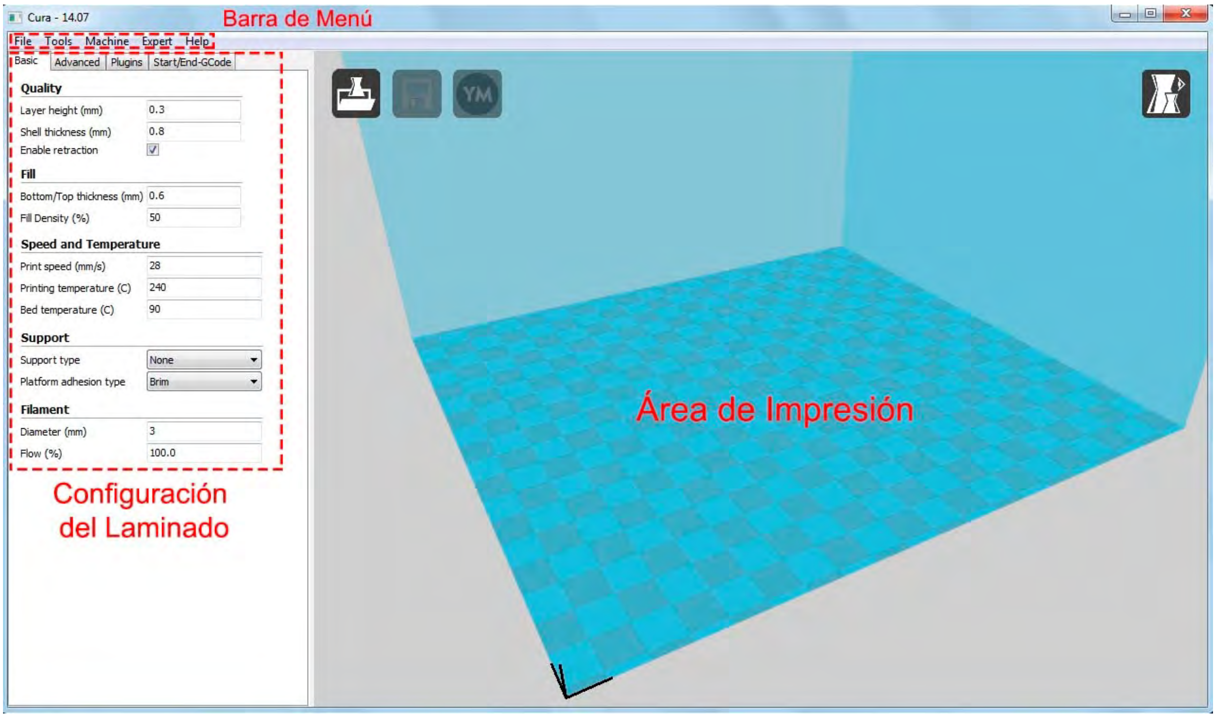

Si lo que os aparece en pantalla no se corresponde con la imagen anterior, aseguraos que estáis trabajando con CURA en el modo "full settings" , para ello id a la barra de herramientas "Expert" y seleccionar la opción "Switch to full settings"

El programa está estructurado en 3 partes, el área de impresión, configuración de los parámetros de laminado y barra de herramientas. En la imagen superior podéis ver cada una de estas partes de manera detallada.

Área de impresión

El área de impresión es una representación tridimensional del volumen de impresión de la impresora. Este es el espacio con el que contamos para imprimir y no podremos exceder sus límites, ya que quedarían fuera de los limites de impresión reales de nuestra máquina.

En este área nos encontraremos las herramientas necesarias para cargar las figuras que queramos imprimir, modificarlas y visualizar las diferentes capas.

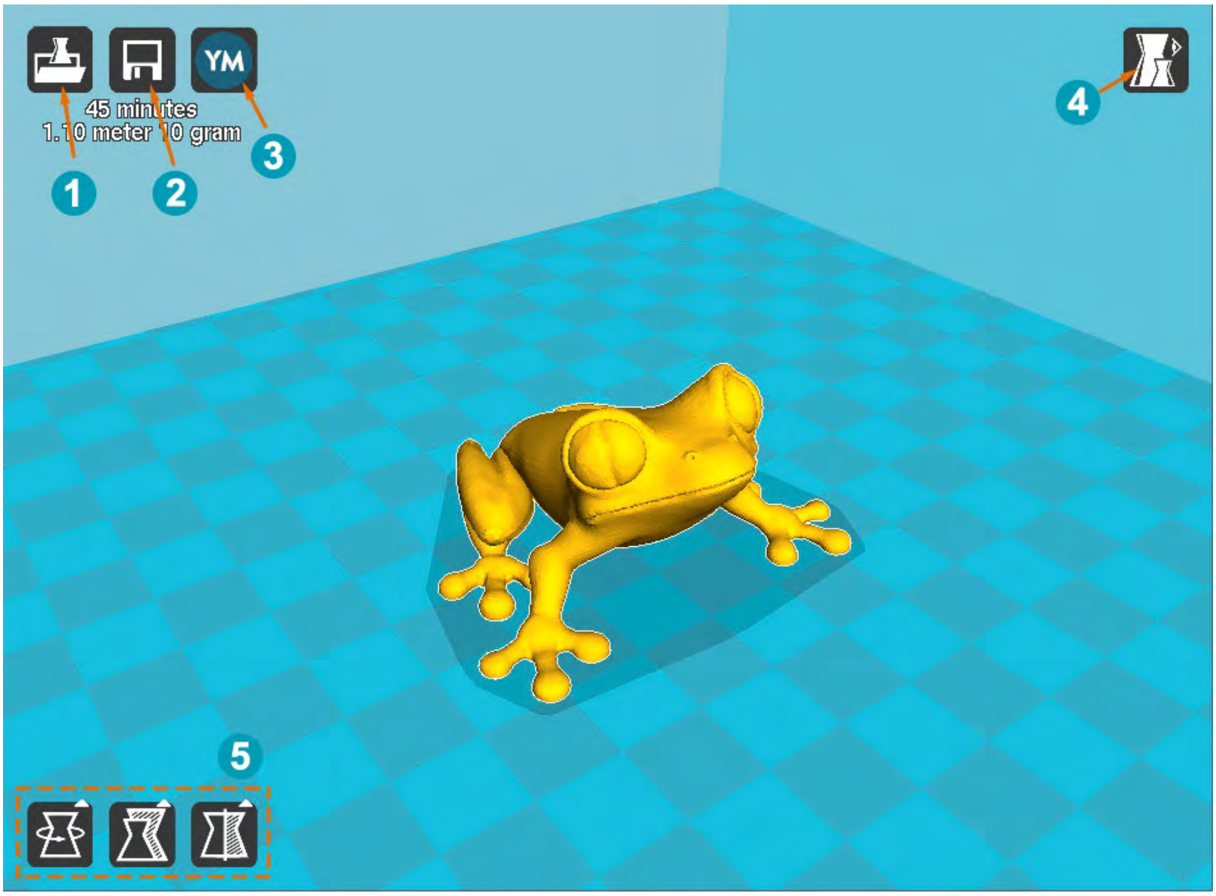

1 Load: Carga el modelo 3D que queramos imprimir. También se puede cargar arrastrando el archivo del modelo dentro del área de impresión.

2 Print With USB: Inicia la conexión con la impresora y abre el panel de impresión (si la impresora no está conectada, el icono será diferente y pondrá "save toolpath", que guardará el proyecto en un archivo gcode imprimible desde la tarjeta SD de la impresora)

3 Share on YouMagine: Con esta opción podrás compartir tus diseños en "YouMagine", una comunidad con un gran repositorio de diseños 3D donde usuarios de todo el mundo suben sus creaciones.

4 View Mode: El icono view mode es un icono desplegable que ofrece 5 tipos de vistas diferentes del objeto que tengamos en el área de impresión. Podemos intercambiar las vistas para ver con detalle algunos elementos de la figura.

- **Normal**: Muestra la figura como un sólido, permitiendo ver el resultado final de la pieza impresa

- **Overhang**: Esta vista realza las zonas que tienen un ángulo superior al ángulo máximo que tengamos configurado. Esto es muy útil para ver qué zonas pueden ser problemáticas a la hora de imprimir y determinar si necesitan soporte o no.
- **Transparent**: Hace que la figura sea transparente permitiendo ver a través de ella.
- **X-Ray**: Esta vista, además de permitir ver a través del objeto, mostrará cavidades o elementos internos a las propias piezas.
- **Layers**: De todas las vistas esta es quizás la más útil, ya que podemos ver el diseño por capas, esto nos permite ver como actuará realmente la impresora a la hora de imprimir y si hay alguna zona en la que el laminado de la pieza sea complejo o simplemente no lo haga como nosotros queremos.

5 Opciones de transformación: en la parte interior izquierda del área de impresión, podemos encontrar varias opciones que nos permiten aplicar transformaciones simples al modelo 3d, estas transformaciones sirven para adaptar el modelo al área de impresión o ajustarlo al tamaño deseado.

> Para que aparezcan estas opciones, primero debemos de seleccionar el modelo 3D sobre el que queremos aplicar los cambios.

- **Rotate**: Permite rotar el modelo en cualquiera de los 3 ejes. También da la opción de retornar los cambios que hayamos realizado pulsando "**reset**" o apoyar el modelo por su parte plana dando al botón "**lay flat**"

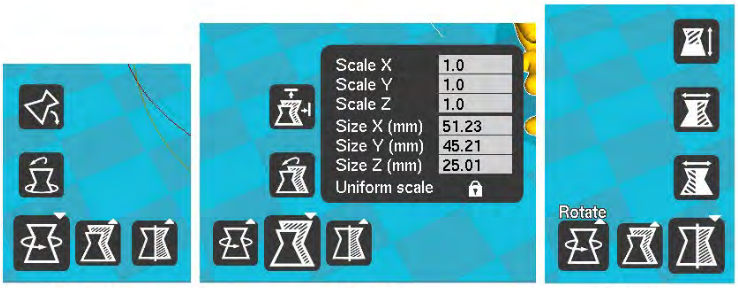

Rotate Scale Mirror

- **Scale**: Con esta función se puede modificar el tamaño del modelo 3D. Al pulsar este icono, se despliega un menú donde podemos aplicar un factor de multiplicación a la escala del objeto o bien indicar las medidas que queremos que tenga el mismo. Este redimensionado puede hacerse de manera proporcional al objeto inicial o de manera totalmente libre en función de si tenemos la opción "**Uniform Scale**" activada o desactivada. Dentro de "Scale", también podemos encontrar la opción de deshacer los cambios aplicados pulsando "Reset" o escalar al tamaño máximo permitido por el área de impresión pulsando sobre "To max".

- Mirror: Esta opción crea una figura espejo de la figura inicial. Se puede espejar la figura en cualquiera de los 3 ejes.

Al seleccionar una pieza contenida en el área de impresión y hacer clic derecho, nos van a aparecer una serie de opciones que nos va a permitir cosas como multiplicar el número de objetos, eliminarlos, centrarlos en la superficie de impresión...

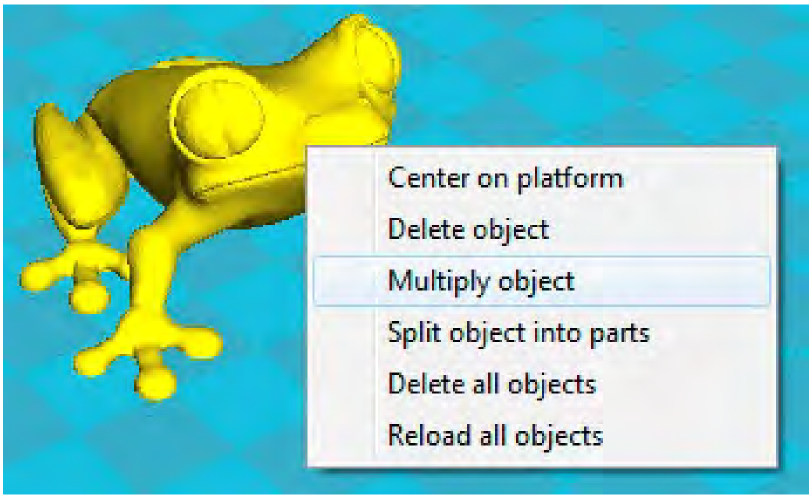

La opción "multiply object" es una opción muy interesante para crear copias idénticas de un objeto sin tener que cargar varias veces el objeto, tan solo hay que indicar el número de copias que se desea del objeto y aparecerán ordenadas en la superficie de impresión.

Configuración del laminado

Tener una configuración adecuada a la hora de laminar la pieza que queremos imprimir, es casi tan importante como tener la impresora bien calibrada, una configuración deficiente o que no se adapte a las características de nuestra impresora va a dar como resultado impresiones de mala calidad. Para saber los parámetros exactos con los que nuestra maquina trabaja bien, no queda otra que hacer pruebas hasta conseguir los valores a los que saquemos la máxima resolución.

Los valores que dé a continuación son valores orientativos y que en la mayoría de los casos darán buenos resultados, pero cada máquina tiene unas características concretas y puede que estos valores no saquen el mayor rendimiento de vuestra máquina.

Para configurar la forma en la que nuestra maquina va a realizar el laminado, tenemos una serie de pestañas en la parte izquierda de la pantalla, en estas pestañas vamos a encontrar las opciones más comunes a la hora de laminar, aunque no son las únicas opciones del programa que van a afectar al laminado, son con las que trabajaremos normalmente.

Basic (Configuración básica)

Quality (Calidad)

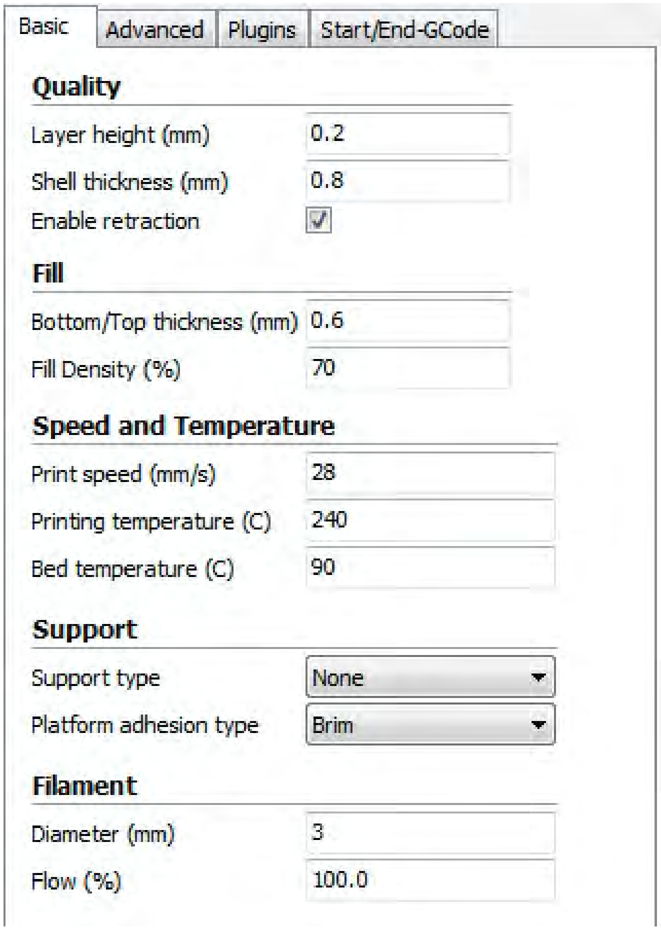

- Layer height (Altura de capa): Este parámetro indica la altura de capa a la que se va a realizar la impresión. La altura de capa es un parámetro ligado directamente a la calidad de la pieza, a menor altura de capa mayor calidad, pero también va a incrementar considerablemente los tiempos de impresión, por ello lo mejor es llegar a un punto intermedio que de suficiente calidad sin alargar demasiado la impresión. Los valores de este parámetro estarán comprendidos entre 0.1 y 0.4mm. Se ha que tener en cuenta que el valor de la altura de capa no debe de ser igual o mayor al diámetro de la boquilla del HotEnd, ya que esto puede dar como resultado piezas quebradizas o con rajas entre las capas.

- Shell Thickness (Grosor del borde): Este parámetro determina la anchura del borde del objeto. El valor de este parámetro va a estar influido directamente por el diámetro de la boquilla del HotEnd, siendo este valor igual al diámetro de la boquilla del HotEnd multiplicado por el numero que vueltas que queramos dar al objeto. Por ejemplo, si nuestro HotEnd tiene una boquilla de 4mm y queremos que al menos de 2 vueltas al borde del objeto, debemos de poner un valor de 0.8mm. El valor que debemos de introducir en este parámetro dependerá de la tipología de la pieza y del relleno que usemos, pero lo normal es hacer un borde con 2 o 3 vueltas.

- Enable retraction (Habilitar retracción): Esta opción hace que en los desplazamientos el extrusor retraiga un poco el plástico para que no gotee, evitando así pequeños defectos en la impresión. Esta opción es muy recomendable tenerla activada.

Fill (Relleno)

- Bottom/Top thickness (Grosor de la capa inferior y superior): Con este parámetro indicaremos que grosor tendrán las capas superior e inferior. Estas capas no se ven afectadas por la configuración de relleno, por lo que serán capas macizas. Dependiendo de la figura que queramos imprimir y del relleno que usemos vamos a necesitar más o menos capas, lo normal es usar 3 o 4 capas macizas, pero en algunas piezas para tener un buen acabado vamos a necesitar algunas mas. El valor del grosor de capa hay que indicarlo en milímetros, por lo que hay que multiplicar el valor de la altura de capa por el numero de capa que queramos, por ejemplo, si estamos imprimiendo con una altura de capa de 0.2mm y queremos tener 3 capas macizas, habrá que introducir en este parámetro 0.6mm.
- Fill Density (Densidad de relleno): Este valor indica el relleno que va a tener la figura. El relleno va a repercutir directamente en el tiempo de impresión y en el coste de la pieza, por ello el hacer las piezas con poco relleno va a ser muy beneficioso, pero al mismo tiempo va a mermar la resistencia de la pieza, por lo que el relleno va a depender de las características mecánicas que queramos conseguir. Para creaciones artísticas, figuras o elementos decorativos, podemos usar un relleno del 20%, mientras que para piezas que deban soportar peso o esfuerzos podemos darle un 80% de relleno.

Speed and Temperature (velocidad y temperatura)

La velocidad y la temperatura son parámetros que están íntimamente ligados en la impresora 3D y de los que depende en gran medida la calidad de impresión. Por regla general a mayor temperatura de impresión podremos imprimir a mayor velocidad sin disminuir la calidad, pero la temperatura es un parámetro que no podemos subir todo lo que queramos ya que podemos dañar el HotEnd o provocar atascos por exceso de calor.

- Print speed (velocidad de impresión): En este parámetro vamos a fijar la velocidad de impresión. A mayor velocidad conseguiremos menor calidad en la impresión, por lo que hay que ajustar el valor en función de la calidad que deseemos obtener. También va a depender mucho que máquina estemos usando, ya que no todas pueden alcanzar las mismas velocidades con la misma resolución. A modo orientativo, podéis fijar la velocidad en 28mm/s (que es una velocidad muy prudente) e ir subiendo la velocidad progresivamente hasta determinar la velocidad optima de vuestra máquina.
- Printing Temperature (temperatura de impresión): Fija la temperatura del HotEnd a la que se va a imprimir. En función del plástico utilizado vamos a usar una u otra

temperatura. Los plásticos más comunes son el ABS y el PLA, para ABS fijaremos una temperatura de 220-240º y para el PLA de 190-210º

- Bed Temperature (temperatura de la cama caliente): Fija la temperatura de la cama caliente. La temperatura de la cama caliente cambiará en función del plástico que usemos, para el PLA no es necesario calentar la cama (aunque se adquiere mejor si se templa a unos 30º) y para el ABS fijaremos la cama de 80 a 110º (dependiendo del ABS que usemos).

Support (soporte)

Para muchas de las impresiones debemos de usar elementos que aseguren una correcta impresión como pueden ser los elementos de soporte o de mejora de la adherencia.

- Support type (tipo de soporte): Esta opción creará soportes donde sea necesario. Los soportes se emplean cuando la pieza tiene partes en el aire que no se pueden sustentar o cuando esta crece con un ángulo superior al que tengamos fijado. En las opciones podemos seleccionar 2 tipos de soporte, "Touching Buildplate" o "Everywhere", la primera opción crea soportes apoyándose solo en la base y la segunda crea soportes que apoyan en cualquier parte de la pieza.
- Platform adhesion type (plataforma de adhesión): Con esta opción podemos crear una plataforma en la base que mejore la adhesión de la pieza. Existen 2 tipos de bases, la primera "Brim" crea una especie de visera en todos los bordes de la figura y la segunda "Raft" va a generar una base completa sobre la cual se va a construir la pieza. Tened en cuenta que al aplicar "Raft" la figura no va a apoyar su base sobre el cristal de impresión, por lo que esta superficie no va a quedar con una terminación tan buena como si se imprimiera directamente sobre el cristal.

Filament (Filamento)

- Diameter (Diámetro de filamento): Establece el diámetro del filamento que estemos usando. Los diámetros que se usan comúnmente son de 3mm y 1.75mm
- Flow (Multiplicador del flujo de filamento): Este parámetro modifica la cantidad de filamento que extruye la impresora. Este parámetro se usa para corregir la cantidad de plástico extruido, ya que podemos tener mal calibrado el extrusor o el filamento puede ser de un diámetro ligeramente diferente al indicado.

Advanced (Configuración avanzada)

Machine (Maquina)

- Nozzle size (Diametro de la boquilla del Hotend): En este parámetro especificaremos el diámetro de la boquilla del HotEnd que estemos usando. Los diámetros más comunes son 0.5mm 0.4mm y 0.35mm.

Retraction (Retracción)

- Speed (velocidad): Velocidad a la que realiza la retracción. Este parámetro tiene un amplio margen de trabajo, por defecto trae 40mm/s que es una velocidad a la que funciona bien, se puede aumentar la velocidad mucho mas, pero una velocidad muy elevada puede mellar el filamento y estropear la impresión.
- Distance (Distancia): Indica la cantidad de filamento que va a retraer. Por defecto trae 4.5mm que es un valor que funciona bien.

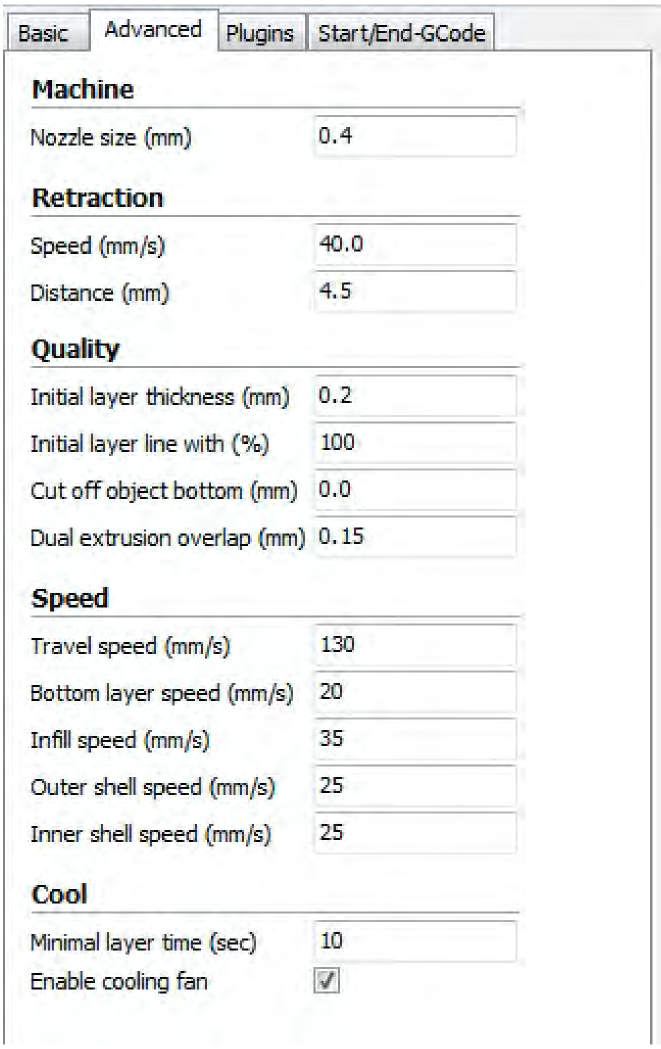

Quality (Calidad)

- Initial layer thickness (grosor de la capa inicial): Este parámetro fija el grosor de la capa inicial. Si queremos hacer que la capa inicial tenga el mismo valor que el resto de capas, le asignaremos el valor 0. No es recomendable que la capa inicial sea demasiado gruesa, ya que esto va a repercutir en la adherencia, no es recomendable que la altura de la capa inicial sea mayor de 0.3mm.
- Initial layer line with (Ancho de linea inicial): Establece el ancho de línea en la primera capa. Este parámetro va a afectar directamente al "flow" de la primera capa, mejorándose la adherencia de la figura al depositar mayor cantidad de plástico en la primera capa.
- Cut off object botton (Corta la base del objeto): Con este parámetro podemos cortar la figura a la altura deseada. Este parámetro hundirá la figura en la base empezando la impresión a la altura que deseemos.

Speed (Velocidad)

- Travel speed (Velocidad de desplazamiento): Fija la velocidad a la que se va a mover el extrusor al desplazarse de un punto a otro de la maquina. Está configurado por defecto a 150mm/s, aunque con algunas impresoras puede ser un movimiento demasiado rápido por lo que recomiendo bajarlo a 130mm/s.
- Bottom layer speed (velocidad de la primera capa): Este parámetro establece la velocidad de impresión de la primera capa. Es muy importante para la adherencia de la pieza realizar la primera capa a baja velocidad, por lo que se deberá de fijar a un valor inferior a la velocidad de impresión normal. Un valor con el que se obtiene un buen resultado en la mayoría de impresoras es 22mm/s.
- Infill speed (velocidad de relleno): Fija la velocidad a la que se va a realizar el relleno de la figura. Para realizar el relleno de la figura se puede aumentar la velocidad considerablemente sin que la calidad de la pieza se vea afectada, reduciendo así el tiempo de impresión. Como referencia, podéis fijar este valor en 40mm/s e ir aumentándolo progresivamente hasta determinar la velocidad ideal para vuestra máquina.
- Outer shell speed (Velocidad de la capa externa): Este parámetro establece la velocidad de la capa exterior de la pieza. Es un parámetro del que va a depender en gran medida el acabado de la pieza, por ello conviene establecer una velocidad baja para este parámetro. En torno a 25mm/s es una velocidad adecuada.
- Inner shell speed (Velocidad de los bordes interiores): Establece la velocidad de los bordes interiores (lo que no se ven). Este parámetro va a fijar la velocidad de los bordes que no son externos (dependiendo de la configuración del "Shell Thickness", vamos a tener mayor o menor número de estos bordes). Al ser bordes no visibles, podemos aumentar la velocidad con respecto a los bordes visibles sin que afecte a la terminación de la pieza, fijad inicialmente este valor en 30mm/s.

Cool

- Minimal layer time (tiempo mínimo de capa): Fija el tiempo mínimo para terminar una capa antes de empezar con la siguiente. Si empezamos una capa sin que la anterior se haya enfriado, el acabado va a ser muy malo e incluso vamos a tener una figura deforme, por ello hay que fijar un valor mínimo. Este valor va a depender del tipo de plástico que estemos usando y de la temperatura de impresión, fijad este valor al menos en 10 segundos.
- Enable cooling fan (Habilitar ventilador de capa): Esta opción habilita el ventilador de capa (si nuestra impresora cuenta con uno). El ventilador de capa nos va a ayudar a enfriar las capas de manera uniforme, mejorando en gran medida la calidad de piezas que por su pequeño tamaño no se enfrían correctamente antes de depositar las siguientes capas.

Plugins

En este apartado se pueden añadir plugins que doten al programa de funcionalidades que inicialmente no tiene. Es posible diseñarse plugins para un fin especifico o descargarse plugins ya creados. Por defecto CURA trae dos plugins instalados.

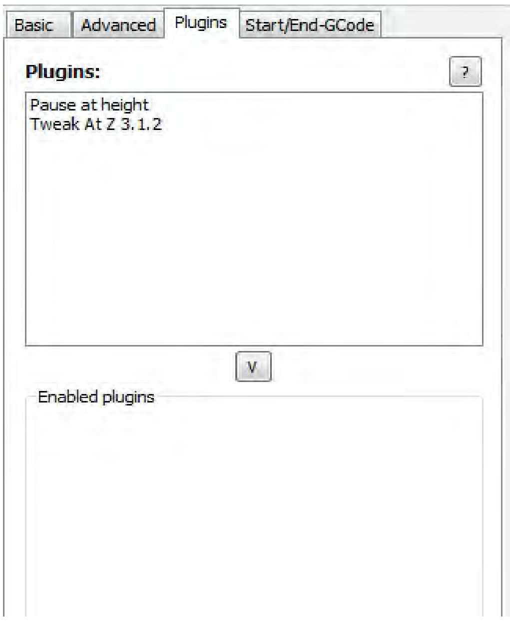

- Pause at height (Pausar a una altura): Es un plugin que pausa la impresión a una altura determinada.
- Tweak at Z (Cambio a Z): Es un plugin que cambia los valores de impresión que hemos fijado al llegar a una determinada altura de impresión

Para habilitar estos plugins, debemos seleccionarlos y pulsar la flecha inferior que los moverá a "enable plugins", una vez aquí, podemos configurar el plugin con los valores que queramos.

Start/End gcode

En este apartado podemos añadir parámetros directamente al gcode de inicio y fin de impresión.

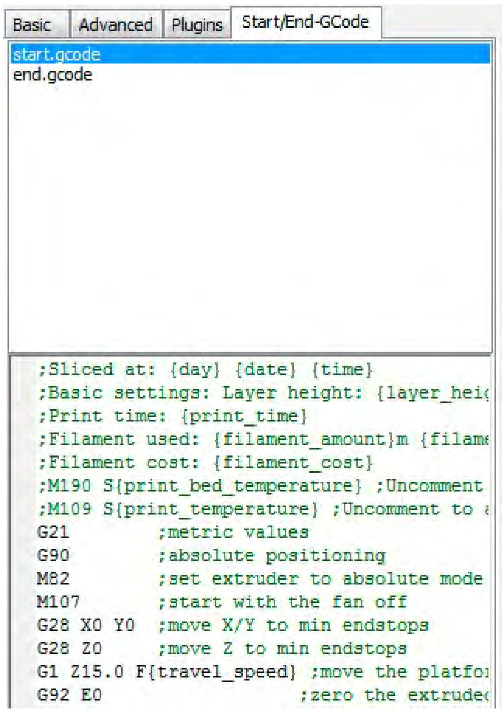

El gcode, es el archivo que va a reconocer nuestra impresora y tiene todos los comandos necesarios para el control de la misma. En este apartado, podemos modificar el funcionamiento inicial y final de la impresora añadiendo comandos o modificando los comando existentes.

En el gcode de inicio que trae precargado CURA, se indica que antes de la impresión haga un "homing", suba el eje Z, extruya una pequeña cantidad de filamento y posteriormente comience la impresión. En el código de fin, apagará tanto el HotEnd como la cama caliente, retrae filamento, sube el eje Z y va a una posición especifica. Si nos interesa cambiar alguno de estos parámetros podemos hacerlo directamente sobre este código.

Barra de Menú

En la barra de menú podemos encontrar un montón de opciones e información tanto para la configuración de la impresora como del propio laminador. Estas opciones están divididas en 5 pestañas, "File", "Tools", "Machine", "Expert" y "Help". Muchas de las opciones que podemos encontrar en estas pestañas son accesibles desde diferentes partes del programa o son las típicas opciones que podemos encontrar en la mayoría de los programas, por lo que tan solo pasaré a detallar las opciones más mas importantes.

File

- Open profile/Save profile: Esta opción nos permite guardar nuestras configuraciones de CURA o cargar configuraciones guardadas con anterioridad. Es muy útil tener varias configuraciones guardadas con acabados diferentes o configuraciones para diferentes maquinas, así no es necesario cambiar una y otra vez los parámetros de impresión cada vez que cambiamos de maquina o de filamento.

- Preferences (Preferencias): En esta opción podemos encontrar parámetros muy diferentes que van a cambiar desde el aspecto visual de algunos elementos hasta opciones de programa.

  - Print window (Ventana de impresión): En esta pestaña podemos seleccionar el aspecto de la ventana de impresión, CURA ofrece dos posibilidades, la que trae por defecto (Basic) y una ventana que imita el entorno del Pronterface (Pronterface UI).

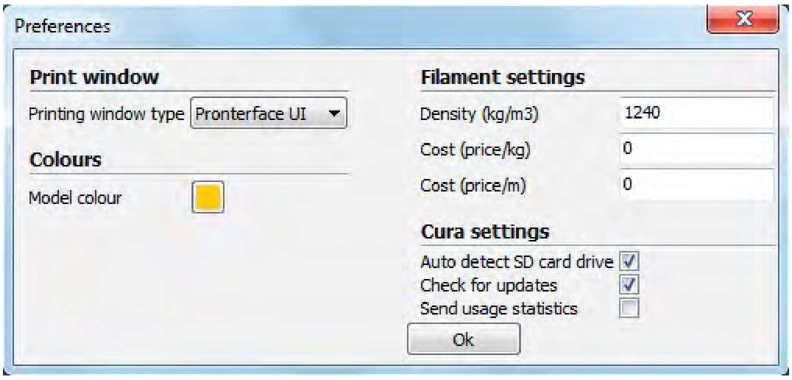

    Por defecto trae seleccionada "Basic", recomiendo cambiar esta opción a "Pronterface UI", ya que es mucho mas visual y tiene un entorno más agradable.

  - Colours (colores): Con esta opción podemos cambiar el color del modelo 3D que aparece en el área de impresión.

  - Filament Settings (Ajuste del filamento): En esta ventana podemos introducir los parámetros reales del filamento que estemos usando. Un parámetro muy interesante que conviene rellenar es el que indica el precio por kg de filamento, ya que al rellenar este parámetro, además de conocer los tiempo de impresión y metros de filamento necesarios, el programa nos va a mostrar en pantalla el coste de la impresión.

  - Cura Settings (Configuración de CURA): En este apartado se muestran 3 opciones del programa, la primera "auto detect SD card drive" va a detectar cuando conectemos una tarjeta SD en el ordenador para guardar directamente el proyecto creado en gcode. La segunda opción "Check for updates" hace que el programa compruebe si existen nuevas versiones de CURA al inicio de cada sesión y la tercera opción "Send usage statistics" mandará información a Ultimaker.

- Machine Settings (Configuración de la maquina): Aquí podemos encontrar un gran número de parámetros que se deben configurar en función de las características físicas de nuestra máquina.

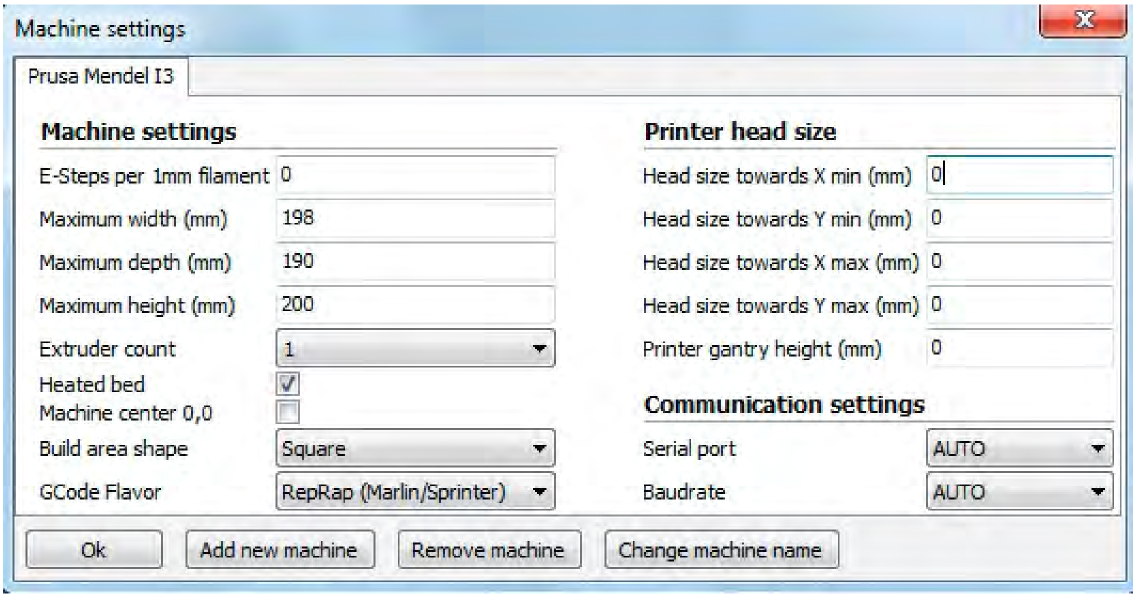

  - E-Steeps per 1mm filament: Va a definir los pasos que tiene que dar el motor del extrusor por cada milímetro de filamento extruido. Recomiendo configurar este parámetro en el firmware e introducir aquí el valor "0"
  - Maximun width/depth/heigth: En estos parámetros hay que introducir la medida real del volumen de impresión. Estos valores van a ser los valores límite a los que se van a poder mover los ejes de la impresora.
  - Extruder count: Aquí hay que indicar el numero de extrusores con los que cuenta nuestra máquina. El tener más o menos extrusores va a cambiar algunas opciones de programa, ya que hay parámetros que deben ser configurados para cada extrusor de manera independiente.
  - Heated bed: Si nuestra impresora cuenta con una cama caliente hay que marcar esta opción para activarla.
  - Machine center 0,0: Si esta opción está habilitada, establece el centro de la máquina en el punto 0,0. Lo más común es trabajar con esta opción deshabilitada.
  - Build area shape: Determina la forma del área de impresión. Dependiendo del modelo de impresora, el área de impresión puede ser cuadrada o circular (impresoras tipo delta), seleccionar el tipo de área en función de la impresora.

- Gcode flavor: En función del tipo de máquina y del firmware que tenga cargado, va a reconocer un tipo de gcode u otro. Seleccionar el que se adapte a vuestra impresora.
- Printer head size: Estos parámetros se usan para determinar el tamaño del HotEnd y de los elementos que tengamos entorno a este. Es necesario rellenar estos parámetros si queremos imprimir múltiples objetos de forma simultánea y que ninguna parte del extrusor golpee a las piezas ya creadas.
- Communicatión settings: estos parámetros establecen tanto el puerto al que tenemos conectado la impresora como la tasa de transferencia de datos (baud rate). Se pueden poner ambas opciones en "AUTO" siendo el programa el determine estos parámetros.

Tools

En la pestaña "tools" podemos encontrar 2 opciones que van a cambiar la forma en la que la impresora va a imprimir cuando tenemos múltiples objetos en el área de impresión.

Cuando situamos varios objeto en el área de impresión, por defecto los va a imprimir todos a la vez (print all at once), pero podemos configurar la impresora para que imprima estos objetos de uno en uno, para ello hay que marcar la opción "print once at time". Con esta opción marcada, la impresora hará cada objeto de manera independiente, comenzando un objeto siempre que haya terminado el anterior, esta es una buena opción para impresiones largas con múltiples objetos, ya que si en algún momento falla la impresión puede que tengamos algún objeto completo y no tengamos que desechar la bandeja entera.

Machine

En la pestaña machine podemos tener varias configuraciones preestablecidas si tenemos varias máquinas que usan configuraciones diferentes. Al imprimir con una u otra máquina, tan solo debemos de seleccionar aquí la máquina que estemos usando y se cargaran los valores que tenemos guardados por defecto.

También podemos encontrar un acceso a "Machine settings" que nos llevará al mismo menú que "file/Machine_settings"

Este menú también da la opción de cargar un firmware especifico a la impresora (install custom firmware).

Expert

En la pestaña "Expert", las dos primeras opciones que nos encontramos nos van a permitir conmutar el modo en que aparecen las opciones de impresión entre una "impresión rápida" (sin apenas configuración) y una "impresión completa" (con todas las opciones). En la impresión rápida, tan solo hay que introducir la calidad que queremos obtener, el tipo de filamento que estamos usando y su diámetro, mientras que en la opción completa, aparecen todos los parámetros que afectan a la impresión.

> Recomiendo usar la configuración completa, ya que permite adaptar los parámetros de impresión a cada máquina.

La siguiente opción "Open Expert Settings", abrirá una ventana de configuración donde se pueden alterar parámetros de impresión que no aparecen en las opciones de impresión básicas.

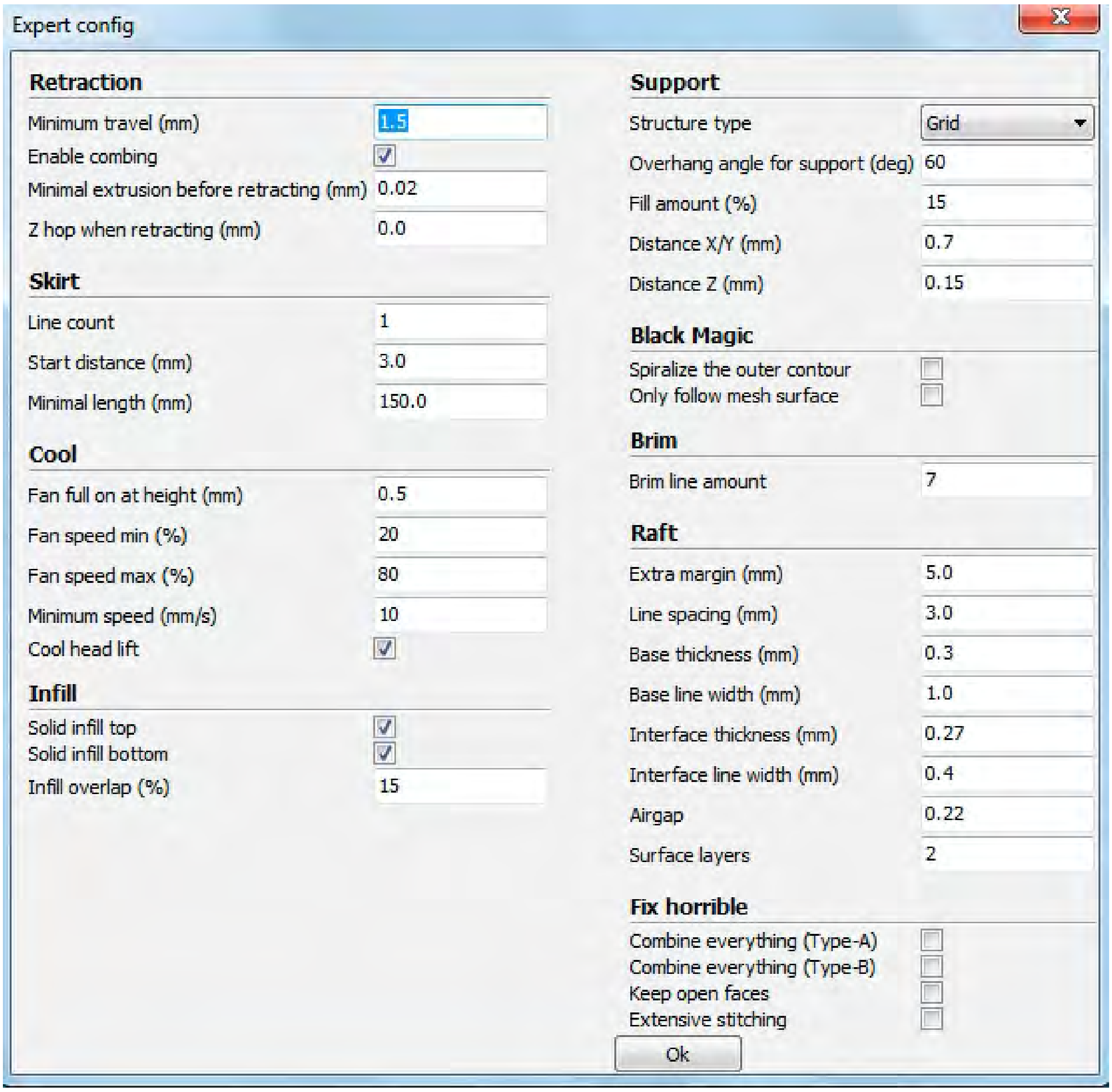

Retraction (retracción)

La impresora hará la retracción del filamento siempre que tenga que moverse de un punto a otro sin imprimir. Esta retracción se realiza para evitar que gotee el plástico.

- Minimun travel (desplazamiento mínimo): Fija el desplazamiento mínimo para el que se realizará la retracción del filamento.
- Enable combining: Si esta opción está marcada, además de realizarse la retracción, la impresora va a evitar que el HotEnd pase sobre los orificios o huecos.
- Minimal extrusion before retracting (mínima extrusión antes de retraerse): Fija la cantidad mínima de plástico que se debe de extruir antes de realizar la retracción. Si no se extruye al menos esta cantidad de filamento, la retracción será ignorada.
- Z hop when retracting (elevación del eje Z al retraer): Esta opción hace que se eleve el eje Z cuando se realizan desplazamientos. Es una opción muy útil y que va a mejorar la calidad de piezas que tengan detalles pequeños, evitando junto con la retracción que aparezcan hilos que afeen la impresión. Para piezas simples recomiendo tenerla desactivada (ya que activarla va a incrementar el tiempo de impresión), si la pieza es compleja y tiene detalles, se puede introducir en este parámetro una altura que sea el doble de la altura de capa que se esté usando.

Skirt

El skirt o falda es una línea que va a rodear el modelo que estemos imprimiendo. Esta línea tiene 2 propósitos, el primero es determinar los límites donde estará contenido el modelo y el segundo es limpiar el HotEnd eliminando posibles burbujas de aire de su interior o suciedad de la propia boquilla.

- Line count (Número de líneas): Fija el numero de vueltas que dará rodeando al objeto.
- Start distance (Distancia al objeto): Establece la distancia de separación entre el objeto y la falda.
- Minimal length: (longitud mínima): Establece la longitud mínima que tendrá la falda. En piezas pequeñas la falda no será suficientemente grande para limpiar correctamente el HotEnd, por lo que se fija una distancia mínima, incrementando el número de vueltas hasta llegar a esta distancia.

Cool

Los parámetros contenidos en "Cool" afectan a la forma en la que se va a enfriar la pieza, pudiendo modificar las opciones del ventilador de capa o los tiempos mínimos de impresión.

- Fan full on at height (Ventilador activo a cierta altura): Esta opción va a activar completamente el ventilador de capa a partir de la altura seleccionada. Para las capas inferiores, el ventilador funcionará a una velocidad proporcional, estando siempre desactivado para la capa inicial.

- Fan speed min/max (velocidad máxima y mínima del ventilador): Estos parámetros establecen la velocidad máxima y mínima del ventilador de capa. Dependiendo del ventilador instalado en la impresora, hay que regularlo para que el flujo de aire sea correcto, ya que un flujo excesivo enfriará la pieza demasiado rápido y puede hacer que aparezcan rajas en la pieza.
- Minimun speed (velocidad mínima): Establece la velocidad mínima de impresión. Este parámetro es muy importante, ya que al imprimir a muy baja velocidad el plástico se va a recalentar demasiado deformando la impresión, por ello es necesario fijar una velocidad mínima para que esto no suceda. Este valor va a depender del tipo de filamento con el que estemos imprimiendo, para la mayoría de filamentos un valor de 10 a 15mm/s es suficiente.
- Cool head lift (Sube para enfriar): Si esta opción esta seleccionada, va a elevar el HotEnd al completar una capa si no se ha cumplido el tiempo mínimo establecido para cada capa, dándole tiempo a enfriarse y separándose para no recalentar el plástico.

Infill

- Solid infill top/bottom (relleno sólido superior e inferior): Al seleccionar estas opciones, tanto la capa inferior como la superior serán sólidas y no se verán afectadas por el factor de relleno que se tenga aplicado al diseño. Es recomendable tenerlas siempre activadas.
- Infill overlap (solapamiento del relleno): Este parámetro controla la cantidad de relleno que se va a solapar con los bordes. El valor que trae por defecto (15%) funciona bien.

Support

Los soportes son elementos que en muchas ocasiones son totalmente necesarios para imprimir el modelo, y en función de las características del mismo, habrá que modificar los soportes para que se adapten lo mejor posible al diseño y sean fácilmente retirables.

- Strunture type (tipo de estructura): Podemos seleccionar entre dos tipos de estructuras, una compuesta por una cuadricula (grid) y otra compuesta por líneas (lines). Elegid la que mejor se adapte a vuestro modelo, aunque la estructura "grid" da por lo general mejores resultados.
- Overhang angle for support (ángulo máximo para suportes): Indica el ángulo máximo para el que se empezarán a usar los soportes. Este ángulo toma como referencia la vertical, tenido un muro vertical un ángulo de 0º y un puente horizontal un ángulo de 90º. La mayoría de impresoras son capaces de crecer con ángulos de al menos 45º,

por lo que los soportes no son necesarios para ángulos inferiores. Fijad el valor en 45º y aumentar el valor hasta determinar el límite de vuestra máquina.

- Fill amount (Cantidad de relleno): Fija el relleno que se va a usar para los soportes. El relleno va a definir la separación entre las líneas de soporte, vuestra impresora deberá de crear puentes usando estas líneas y salvando estos huecos. Suelen funcionar bien valores de relleno del 20% al 50% (en función del diseño).
- Distance X/Y (Distancia X/Y): Establece la separación entre los bordes del objeto y los soportes. Si esta distancia es muy pequeña, se pueden unir los bordes con los soportes haciendo que los soportes sean muy complejos de retirar y afeando la terminación final de la pieza. Una separación de 0.7mm será suficiente para HotEnds con boquillas de hasta 5mm.
- Distance Z (Distancia Z): Establece la separación en Z (altura) que habrá entre el soporte y la pieza. Esta distancia está determinada en gran medida por la altura de capa que se use, siendo lo más correcto introducir aquí un valor que sea la mitad de la altura de capa. Los valores 0.1mm o 0.15mm funcionan bien.

Black magic

- Spiralize the outer contour: Esta opción imprime el contorno del objeto con una base sólida. Convierte un elemento sólido en un objeto hueco.
- Only follow mesh surface: Esta opción imprime la superficie o cáscara del objeto, sin que se tengan en cuenta la base, el relleno o la capa superior.

Brim

- Brim line amount (Ancho de la visera): En este parámetro se indica el ancho que va a tener la visera. Cuanto mayor sea el ancho de la visera, mayor va a ser la adhesión que tendrá el objeto. El tamaño de la visera va a depender de la superficie de contacto y de la forma que tenga la pieza, siendo valores comunes los que están comprendidos entre 5 y 20 milímetros.

Raft

Aquí podemos configurar todos los parámetros de la base de impresión. Esta base, como se comentó en la "configuración del laminado", va a mejorar la adhesión de la pieza creando una especie de malla sobre la que se imprimirá el objeto.

- Extra margin (Margen extra): Este parámetro fija el margen que sobresaldrá la base del objeto.
- Line spacing (Espacio entre líneas): Fija la distancia entre las líneas que formaran la malla.
- Base thickness (Espesor de la base): Establece el espesor que tendrá la base. Por defecto se suelen hacer 1 o2 capas de base (en función del espesor de capa).

- Base line width (Ancho de la línea de base): Este parámetro modifica el grosor de las líneas con las que se confecciona la base. Da buenos resultados usar líneas que tengan el doble de ancho que la boquilla del HotEnd (dará dos pasadas por línea).
- Interface thickness (Espesor de la capa intermedia): Establece el grosor de la capa intermedia que tiene la base.
- Interface line width (Espesor de la línea intermedia): Establece el grosor de las líneas que forman la capa intermedia de la base.
- Airgap: Este parámetro modifica el espacio entre la última capa de la base y la primera capa del objeto. Esta separación va a influir en la facilidad a la hora de retirar la base del objeto.
- Surface layers (capas de la superficie): Fija el número de capas de la parte superior de la base

Fix Horrible

Las opciones incluidas en "Fix horrible" son opciones para intentar mejorar o reparar los objetos. El programa por defecto realiza modificaciones en el diseño 3D que puede dar como resultado efectos no deseados y que alteren el modelo original. Las opciones contenidas en "fix horrible" por si solas o combinadas entre sí, cambian la manera en que CURA va a interpretar el modelo 3D, solventando posibles problemas a la hora de imprimir.

Por defecto CURA suele reparar correctamente todos los errores del modelo 3D, estas opciones solo son recomendables activarlas en casos excepcionales, ya que pueden afectar negativamente a la impresión.

- Combine everything (Type A): Une todas las partes del modelo en base a las normales intentando mantener los orificios internos intactos.
- Combine everything (Type B): Une todas las partes del modelo ignorando orificios internos y conservando la capa exterior.
- Keep open face: Mantiene abiertos pequeños huecos que pudiera tener el modelo. Por defecto CURA cierra los huecos o grietas pequeñas del modelo, ya que los toma como errores del diseño.
- Extensive stitching: Repara los agujeros o grietas del modelo, cerrando los orificios que tengan polígonos que se toquen.

Las dos últimas opciones que podemos encontrar dentro de la pestaña "Expert" son:

Run first run wizard, con esta opción podemos ejecutar el asistente para la configuración inicial. Este asistente se ejecuta por defecto la primera vez que instalamos el programa

Run bed leveling wizard, al pulsar esta opción, se va a ejecutar un asistente que ayuda en el proceso de nivelación de la cama.

Menú de **impresión**

Imprimiendo el modelo 3D

Una vez cargado el modelo en el área de impresión y configurado los parámetros de laminado, podemos guardar estos valores en la tarjeta SD e imprimir la figura usando para ello la pantalla LCD de la impresora 3D o bien podemos establecer una conexión entre la impresora y el ordenador abriendo para ello el menú de impresión.

Podemos abrir el menú de impresión pulsando sobre el icono "print with USB" que encontraremos en la parte superior del área de impresión o haciendo clic sobre la opción "print" que está dentro del menú "file" de la barra de tareas.

Al hacer esto se nos abrirá una nueva ventana con el menú de impresión. Esta ventana puede mostrar dos entornos visuales distintos en función de la configuración que tengamos (ver "preferences" pag. 19), puede mostrar la vista clásica de CURA o cargar el entorno de pronterface.

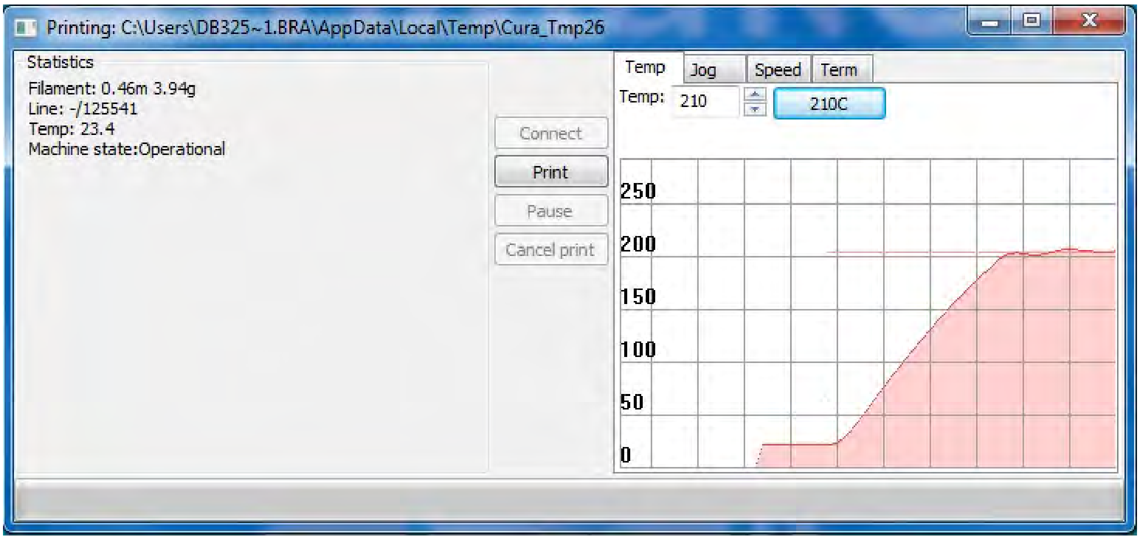

En la imagen superior se puede ver el panel de impresión que usa CURA por defecto, en este panel tenemos acceso a la información básica, como puede ser la temperatura de la cama caliente y del HotEnd. Tambien encontraremos opciones para desplazar cada uno de los ejes (en la pestaña "Jog") y podremos modificar la velocidad de impresión en la pestaña "Speed".

En ambos entornos de impresión vamos a encontrar las mismas opciones, mover los ejes en todas direcciones, extruir, fijar la temperatura tanto de la cama caliente como del HotEnd y visualizarla en el monitor de temperaturas.

Cuando la impresora tenga la temperatura deseada y tengamos todo listo, tan solo hay que hacer clic sobre el botón "print" para que comience la impresión.

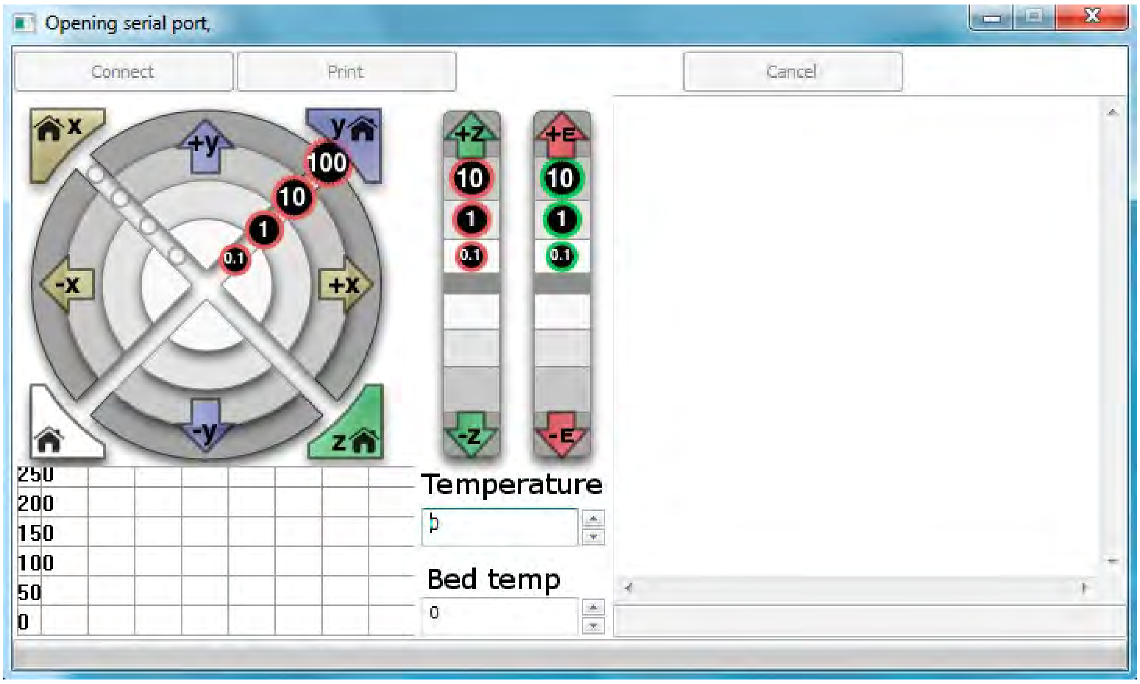

Una vez iniciada la impresión, se podrá variar la temperatura tanto de la cama caliente como del HotEnd, o la velocidad de impresión. El menú de impresión también nos da la opción de cancelar si detectamos algún error en el transcurso de la misma.

Una vez iniciada la impresión, recomiendo hacer los cambios de velocidad, temperatura, flow... preferiblemente a través de la pantalla LCD de la impresora.

Anexo 5. Planos de hélice.

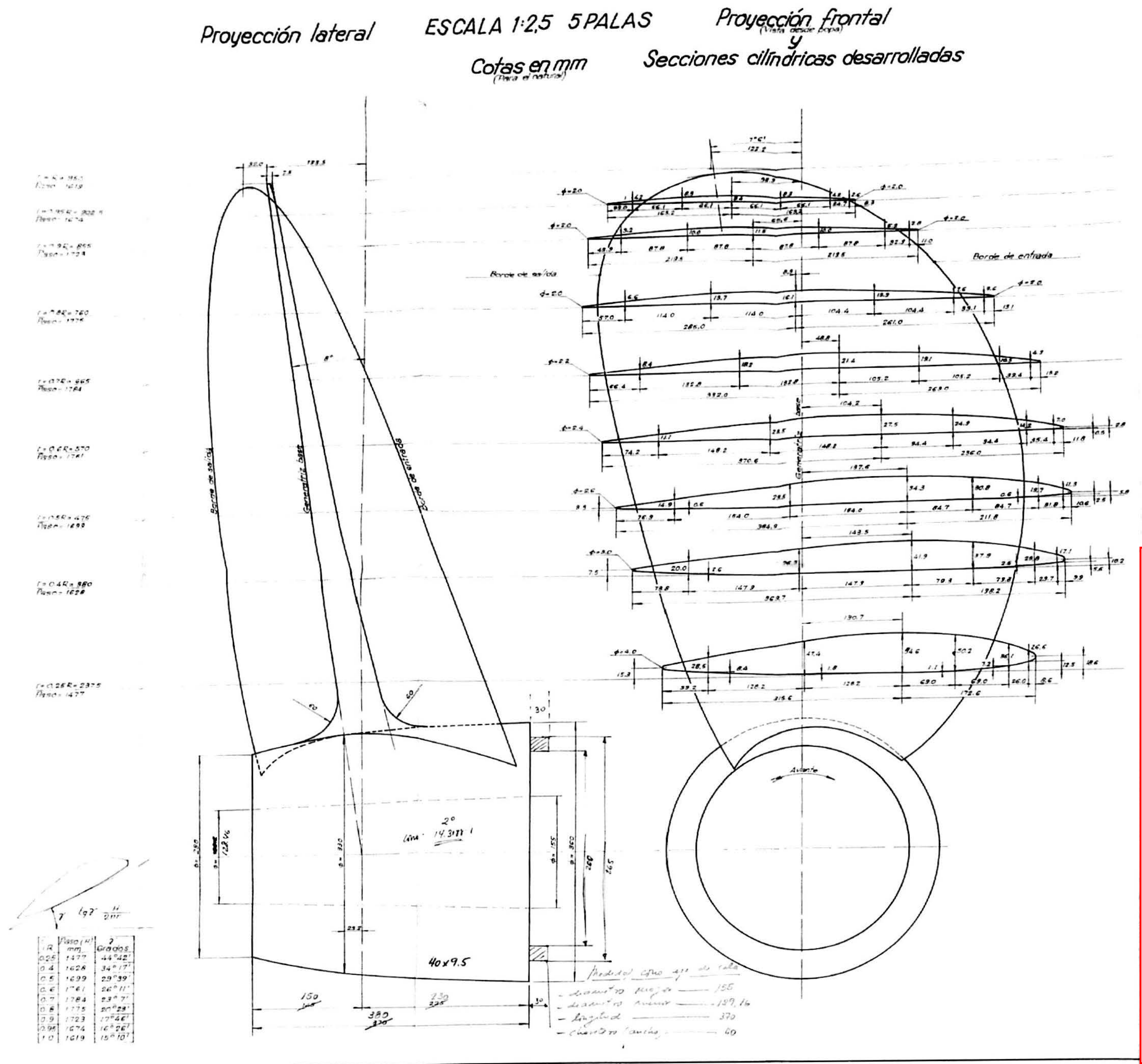
Proyección lateral
ESCALA 1:2,5 5 PALAS
Cotas en mm
(Para el natural)
Proyección frontal
(Vista desde popa)
y
Secciones cilíndricas desarrolladas
Borde de salida
Generatriz base
Borde de entrada
Avante
40x9.5

A-VALUE = -35

RAKE = 25.0

CTE	CLE	R/R	RADIUS	PITCH	THICKNESS
178	-150	1.00	350.00	850	6.0
224	-26	0.95	332.50	850	6.9
224	42	0.90	315.00	850	7.9
205	130	0.80	280.00	850	10.3
179	179	0.70	245.00	850	12.9
151	197	0.60	210.00	850	16.0
123	192	0.50	175.00	850	19.4
97	169	0.40	140.00	850	23.3
73	136	0.30	105.00	850	27.4
63	117	0.25	87.50	850	29.7
51	96	0.20	70.00	850	32.0

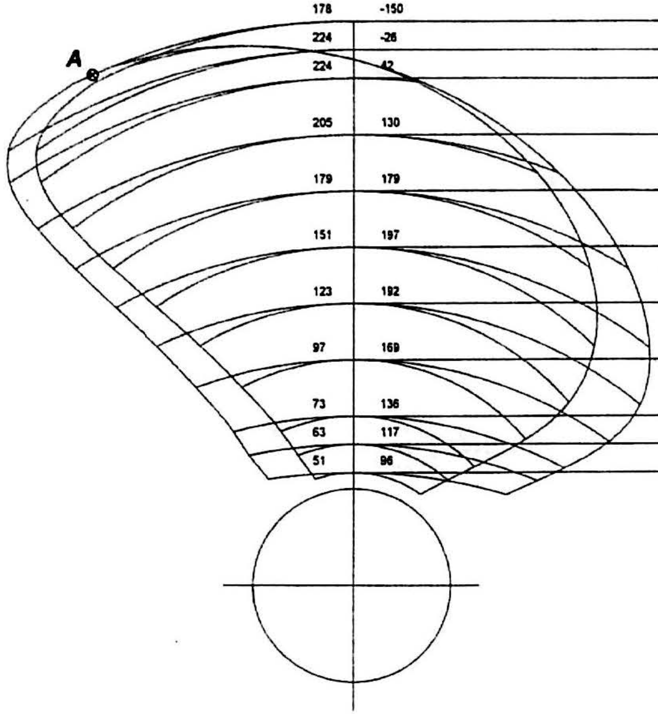

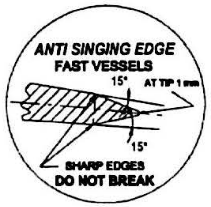

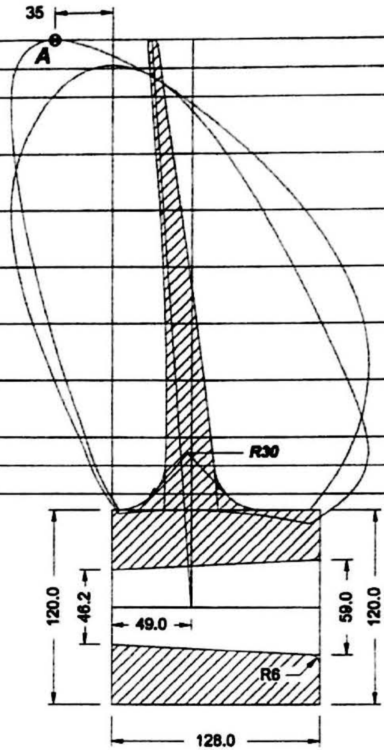

ATTENTION: FAST VESSEL - LEAN PROFILES ROOT-THICKNESS TO BE AT THE MINIMUM!!!

NOTES:

1. BOTH SIDES ANTI-SINGING-EDGE FROM R 0,2 TO R 1,0 (TRAILING EDGE)
2. FILLET RADIUS DECREASING TO LEADING EDGE AND TRAILING EDGE
3. FRONT FILLET RADIUS LEADING EDGE 10% OF MAX.
4. AFT FILLET RADIUS TRAILING EDGE 10% OF MAX.

TOLERANCE FOR A-VALUE: +/- 1mm

PAY ATTENTION TO SKEW-CENTERLINE

1. MAXIMUM THICKNESS PER RADIUS IS BASED ON CENTERLINE!
2. POSITION OF BLADE TIP = 'A'-VALUE = DISTANCE OF SMALLER HUB-FACE TO POINT OF MAX. THICKNESS AT RADIUS 1.00 (ON CENTERLINE). MARK REFERENCE POINT FOR 'A' ON PATTERN!

Aviso responsabilidad UC

Este documento es el resultado del Trabajo Fin de Grado de un alumno, siendo su autor responsable de su contenido.

Se trata por tanto de un trabajo académico que puede contener errores detectados por el tribunal y que pueden no haber sido corregidos por el autor en la presente edición.

Debido a dicha orientación académica no debe hacerse un uso profesional de su contenido.

Este tipo de trabajos, junto con su defensa, pueden haber obtenido una nota que oscila entre 5 y 10 puntos, por lo que la calidad y el número de errores que puedan contener difieren en gran medida entre unos trabajos y otros,

La Universidad de Cantabria, la Escuela Técnica Superior de Náutica, los miembros del Tribunal de Trabajos Fin de Grado así como el profesor tutor/director no son responsables del contenido último de este Trabajo.”